EFFECTS OF A STIFFENED ARTERIAL TREE ON VENTRICULAR-ARTERIAL COUPLING IN HEALTHY AND DISEASED HEARTS

THÈSE N^{O} 3582 (2006)

PRÉSENTÉE LE 25 AOÛT 2006

À LA FACULTÉ SCIENCES DE LA VIE

Laboratoire d'hémodynamique et de technologie cardiovasculaire

SECTION SCIENCES ET TECHNOLOGIES DU VIVANT

ÉCOLE POLYTECHNIQUE FÉDÉRALE DE LAUSANNE

POUR L'OBTENTION DU GRADE DE DOCTEUR ÈS SCIENCES

PAR

David JEGGER

M. Eng., Open University Londres, Royaume-Uni

de nationalité suisse et originaire de Fribourg (FR)

acceptée sur proposition du jury:

Prof. W. Pralong, président du jury

Prof. N. Stergiopulos, directeur de thèse

Prof. P. Segers, rapporteur

Prof. P. Niederer, rapporteur

Prof. L. Von Segesser, rapporteur

ÉCOLE POLYTECHNIQUE FÉDÉRALE DE LAUSANNE

Lausanne, EPFL

2006

Summary

In this thesis we study ventricular-arterial coupling in rodents under the influence of arterial stiffening and myocardial infarction (MI), combination of the two considered as a novel cardiovascular research model for diseased hearts pumping against an aged, stiffened arterial tree. The stiffened arterial tree yields isolated systolic hypertension and is obtained by administration of vitamin D and nicotine (VDN). The investigation cardiac performance and ventricular-arterial coupling using such a combined model (VDN/MI) is of particular relevance to cardiac research, as cardiac disease in elderly often takes place in presence of a atherosclerotic or stiff arterial tree.. The thesis consists of an Introduction, 4 scientific papers and a brief Conclusion.

The Introduction is an overview of the epidemiology of heart failure, structure and functional changes that occur during MI and VDN, material and methods used in evaluating cardiac function invasively and non-invasively (using trans-thoracic echocardiography, TTE), methods for evaluating arterial function, and finally an overview of the interaction between the heart and vessels.

Paper 1: This paper addresses the issue of the universality of the normalized time-varying elastance curve. It is demonstrated that the waveform of the normalized time-varying elastance curve ($E_n(t_n)$) is qualitatively comparable between the control and MI hearts, however, when $E_n(t_n)$ is compared quantitatively between the two groups, statistical significance is found at the ejection phase and during diastole. These differences need to be taken into account when assessing cardiac contractility based on a generalized $E_n(t_n)$ in different animal models or in the human in different physiological or pathological states.

Paper 2: Using trans-thoracic echo (TTE), we were able to follow serial changes of cardiac function post MI using two novel parameters, the myocardioal performance index (MPI) and its ratio to left ventricular fractional shortening (LVFS/MPI), both indices being monitor

successfully and as efficiently as other classical TTE parameters. More so, LVFS/MPI visually expressed better the serial modifications in cardiac function. Both MPI and LVFS/MPI were correlated to the load-independent contractile parameter, PRSW, and to the preload parameter, LVEDP, being thus pertinent in following preload changes post MI. Finally, chamber remodeling post MI can successfully be followed due to the fact that ESV and EDV both correlate to MPI and LVFS/MPI.

Paper 3: We studied hemodynamics, arterial function, cardiac function and ventricular-arterial coupling in a rat model of reduced arterial compliance. The results show that arterial stiffening after VDN treatment provokes important changes in vascular impedance and wave reflections, leading to isolated systolic hypertension and LV hypertrophy, Ventricular-arterial coupling was also altered. The effects are quantitatively similar to those of arterial stiffening with age.

Paper 4: We studied changes in cardiac geometry, structure and function in response to MI in control and VDN-treated (stiffened aorta) rats. The combined VDN/MI model showed the largest compromise in cardiac structure and function and exhibited the strongest biochemical signs of heart failure as compared to all other groups. The addition of MI on top of a raised afterload, seems to have accelerated the progression of heart failure. Vascular alterations also reflected well a model of ageing and calcification. This combined pathology model of failing hearts in presence of a stiff arterial tree might be fruitful in better understanding the evolution of disease and may help improving or developing novel treatment therapies.

The Conclusion chapter summarizes the findings of the thesis and brings into perspective their importance and future relevance into cardiovascular research models.

Keywords: calcium, echocardiography, heart failure, hypertension, myocardial infarction.

Résumé

Dans cette thèse, nous étudions le couple ventriculo-artériel chez les rongeurs sous l'influence de rigidification artérielle et d'infarctus du myocarde (IM). La combinaison des deux est considérée comme le nouveau modèle de recherche cardio-vasculaire dans le cadre de cœurs malades devant pomper dans un arbre artériel âgé et rigidifié. Cet arbre artériel rigidifié se focalise sur l'hypertension systolique et est obtenu par administration de vitamine D et de nicotine (VDN). Les investigation des performances cardiaques et du couple ventriculo-artériel utilisant un tel modèle combiné (VDN/IM) sont d'une importance toute particulière dans la recherche cardiaque, surtout sous le point de vue des maladies cardiaques liées au grand âge, qui recèlent souvent un arbre artériel athérosclérotique ou rigidifié. Cette thèse consiste en une introduction, quatre publications scientifiques et une brève conclusion.

L'introduction fait un tour d'horizon sur l'épidémiologie de l'insuffisance cardiaque, les changements structurels et fonctionnels apparaissant durant un IM et la VDN, le matériel et les méthodes utilisées pour l'évaluation invasive et non-invasive de la fonction cardiaque (échocardiographie trans-thoracique, ETT), les méthodes utilisées pour évaluer la fonction artérielle, ainsi que, pour terminer, un point sur les interactions entre cœur et vaisseaux.

Publication 1) Consacrée à la courbe d'élastance normalisée en fonction du temps. Il a été démontré que la forme de la courbe d'élastance normalisée en fonction du temps ($E_n(t_n)$) est qualitativement comparable entre le groupe de contrôle et les cœurs avec IM ; néanmoins, lorsque $E_n(t_n)$ est comparé quantitativement, l'on trouve une différence statistiquement significative entre la phase d'éjection et durant la diastole. Ces différences sont à prendre en compte lors de l'évaluation de la contractilité cardiaque basée sur un $E_n(t_n)$ généralisé pour différents modèles animaux ou pour l'être humain dans différents états physiologiques ou pathologiques.

Publication 2) En utilisant l'échocardiographie trans-thoracique (ETT), il nous a été possible

de suivre les changements de la fonction cardiaque après IM en nous servant de deux nouveaux paramètres, l'index de performance myocardique (IPM) et sa proportion dans la fraction de raccourcissement ventriculaire gauche (FRVG/IPM). Tous deux ont été monitorisés avec succès et avec la même efficacité que pour les paramètres classique de l'ETT. De plus, FRVG/IPM exprime mieux visuellement les changements dans la fonction cardiaque. IPM et FRVG/IPM ont été corrélés avec le paramètre contractile indépendant de la charge (PRSW), et avec le paramètre de précharge LVEDP, valables pour suivre les changements de précharge après IM. Le remodelage des cavités cardiaque après IM peut être suivi efficacement grâce au fait que ESV et EDV corrèlent tous deux avec IPM et FRVG/IPM.

Publication 3) Nous avons examinés l'hémodynamique, la fonction artérielle, la fonction cardiaque et le couple ventriculo-artériel sur un modèle de rat à compliance artérielle réduite. Les résultats mettent en évidence qu'une rigidification artérielle près VDN provoque un important changement de l'impédance vasculaire et aussi des réflexions des ondes, conduisant à une hypertension systolique isolée et une hypertrophie du VG, ainsi qu'une altération du couple ventriculo-artériel. Ces effets sont quantitativement comparables à ceux de la rigidification artérielle liée à l'âge.

Publication 4) Nous avons examinés les changements de la géométrie cardiaque, des structures et des fonctions en réponse à un IM, comparé au groupe de contrôle et aux rats traités par VDN (aorte rigidifiée). Le modèle combiné VDN/IM montre le plus grand compromis dans les structure et fonction cardiaques et montre les signes biochimiques d'insuffisance cardiaque les plus marqués en comparaison avec tous les autres groupes. L'ajout d'un IM sur une postcharge augmentée semble accélérer l'apparition d'insuffisance cardiaque. Les altérations vasculaires reflétaient bien un modèle de vieillissement et de calcification vasculaire. Cette combinaison de modèles pathologiques d'insuffisance

cardiaques en présence d'un arbre artériel rigidifié pourrait aider à mieux comprendre l'évolution de la maladie et pourrait contribuer à l'amélioration ou au développement de nouvelles thérapies.

Le chapitre de conclusion fait le bilan des résultats obtenus dans cette thèse et met en perspective leur importance présente et future dans les différents modèles de recherche cardiovasculaire.

Mots-clés : calcium, échocardiographie, insuffisance cardiaque, hypertension, infarctus du myocarde.

Acknowledgements

This PhD thesis could not have been performed without the help from numerous sources including personal and professional ones not forgetting the keen collaboration between many centres of excellence.

Initially, I would like to express my deepest thanks to Prof N Stergiopulos for his advice, support, encouragement and expertise in cardiovascular biomechanics. Apart from being a friendly and kind person, his professionalism concerning biomechanics and ventricular-arterial coupling interactions were deeply appreciated throughout the duration of my project.

A great appreciation is expressed to Dr AS Mallik, Dr R da Silva, Dr P Fridez, Caroline Di Gilio, Gilles Prod'hom and the rest of the LHCT group for their support and motivation.

Special thanks to Dr H Tevaearai in Bern for his personal support and motivation. His scientific and medical advice laid the foundation to the final chapters of the thesis and to the eventual application of it to further pursue a postdoc research proposal using gene therapy and later reverse remodelling in the USA. Collaborators will be Prof D Burkhoff (Columbia University, NY, USA) and Prof P Hunter (Auckland University, New Zealand).

A great deal of appreciation is expressed to Prof LK von Segesser, Mrs J Horisberger and the perfusion team at the CHUV for their support and flexibility concerning the time allocated to me in order to pursue my thesis at the EPFL. Also, the technical and medical insight provided by Dr P-G Chassot, Dr M Nasratullah and Dr X Jeanrenaud re Trans-Thoracic Echocardiography.

The efficiency, statistical insight and innovation provided by Prof P Segers will not be forgotten and my utmost appreciation is hereby expressed for it.

The undertaking of the thesis could not have been done without the help from Dr I Lartaud and Prof J Atkinson whom studied extensively the role of VDN on cardiac and vascular function in Nancy, France. Also, Dr D Hayoz who introduced me to the VDN model.

This work was supported by an award from the Swiss National Research Foundation (3100AO-104257/1), Cardiovascular Scientific Foundation (Fonds Scientifique Cardiovasculaire), Swiss Life Anniversary Foundation for Public Health and Medical Research, Novartis Foundation for Medico-Biological Research, the French Ministry of Education and Research (EA3448) Paris. Also, an exchange grant (PBOIA-102080) was obtained from the FNS to spend expertise training with Prof P Hunter in Auckland, New Zealand.

A direct and indirect inspiration from my family and friends will not be forgotten. Special motivation was obtained from my son and brother whom are always in my thoughts even in the absence of their presence.

Contents

Introduction

Heart failure in relation to myocardial infarction and hypertension

One of the most cited and a coherent study on the epidemiology of congestive heart failure (CHF) in the USA is The Framingham Heart Study, which followed a cohort of 9405 patients over a 40 year period [20]. In a subgroup analysis of 331 men and 321 women who developed CHF, the majority had coronary artery disease (CAD) with or without hypertension (HTN), and approximately 1/3 had HTN alone.

Epidemiological studies have shown that coronary heart disease (CHD) and essential hypertension are independent predictors of congestive heart failure with an occurrence rate of 40% in both male and female populations when the two pathologies are combined (Figure 1)[20]. Figure 1 demonstrates the risk of several conditions on the development of CHF in men with a similar occurrence in woman. Serum cholesterol was not associated with an increased risk of HF. However, smoking, HTN, diabetes and ECG-LV hypertrophy did. There were also age-dependent differences in risk rates. Therefore, the combination of myocardial infarction (MI) together with hypertension would also seem to be an interesting research model to pursue.

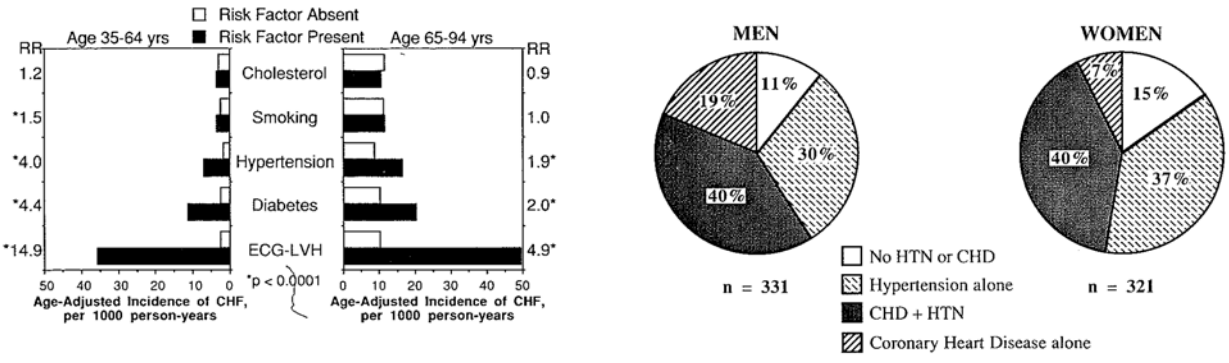

Figure 1 Demonstrates the risk of several conditions on the development of CHF in men with a similar occurrence in woman.

Physiology of myocardial infarction (MI) and hypertension (VDN)

Despite the multiple different causes, LV failure typically progresses by the common pathways of myocyte hypertrophy, fibrosis deposition, and left ventricular chamber enlargement. Abnormalities of function during systole, diastole or both may contribute to diminished cardiovascular performance. The evolution of cardiac function depends on the pathology inflicting the damage.

Myocardial Infarction (MI) causes chamber dilatation and loss in contractile function often referred to as "volume overload" while HTN raises the afterload of the heart and causes a state called "pressure overload". These two models lead to different changes in cardiac function as a response to workload. A pattern of hypertrophic growth characterized as concentric, in which increased mass is out of proportion to chamber volume, is particularly effective in reducing systolic wall stress under conditions of increased pressure load. In contrast, in volume overload conditions, in which the major stimulus is diastolic loading, a predominant finding is a great increase in the cavity volume or size, the relationship between mass and volume is either preserved or, in severe cases, reduced. The fundamental response is generated by cellular hypertrophy. However, the configuration of the new contractile tissue is specific and offsets the major mechanical stimulus of pressure or volume overload (Figure 2)[16].

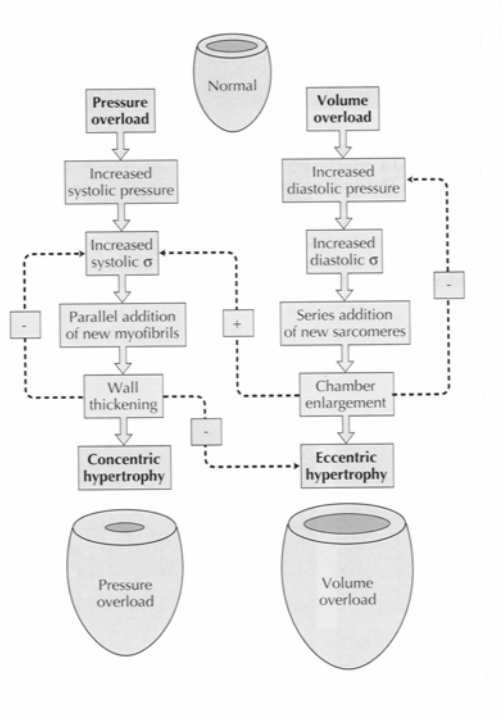

Figure 2. Schematic representation of the two models of pressure and volume overload.

During aging, alterations in aortic structure and function occur, leading to a decrease in aortic compliance. Degeneration and fragmentation of elastic fibers contribute to the increase in aortic stiffness [4]. To study the effects of arterial stiffening on arterial and cardiac function, many experimental animal models have been used, ranging from acute animal models where the aorta was either replaced by a stiff tube [26,42] or wrapped with a non-compliant Dacron band [21], to chronic models, where aortic stiffness is increased by inbreeding [19], as a result of hypertension-induced remodeling [23] through some chemical or biological treatment or old age [4,12,32]. Of particular importance is a model of aortic elastocalcinosis induced by the administration of vitamin D_3 and nicotine (VDN), developed originally by Hass et al. [18]. The VDN model leads to arterial stiffening by decimation of the arterial wall elastic fibre network [38]. Earlier studies on the effects of VDN on arterial hemodynamics showed that arterial stiffening caused by VDN decreased compliance and increased wave speed, aortic characteristic impedance, and wave reflections leading to isolated systolic hypertension (ISH) and the development of compensatory LV hypertrophy [28,29].

Thus, the type of remodeling occurring in the combined model (MI and ISH provoked by VDN) would be interesting to elucidate and understand the mechanisms involved in its development. The cardiac function can be modeled invasively (using the conductance catheter, CC) and/or non-invasively using trans-thoracic echocardiography (TTE)[5,62].

Cardiac function using conductance catheter: Invasive measurements

The cardiac cycle in brief

The principle function of the heart is to pump oxygenated blood to the peripheral tissues to meet their metabolic demands. The systemic arterial and venous systems provide the conduits. The interaction of the LV with the arterial and venous systems is therefore integral to the satisfactory performance of this vital function. It is important to understand how the normal

heart functions and how it interacts with the systemic arterial and venous systems as prelude to comprehending how it is affected by various pathologic conditions.

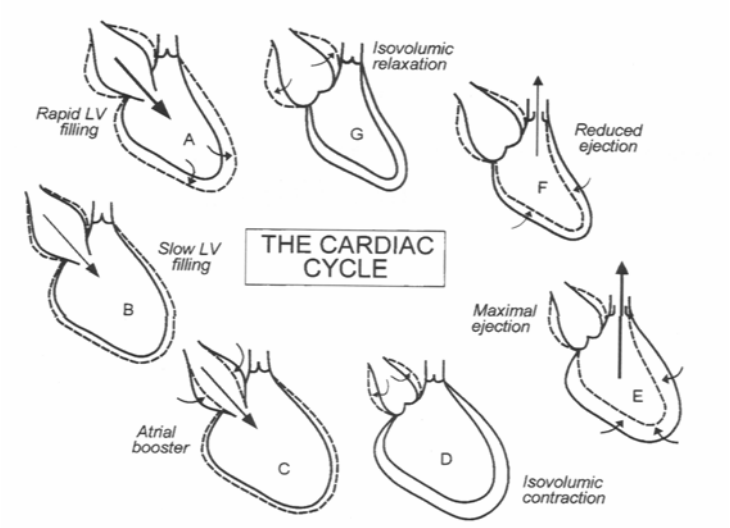

Figure 3. The cardiac cycle representing the different phases within it.

In brief, the cardiac cycle, with electrical activation there is an abrupt increase in isovolumic LV pressure, followed by rapid ejection. Reduced ejection follows until closure of the aortic valve, establishment of zero flow, minimal volume, and maximal LV wall thickness, at which time diastolic events are initiated. The initial diastolic event, active LV pressure decline, is followed by rapid filling, which manifests as a rapid increase in LV volume and thinning of the LV wall, followed by diastasis. Diastole is completed with atrial contraction (Figure 3)[6].

The pressure-volume relationship

The diastolic and systolic pressure-volume (P-V) relations can be obtained in vivo by measuring ventricular volume and pressure while cardiac filling is changed, for instance by partial occlusions of the vena cava which is, in fact, the preferred way to obtain the ESPVR (Figure 4). At each moment in the cardiac cycle a P-V graph exists, which can be obtained by constructing isochrones. This family of curves, when approximated by straight lines, allows for the determination of slope as a function of time, E(t) [58]. The time pattern of this slope, E(t), when normalised with respect to magnitude and time to peak (En(tn)), is maintained under normal conditions and during diseased states like MI [40]. From the P-V loops, the E (t)

(Figure 4) and En(tn) curves [58] can be established, as well as the functional parameters [10, 51] and finally the cardiac energetics [59-61](Figure 5). In MI induced HF, the ESPVR is compromised contrary to the initial effect of HTN, which causes enhanced contractility thus a higher ESPVR.

Sagawa et al. performed various preload, afterload, ino and chronotropic manipulations in a canine model and came to the conclusion that the LV has time-varying elastic characteristics and elastance is maximal at end-systole [50]. During different cardiac pathologies, the E(t) curve is presumed to be conserved; however, this is a controversial topic as Kass et al. describes this phenomenon [25]. However, we hypothesise, that MI does in effect alter the E(t) curve.

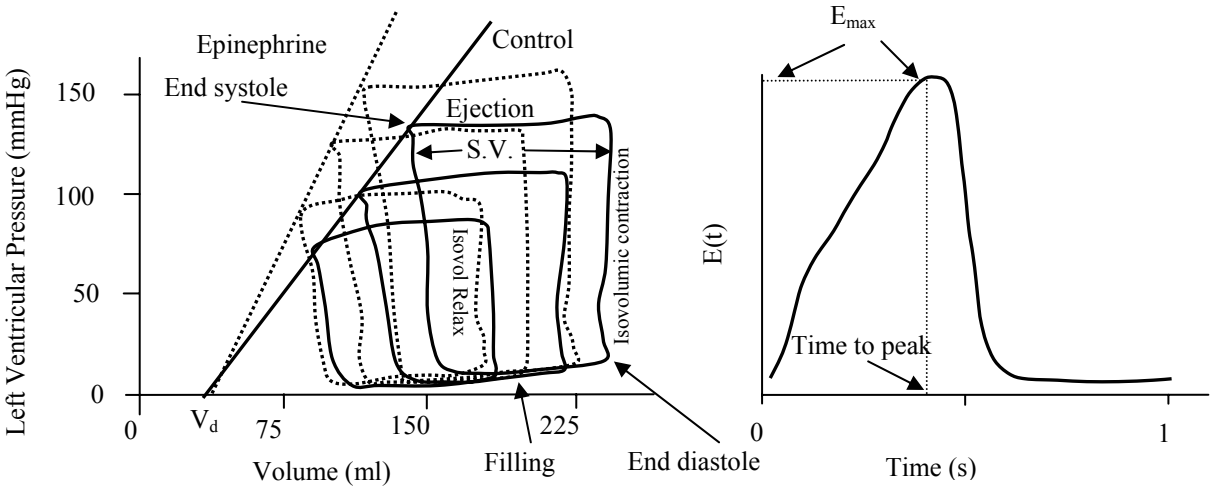

Figure 4 Pressure-volume relationships during control and epinephrine stimulation.

Energetics: total mechanical energy and PVA

Suga et al. came to the conclusion that the E (t) can lead to a new measure of total mechanical energy of contraction as an analogy of the mechanical energy stored in a stretched spring and mechanical work performed by its shortening (Figure 5C) [50]. This measure corresponds to the systolic P-V area (PVA) in the P-V diagram (Figure 5D,E). PVA is the sum of the areas

for external work (EW) within the P-V loop and elastic potential energy (PE) under the Emax line on the origin side of the P-V loop. Consequently, Suga et al. established the relationship between PVA and myocardial oxygen consumption (mVO2)[58]. Efficiency is inversely proportional to PVA.

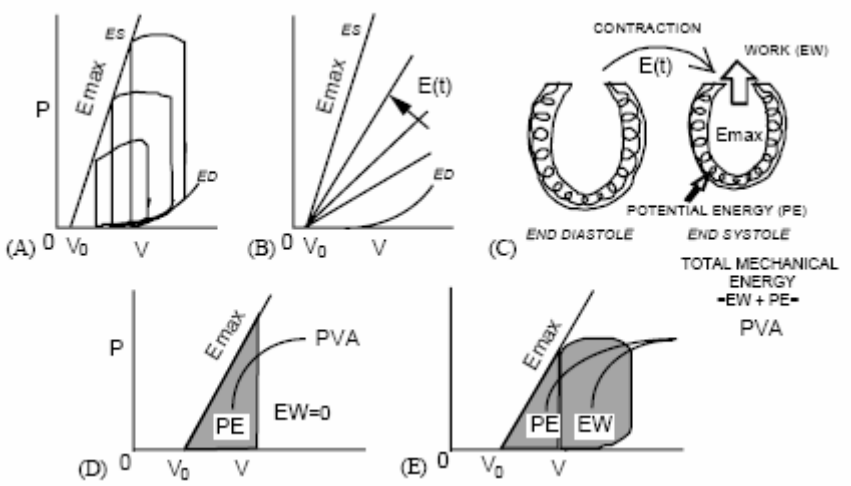

Figure 5. Information contained in the P-V diagram. Ventricular contractility index Emax (A), time-varying elastance E(t) (B), external work (EW) and potential energy (PE) in the time-varing elastance model of the ventricle (C), and systolic PVA (shaded area) as a measure of ventricular total mechanical energy in isovolumic (D) and ejecting contraction (E). Vo: unstressed ventricular volume, ES: end systole, ED: end diastole.

Assessment of LV function

dP/dt_{max} is the most widely used index of contractility, assumingly afterload independent but sensitive to preload. Its relationship with EDV is linear and is load independent. However, a more useful indicator, ESPVR is preload and afterload independent [51]. ESPVR can be characterized by a slope (Ees) and a volume axis intercept (Vo), so that Pes=Ees(Ves-Vo). The Vo is the volume left in the LV when no load is applied. ESPVR can also vary with heart size so normalization has been considered [61].

Cardiac output (CO), ejection fraction (EF), left ventricular fractional shortening (LVFS) and stroke work (SW) are all load dependent. However, SW can be indexed to EDV becoming preload recruitable stroke work (PRSW) which is sensitive to contractile changes but insensitive to pre, afterload and heart size.

Tau (τ), an index of isovolumic relaxation, is defined as the time required to decline 1/e or

37% of its value at dP/dt_{min}. EDPVR is a measure of diastolic stiffness and is influenced by EDV. It can be linear or nonlinear depending on the filling pressure. It reflects the net effect of all facets of myocardial material properties, chamber structure properties, and extracellular matrix [10].

Cardiac function using Trans-Thoracic Echocardiography (TTE): non-invasive measurements

The use of TTE has already been validated in rats [44], using different models including MI [22,33,41], hypertension and aging [55], and a comparison between both pressure-volume overloaded ones [13]. The M-mode (Figure 6) is used to evaluate parameters which utilise the following dimensional parameters seen in Figure 6 i.e. end-diastolic LV dimension (LVDed), end systolic LV dimension (LVDes), septal and posterior wall thickness's (SWth and PWth respectively).

Indicators of systolic function:

1. Ejection fraction (EF): A 2-dimensional long axis view is obtained during end-systole and end-diastole of the LV. The images are sectioned and a length, L is obtained. The following formula is applied: (EDV-ESV)/EDV= % where the volumes are calculated from: $(\pi/ 4) \bullet \Sigma D \bullet (L / n)$ where n = 20 discs of diameter D. This is referred to as the Simpson rule (Figure 7).
2. LV fractional shortening (LVFS): (LVDed-LVDes)/LVDed x100= %. LVFS is preload and afterload dependent.
3. LV mass: $(((LVDed+SWth+PWth)^3 LVDed^3)*1.04)*0.8+0.14 = g$
4. Relative wall thickness (RWT): (PWth+SWth)/(LVDed)
5. Velocity of circumferential fibre shortening (Vcf) : (LVDed-LVDes)/(ET x LVDed)= circ/s

6. Myocardial performance index (MPI): an indicator of combined systolic and diastolic function (Figure 8)[63]. It comprises of the isovolumic contraction time (ICT) plus isovolumic relaxation time (IRT) divided by the ejection time (ET).
7. Cardiac output (CO): Instantaneous blood flow: Vmax (cm/s) • A (cm2) = Q (cm^3/s)= ml/s x 60 = ml/min.

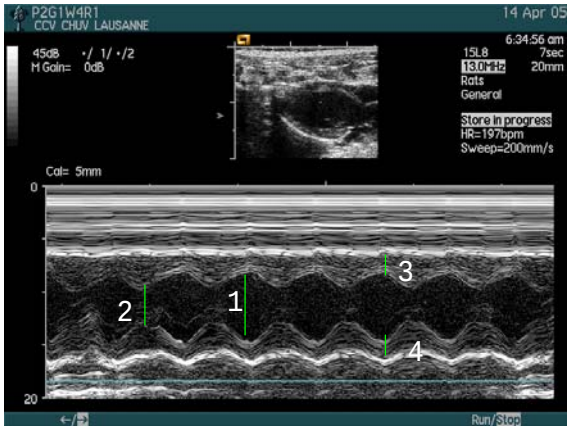

Figure 6. Representation of the M mode showing the LVDed (1), LVDes (2), SWth (3) and PWth (4).

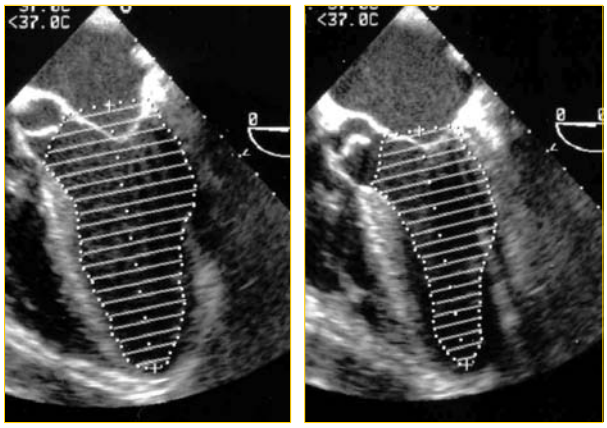

Figure 7. Representation of the Simpson rule showing the LV in diastole (left) and systole (right).

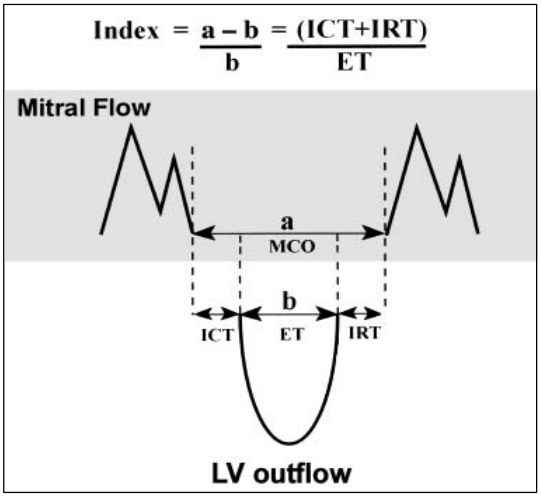

Figure 8. Sketch showing the principle of the MPI.

Indicators of diastolic function:

Diastolic function is assessed indirectly from flow across the mitral valve and by pulmonary venous flow (Figure 6). The E wave is developed from early atrial filling and the A wave

from atrial contraction. Their ratio is often used to express an indication of diastolic function in a clinical setting but has certain limitations. In rats, the major limitation is the high HR which causes the two waves to fuse thus rendering the analysis impossible. Therefore, this parameter is inappropriate. Other parameters exist but require Doppler tissue imaging (DTI) or strain functions, which need to be installed in the TTE machine or special probes are necessary.

Thus, we opted to analyze the flow in the pulmonary vein. The parameter that is well known to correlate to any alterations in left atrial pressure being a sign of diastolic dysfunction is the deceleration time of the D (diastolic) wave (Figure 9)[27].

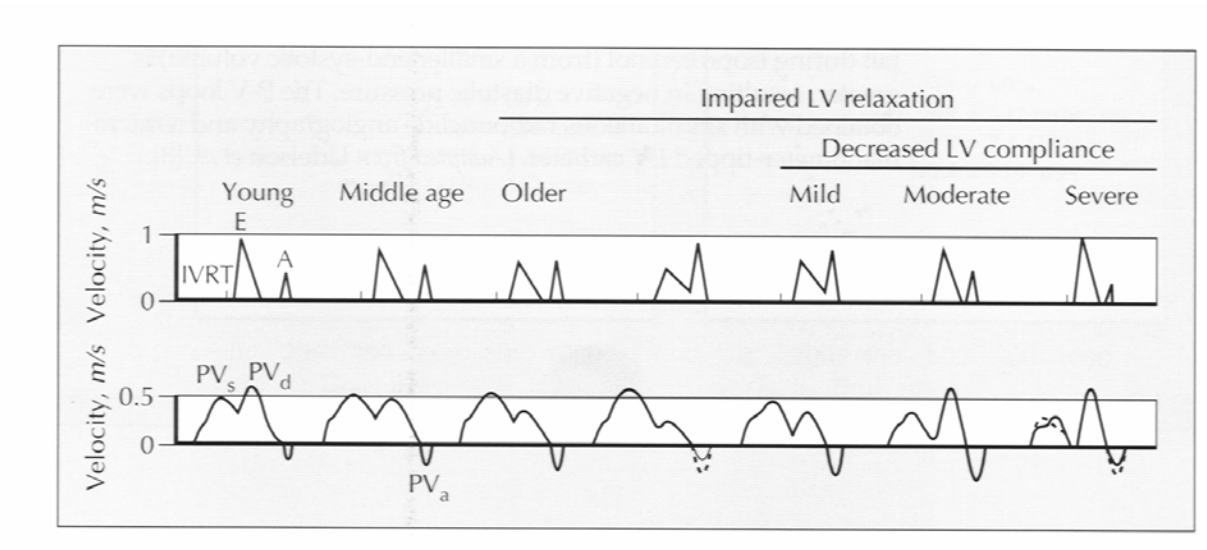

Figure 9. Doppler transmitral (above) and pulmonary (below) venous flow patterns with diastolic dysfunction. In healthy young individuals, most diastolic filling occurs early in diastole so the E/A ratio is >1. The relaxation is impaired, early diastolic filling decreases, and more blood is transported late in diastole by atrial contraction; this is reflected by E/A reversal. With disease progression, LV compliance decreases and filling pressure increases (pseudonormalisation). With a severe decrease in LV compliance, left atrial pressure rises maintaining diastolic filling that result in a restrictive pattern.

Arterial function including wave reflection analysis: effects of HTN

Epidemiological studies have emphasized the close relationship between elevated blood pressure and the incidence of cardiovascular disease [64]. Systolic blood pressure and pulse pressure (PP), in particular, have been demonstrated to be strong independent predictors of cardiovascular mortality [15,47]. PP is on one hand determined by heart-related parameters

such as heart rate and stroke volume (also related to arterial load), but also by the cushioning capacity of arteries (total arterial compliance) and the timing and intensity of wave reflections [37,57]. The former is influenced by arterial stiffness, which is usually expressed as the inverse of stiffness, i.e., as compliance or distensibility. The latter results from the summation of all backward running waves i.e., waves returning towards the heart after reflection at peripheral sites. In a recent review, aortic stiffness (measured from aortic pulse wave velocity, PWV) and an early return of reflected waves to the heart have been established as independent predictors of cardiovascular risk [48].

Aging, environmental and genetic factors are responsible for structural and functional changes of the arterial wall, leading to decreased elasticity and increased stiffness in humans [17,36]. Furthermore, these changes in arterial stiffness are different in proximal elastic arteries compared to distal muscular ones [7,30,39]. This increased stiffness, is responsible for raising the systolic blood pressure and a relative decrease is diastolic blood pressure, thus increasing pulse pressure (PP). More specifically, increased PP, stiffness and thickness of the common carotid artery (CCA) wall were shown to be significant predictors of cardiovascular complications mainly for myocardial infarction [9] but also for stroke in humans [31]. Similarly, the relationship between raised CCA stiffness and left ventricular (LV) hypertrophy has been established [8,45,46].

Assessment of arterial function. Aortic flow is measured using a transit-time ultrasonic flowmeter with the flow probe placed around the ascending aorta. Aortic pressure is measured by retracting the CC from the LV into the ascending aorta. Steady state measurements containing 10 cycles are averaged to construct a representative steady-state beat of aortic pressure (P_{ao}) and flow (Q_{ao}). Discrete Fourier transform (Mathematica 5.2®, Wolfram Research Inc., IL, USA), is applied to obtain pressure and flow in the frequency domain. Aortic input impedance, $Z_{in,}$ was calculated as the ratio of the pressure to flow

harmonics and we considered the steady (or DC component) and the first 10 harmonics.

The ratio of mean P_{ao} and Q_{ao} (DC component of Z_{in}) is systemic vascular resistance (R). Input impedance being a complex quantity, is expressed in terms of its modulus and phase as a function of frequency (figure 10 top). The characteristic impedance of the aorta, $Z_{c,}$ is estimated as the average of impedance modulus between the 5^{th} and the 10^{th} harmonic. Because heart rate differs from animal to animal, impedance values are interpolated and reported at intervals of 10Hz, allowing thus the calculation of standard deviations. Total arterial compliance (C) is estimated using the Pulse Pressure Method [56]. Pulse wave velocity (PWV) is estimated indirectly from the characteristic impedance and ascending aorta dimensions as $PWV= Z_c*A/\rho$, where $A=\pi r^2$ is the luminal cross-sectional area of the ascending aorta measured with Echo Doppler and ρ being the density of blood.

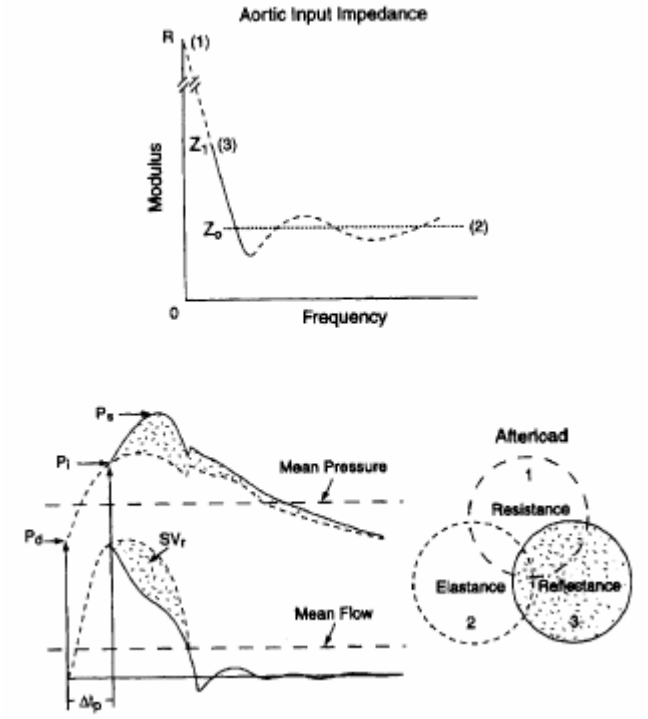

Figure 10. 1) Impedance at zero freqzuency or peripheral resistance (R). 2) Mean value of impedence moduli or characteristic impendence (Zo). Zo is an index of aortic elastance. 3) Fundamental impedence moduli Zi, is an index of wave reflection amplitude Ps-Pi; reflectance. Impedence minimum is related to PWV and distance to the major reflection site. (lower left) High fidelity pressure and flow velocity waveforms. Ps is peak systolic pressure, Pi is inflection point, which indicates the beginning of the upstroke of reflected pressure wave, and Pd is diastolic pressure. Δtp is roundtrip travel time of the forward wave from ascending aorta to major reflecting site and back. The shaded area represents the part of the respective wave that is reflected. SVr is the stroke volume associated with the reflected flow wave i.e. that would be ejected in a reflectionless system. (lower right) Venn diagram showing three components of afterload.

The assessment of arterial function has already been documented in mice and rats and is found to be affected by HTN [43,48,52]. Changes in arterial function also affect afterload which in turn is influenced by internal stresses (stress, viscous resistance, inertial components) and external vascular load (C, Z, R). In HTN, the impedence modulus is raised (Figure 11a) while in aging the arterial waveform is also modified (Figure 11b)[53,54].

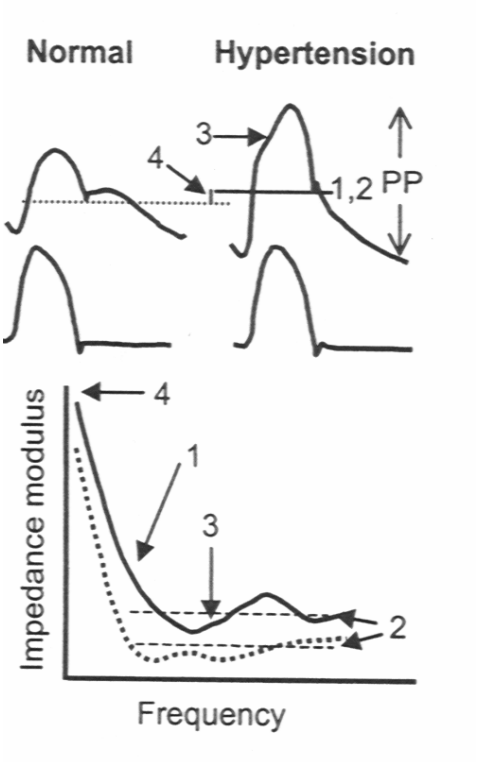

Figure 11a. In hypertension, R and MAP are increased (4). C drops resulting in a less rapid decrease in Z, with frequency, 1, and a higher Zc, 2. PP rises (1,2). Wave speed rises and Z oscillates around Zc (3), and the wave is augmented (3)

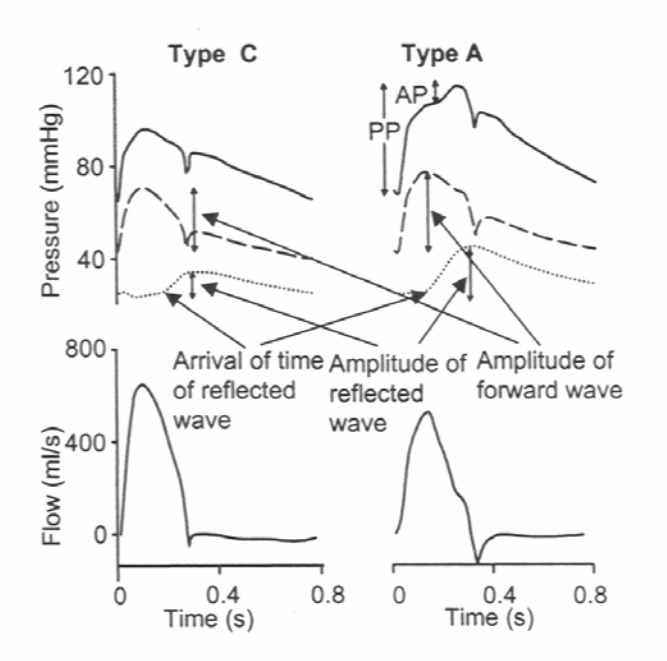

Figure 11b. Analysis of aortic pressure waves with their forward (dashed lines) and reflected, or backward waves (dotted lines). The type C beat pertains to young and the Type A beat to an old subject.

Wave reflection analysis. Aortic pressure, $P_{ao,}$ is separated into its forward (P_f) and backward (P_b) running components using the linear wave separation method [65]:

$$P_f = (P_{ao} + Z_c * Q_{ao})/2 \text{ and } P_b = (P_{ao} - Z_c * Q_{ao})/2$$

An example of the aortic pressure wave and its forward and backward (reflected) components is shown in figure 11b. The backward component is the sum of all reflected waves travelling towards the heart [65]. To characterize wave reflections, the reflection coefficient (Γ) was computed as [66]:

$$\Gamma = (Z_{in} - Z_c)/(Z_{in} + Z_c)$$

Γ is a frequency-dependent complex quantity. In order to facilitate comparison between pathologies one can compute and compare the modulus of the reflection coefficient at the 1st harmonic, $|\Gamma_1|$ which is assumed to be representative of the general wave reflection properties of the arterial tree. The time of the arrival of the foot of the reflected wave was defined as Δt (Figure 10). The shorter the Δt, the stronger the systolic pressure augmentation resulting from wave reflections.

The cushioning effect of arteries. The principal role of arteries as cushions is to dampen the pressure oscillations that are caused by the intermittent nature of ventricular ejection [36].

In performing this cushioning function, the arterial system is able to instantaneously accommodate the entire volume of blood ejected from the heart during systole. Arteries store part of the stroke volume during systolic ejection and drain it during diastole. This so called "Windkessel function" diminishes the pulsatility of the flow. Under normal conditions during systole, roughly 40% of stroke volume is forwarded directly to peripheral tissues, whereas the remainder (60%) is stored in the capacitive arteries (aorta and major arteries), distending the walls and storing part of the energy to be available during diastole (Figure 12). In diastole, the stored energy recoils the aorta, squeezing the stored blood forward into the peripheral circulation.

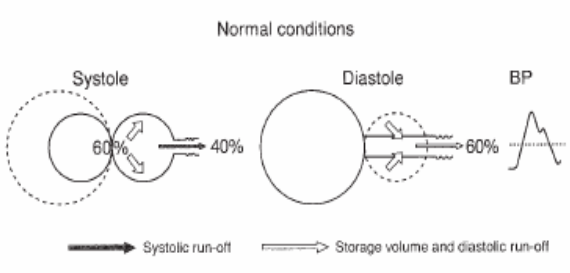

Diagrammatic representation of the cushioning effect of arteries on storage volume, systolic run-off, diastolic run-off, and arterial pulse wave. Normal conditions. *BP,* Blood pressure.

Figure 12

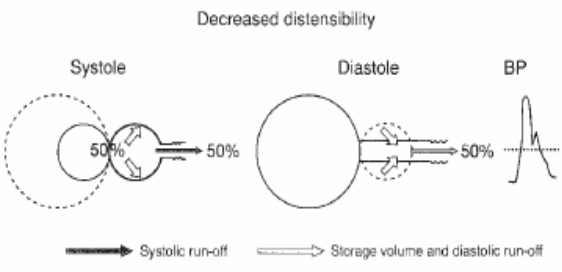

Diagrammatic representation of the cushioning effect of arteries on storage volume, systolic run-off, diastolic run-off, and arterial pulse wave. Conditions of decreased arterial distensibility. *BP,* Blood pressure.

Figure 13

When there is decreased arterial distensibility, a greater proportion of the stroke volume is forwarded to the peripheral circulation (50%), and less can be cushioned in the arterial bed during systole (50%)(Figure 13). Consequently, the amplitude of the arterial pulse wave and, inherently, systolic blood pressure, are increased. After the closure of the aortic valves, arterial pressure begins to fall as blood is drained to the peripheral arteries. The minimum diastolic blood pressure is determined by the duration of the diastolic interval (heart rate) and the rate at which the pressure falls. The rate of pressure fall is influenced by the rate of outflow (i.e., peripheral resistance) and by the compliance of the arterial tree, the product of the two defining the diastolic decay time. Consequently, at a given vascular resistance, the fall in diastolic blood pressure will also be greater if the stiffness of large arteries is increased.

In contrast, increased total peripheral resistance decreases systolic run-off (to perhaps 30% or less of stroke volume) so that a much higher proportion is stored in the capacitive arteries. Consequently, diastolic run-off is increased (70%), producing an elevation of mean blood pressure in parallel to an increase in pulse pressure (Figure 14).

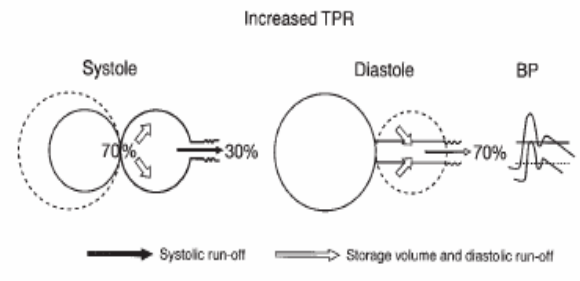

Diagrammatic representation of the cushioning effect of arteries on storage volume, systolic run-off, diastolic run-off, and arterial pulse wave. Conditions of increased total peripheral resistance. *BP*, Blood pressure; *TPR*, Total peripheral resistance.

Figure 14

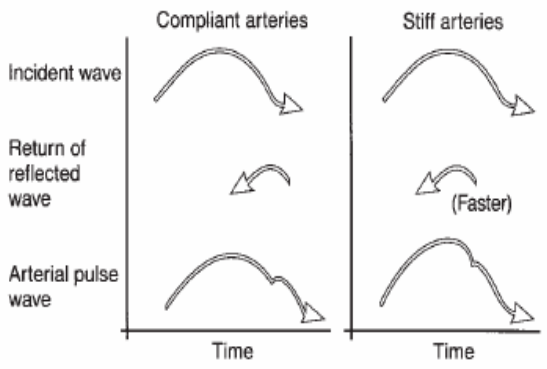

Diagrammatic representation of the effect of arterial compliance on the timing of pulse wave reflections and their effect on the arterial pulse wave.

Figure 15

The mechanical properties of arterial walls are also determinants of the propagation and reflection of pressure waves along the arteries. Ventricular ejection generates a primary (or incident) pressure wave that moves away from the heart at a finite speed, termed pulse wave

velocity, which increases with arterial stiffening. The incident wave is reflected at any point of structural or geometric discontinuity of the arterial tree, generating a reflected wave travelling backward toward the ascending aorta [34,36]. Thus stiffening of the arteries increases the pulse wave velocity and may be responsible for an earlier return of reflected waves. This means that reflected waves may return during the systolic phase rather than the diastolic phase, thus augmenting the systolic part of the incident pressure wave and contributing further to the increase in systolic blood pressure (Figure 15).

Interaction between heart and vessels: ventricular-arterial coupling

Arterial elastance (E_a) is calculated as the ratio of P_{es} divided by SV and the coupling parameter E_a/E_{es} is often computed as an indicator of ventricular-arterial coupling (Figure 16)[58]. Ventricular-arterial coupling is often judged upon optimal cardiac energetics, i.e., the ability of the heart to deliver optimal power or operate under maximal efficiency [65] characterized by the ratio of E_a/E_{es}. It has been suggested that the heart delivers maximum SW when E_a/E_{es} =1, whereas optimal efficiency is obtained when E_a/E_{es} =0.5 [11]. As the ratio augments above 1.3 and below 0.3, the SW and efficiency are both compromised [25] as observed in patients with severe cardiac dysfunction [3]. Efficiency, defined as the ratio of stroke work over pressure-volume area (stroke work plus potential energy) is calculated. Two other important ventricular-arterial coupling parameters are computed: first, the "Compliance Coupling Index, CCI" expressed as the product of characteristic chamber elastance (E_{es}xC), E_{es} being the inverse of ventricular compliance at end systole and C arterial compliance. Second, the "Temporal Coupling Index, TCI", expressed as the ratio of characteristic times (RC/T), T being the heart period and RC the characteristic diastolic pressure decay time which is a combination of the capacitive-resistive properties of the arterial tree [57].

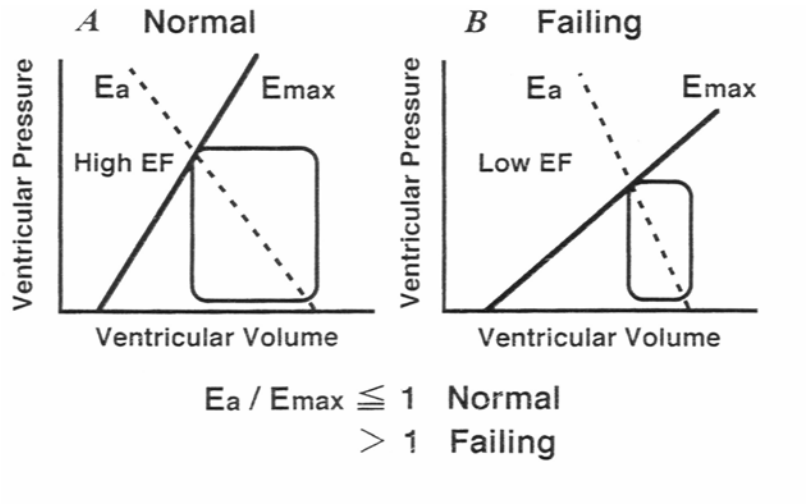

Figure 16. Ventriculo-arterial coupling in terms of Ea/Emax ratio. A: Ea/Emax ratio is comparable to 1 in normal hearts with a high EF. B: Ea/Emax ratio increases from 1 as heart failure proceeds with EF dropping.

Scope and overview of a novel model using MI and VDN

Most experimental models of hypertensive rats developed in the past were based on essential hypertensive principles and not on isolated systolic hypertension (ISH). Early reports of combined models of hypertension and MI were by Fletcher et al., who used spontaneously hypertensive rats (SHR) together with MI [14]. Others used renal hypertensive models [2,35], aortic banding [1] and Dahl salt-sensitive and salt-resistant rats [24]. Alternatively, a mechanical model in an acute setting was studied in dogs, whereby thoracic aorta was replaced by a plastic tube, to mimic severe aortic stiffening during the aging process [26].

The use of ISH together with MI has not been pursued in the cardiovascular research community, whereas, in reality, MI takes place often in aged individuals with stiff arterial trees and ISH. Thus, we found it to be instructive to develop a novel model of MI together with ISH using VDN. The following two hypotheses were central in defining the scope and focus of the thesis: We hypothesized that: 1) the effects of MI on cardiac function and transition towards HF may be enhanced/accelerated when in presence of a stiff arterial tree, 2) the combination of MI and ISH may represent a novel small animal model of HF that mimics the patho-physiological alterations found in clinical situations.

References

1. Anthonio RL, van Veldhuisen DJ, Scholtens E, van Bekkum C, de Boer E, van Gilst WH. Myocardial infarction with aortic banding. A combined rat model of heart failure. *Jpn Heart J* 1997;38:697-708.
2. Anversa P, Li P, ,Malhotra A, Zhang X, Herman MV, Capasso JM. Effects of hypertension and coronary constriction on cardiac function, morphology, and contractile proteins in rats. *Am J Physiol Heart Circ Physiol* 1993;265:H713-H724.
3. Asanoi H, Sasayama S, Kameyama T. Ventriculoarterial coupling in normal and failing heart in humans. *Circ Res* 1989;65:483-493.
4. Atkinson J. Arterial calcification: mechanisms, consequences and animal models. *Path Biol* 1999;47:677-684.
5. Baan J, van der Velde ET, de Bruin HG, Smeenk GJ, Koops J, van Dijk AD et al. Continuous measurement of left ventricular volume in animals and humans by conductance catheter. *Circulation* 1984;70:812-823.
6. Berne RM, Levy MN: Cardiovascular physiology, edn 3. St Louis:CV Mosby ;1977.
7. Boutouyrie P, Laurent S, Benetos A, Girerd XJ, Hoeks APG, Safar ME. Opposing effects of ageing on distal and proximal large arteries in hypertensives. *J Hypertens* 1992;10:S87-S91.
8. Boutouyrie P, Laurent S, Girerd XJ, Benetos A, Lacolley P, Abergel E, Safar ME. Common carotid artery stiffness and patterns of left ventricular hypertrophy in hypertensive patients. *Hypertension* 1995;25:651-659.
9. Boutouyrie P, Tropeano AI, Asmar R, Gautier I, Benetos A, Lacolley P, Laurent S. Aortic stiffness is an independent predictor of primary coronary events in hypertensive patients. A longitudinal study. *Hypertension* 2002;39:10-15.

10. Burkhoff D, Mirsky I, Suga H. Assessment of systolic and diastolic ventricular properties via pressure-volume analysis: a guide for clinical, translational, and basic researchers. *Am J Physiol Heart Circ Physiol* 2005;289:H501-H512.
11. Burkhoff D, Sagawa K. Ventricular efficiency predicted by an analytical model. *Am J Physiol Regulatory Integrative Comp Physiol* 1986;250:R1021-1027.
12. Cantini C, Kieffer P, Corman B, Limiñana P, Atkinson J, Lartaud-Idjouadiene I. Aminoguanidine and Aortic Wall Mechanics, Structure and Composition in Aged Rats. *Hypertension*. 2001;38:943-948.
13. Cantor EJF, Babick AP, Vasanji Z, Dhalla NS, Netticadan T. A comparative serial echocardiographic analysis of cardiac structure and function in rats subjected to pressure and volume overload. *J Mol Cell Cardiol* 2005;38:777-786.
14. Fletcher PJ, Pfeffer JM, Pfeffer MA, Braunwald E. Effects of hypertension on cardiac performance in rats with myocardial infarction. *Am J Cardiol* 1982;50:488-496
15. Franklin SS, Khan SA, Wong ND, Larson MG, Levy D. Is pulse pressure useful in predicting risk of coronary heart disease? The Framington heart study. *Circulation* 1999;100:354-60.
16. Grossman W, Carabello BA,. Gunther S, et al. Ventricular wall stress and the development of cardiac hypertrophy and failure. In *Perspectives in Cardiovascular Research. Myocardial hypertrophy and failure*, vol 7. Edited by Alpert NR. New York: Raven Press;1993:1-15.
17. Hanon O, Luong V, Mourad J, Bortolloto LA,Jeunemaitre X, Girerd X. Aging, carotid artery distensibility, and the Ser422Gly elastin gene polymorphism in humans. *Hypertension* 2001;38:1185-1189.
18. Hass GM, Trueheart RE, Taylor CB, Stumpe M. An experimental histologic study of hypervitaminosis D. *Am J Pathol* 1958;34:395-431.

19. Heyen JRR, Blasi ER, Nikula K, Rocha R, Daust HA, Frierdich G et al. Structural, functional, and molecular characterization of the SHHF model of heart failure. *Am J Physiol Heart Circ Physiol* 2002;283:H1775-H1784.
20. Ho KKL, Pinsky JL, Kannell WB, Levy D. The epidemiology of heart failure: The Framingham study. *J Am Coll Cardiol* 1993;22:6A-13A.
21. Ioannou CV, Stergiopulos N, Katsamouris AN, Startchik I, Kalangos A, Licker MJ, westerhof N, Morel DR. *Eur J Vasc Endovasc Surg* 2003;26:195-204.
22. Iwanaga Y, Hoshijima M, Gu Y, Iwatate M, Dieterle T, Ikeda Y et al. Chronic phospholambin inhibition prevents progressive cardiac dysfunction and pathological remodeling after infarction in rats. *J Clin Invest* 2004;113:727-736.
23. Jaeckel M, Simon G. Altered structure and reduced distensibility of arteries in Dahl salt –sensitive rats. *J Hypertens* 2003;21:311-9.
24. Jain M, Liao R, podesser BK, Ngoy S, Apstein CS, Eberli FR. Influence of gender on the response to hemodynamic overload after myocardial infarction. *Am J Physiol Heart Circ Physiol* 2002;283:H2544-H2550.
25. Kass DA. Age related changes in ventricular-arterial coupling: pathologic implications. *Heart Failure Reviews* 2002;7:51-62.
26. Kass DA, Saeki A, Tunin RS, Recchia FA. Adverse influence of systemic vascular stiffening on cardiac dysfunction and adaptation to acute coronary occlusion. *Circulation* 1996;93:1533-1541.
27. Kinnaird TD, Thompson CR, Munt BI. The deceleration time of pulmonary venous diastolic flow is more accurate than the pulmonary artery occlusion pressure in predicting left atrial pressure. *JACC* 2001;37:2025-30.

28. Lartaud-Idjouadiene I, Lompre A-M, Kieffer P, Colas T, Atkinson J. Cardiac consequences of prolonged exposure to an isolated increase in aortic stiffness. *Hypertension* 1999;34:63-69.
29. Lartaud-Idjouadiene I, Niederhoffer N, Debets JJM, Struijker-Boudier H, Atkinson J, Smits JFM. Cardiac function in a rat model of chronic aortic stiffness. *Am J Physiol Heart Circ Physiol* 1997;272:H2211-H2218.
30. Laurent S, Girerd X, Mourad J-J, Lacolley P, Beck L, Boutouyrie P, Mignot J-P, Safar M. Elastic modulus of the radial artery wall material is not increased in patients with essential hypertension. *Arteriosclerosis and Thrombosis* 1994;14:1223-1231.
31. Laurent S, Katsahian S, Fassot C, Tropeano A-I, Gautier I, Laloux B, Boutouyrie P. Aortic stiffness is an independent predictor of fatal stroke in essential hypertension. *Stroke* 2003;34:1203-1206.
32. Marque V, van Essen H, Struijker-Boudier H, Atkinson J, Lartaud-Idjouadiene I. Determination of aortic elastic modulus by pulse wave velocity and wall tracking in a rat model of aortic stiffness. *J Vasc Res* 2001;38:546-550.
33. Morgan EE, Faulx MD, McElfresh TA, Kung TA, Zawaneh MS, Stanley WC, Chandler MP, Hoit BD. Validation of echocardiographic methods for assessing left ventricular dysfunction in rats with myocardial infarction. *Am J Physiol Heart Circ Physiol* 2004;287:H2049-2053.
34. Murgo JP, Westerhof N, Giolma JP, Altobelli SA. Aortic input impedance in normal man: relationship to pressure wave forms. *Circulation* 1980;62:105-16.
35. Nass O, Yang X-P, Liu Y-H, Carretero OA, Khaja F, Goldstein S, Sabbah HN. Effects of pre-existing left ventricular hypertrophy on ventricular dysfunction and remodeling following myocardial infarction in rats. *J Heart Lung Transplant* 2002;21:1113-1119.

36. Nichols WW, O'Rourke M. McDonald's Blood flow in Arteries: Theoretical, experimental and clinical principles. 4th ed. London, Sydney, Auckland: Arnold, 1998:54-401.

37. Nichols WW, Singh BM. Augmentation index as a measure of peripheral vascular disease state. *Curr Opin Cardiol* 2002;17:543-551.

38. Niederhoffer N, Lartaud-Idjouadiene I, Giummelly P, Duvivier C, Peslin R, Atkinson J. Calcification of medial elastic fibres and aortic elasticity. *Hypertension* 1997;29:999-1006.

39. O'Rourke M. Second Workshop on structure and function of large arteries: Part I. Mechanical principles in arterial diseases. *Hypertension* 1995;26:2-9.

40. Pagliaro P, Senzaki H, Paolocci N, Isoda T, Sunagawa G, Recchia FA, Kass DA. Specificity of synergistic coronary flow enhancement by adenosine and pulsatile perfusion in the dog. *J Physiol* 1999;520:271-80.

41. Palojoki E, Saraste A, Eriksson A, Pulkki K, Kallajoki M, Voipio-Pulkki L-M et al. Cardiomyocyte apoptosis and ventricular remodeling after myocardial infarction in rats. *Am J Physiol Heart Circ Physiol* 2001;280:H2726-H2731.

42. Randall OS, van den Bos GC, Westerhof N. Systemic compliance: does it play a role in the genesis of essential hypertension? *Cardiovasc Res* 1984;18:455-62.

43. Reddy AK, Li Y-H, Pham TT, Ochoa LN, Trevino MT, Hartley CJ, Michael LH, Entman ML, Taffet GE. Measurement of aortic input impedence in mice: effect of age on aortic stiffness. *Am J Physiol Heart Circ Physiol* 2003;285:H1464-H1470.

44. Reffelmann T, Kloner RA. Transthoracic echocardiography in rats. *Basic Res Cardiol* 2003;98:275-284.

45. Roman MJ, Pickering TG, Schwartz JE, Pini R, Devereux RB. Relation of arterial structure and function to left ventricular geometric patterns in hypertensive adults. *J Am Coll Cardiol* 1996;28:751-6.

46. Roman MJ, Saba PS, Pini R, Spitzer M, Pickering TG, Rosen S, Alderman MH and Devereux RB. Parallel cardiac and vascular adaptation in hypertension. *Circulation* 1992;86:1909-1918.

47. Safar ME. Systolic blood pressure, pulse pressure and arterial stiffness as cardiovascular risk factors. *Curr Opin Nephrol Hypertens* 2001;10:257-261.

48. Safar ME, Laurent P. Pulse pressure and arterial stiffness in rats: comparison with humans. *Am J Physiol Heart Circ Physiol* 2003;285:H1363-H1369.

49. Safar M. E. and London G. M. (1994) The arterial system in human hypertension. In *Textbook of Hypertension,* (Edited by Swales J. D.) pp. 85-102.Blackwell Scientific, London.

50. Sagawa K, Maughan L, Suga H, Sunagawa K., 1988. Cardiac contraction and the pressure-volume relationship. Oxford Univ Press, New York.

51. Schertel ER. Assessment of left-ventricular function. *Thorac Cardiovasc Surg* 1998;46:248-254.

52. Segers P, Georgakopoulos D, Afansyeva M, Champio HC, Judge DP, Millar HD, Verdonck P, Kass DA, Stergiopulos N, Westerhof N. Conductance catheter-based assessment of arterial input impedance, arterial function and ventricular-vascular interaction in mice. *Am J Physiol Heart Circ Physiol* 2005;288:H1157–H1164.

53. Segers P, Stergiopulos N, Westerhof N. Quantification of the contribution of cardiac and arterial remodelling to hypertension. *Hypertension* 2000;36:760-765.

54. Segers P, Stergiopulos N, Westerhof N. Relation of effective arterial elastance to arterial system properties. *Am J Physiol Heart Circ Physiol* 2002;282:H1041-1046.

55. Slama M, Ahn J, Varagic J, Susic D, Frohlich ED. Long-term left ventricular echocardiographic follow-up of SHR and WKY rats: effects of hypertension and age. *Am J Physiol Heart Circ Physiol* 2004 ;286 :H181-185.

56. Stergiopulos N, Meister JJ, Westerhof N. Simple and accurate way for estimating total and segmental arterial compliance: the pulse pressure method. *Ann Biomed Eng* 1994;22:392–397.

57. Stergiopulos N, Meister JJ, Westerhof N. Determinants of stroke volume and systolic and diastolic aortic pressure. *Am J Physiol Heart Circ Physiol* 1996;270:H2050-9.

58. Suga H. Paul Dudley White International Lecture: Cardiac Performance as viewed through the Pressure-volume window. *Jpn Heart J* 1994;35:263-280.

59. Suga H. Global cardiac function: mechano-energetico-informatics. *J Biomechanics* 2003;36:713-20.

60. Suga H. Cardiac energetics: from Emax to pressure-volume area. *Clin Exp Pharm Physiol* 2003;30:580-585.

61. Suga H, Yamada O, Goto Y, Igarashi Y, Yasumura Y, Nozawa T. Reconsideration of normalization of Emax for heart size. *Heart and Vessels* 1986;2:67-73.

62. Tanaka N, Dalton N, Rockman HA, Pterson KL, Gottshall KR, Hunter JJ et al. Transthoracic echocardiography in models of cardiac disease in the mouse. *Circulation* 1996;94:1109-17.

63. Tei C. New non-invasive index for combined systolic and diastolic ventricular function. *J Cardiol* 1995;26:135.

64. Weber T, Auer J, O'Rourke MF, Kvas E, Lassnig E, Berent R, Eber B. Arterial stiffness, wave reflections, and the risk of coronary artery disease. *Circulation* 2004;109:184-189.

65. Westerhof N, Sipkema P, van den Bos CG, Elzinga G. Forward and backward waves in the arterial system. *Cardiovasc Res* 1972;6:648–656.

66. Westerhof N, Stergiopulos N, Noble M. Snapshots of Hemodynamics. Berlin: Springer, 2005:1-196.

PAPER 1

Effect of Heart Failure Post Myocardial Infarction on the Normalized Time-Varying Elastance Curve.

David Jegger[1,2], Ajit S Mallik[1], Mohammed Nasratullah[4], Xavier Jeanrenaud[4], Hendrik Tevaearai[3], Nico Westerhof[5], Ludwig K von Segesser[2], Nikolaos Stergiopulos[1].

Laboratory of Haemodynamics and Cardiovascular Technology, EPFL, Lausanne, Switzerland[1] 1015; Department of Cardiovascular Surgery, CHUV, Lausanne, Switzerland[2] 1011; Department of Cardiovascular Surgery, Inselspital, Bern, Switzerland[3] 3010; Department of Cardiology, CHUV, Lausanne, Switzerland[4] 1011; Laboratory for Physiology, Institute for Cardiovascular Research, VU University Medical Center, Amsterdam, Netherlands[5] 1081.

Submitted to: Heart and Vessels

Abstract

It has been suggested that the wave shape of the normalized time-varying elastance curve, $E_n(t_n)$, is conserved in different cardiac pathologies. We hypothesize that the shape of the $E_n(t_n)$ is conserved but that its slopes during systole and diastole as well as its end diastolic value differ quantitatively during heart failure provoked by myocardial infarction (MI).

Sprague-Dawley rats (n=7) were anesthetized with 3% Isofluorane and the left anterior descending coronary artery was ligated to provoke the MI. A sham operated control group (CTRL) (n=9) was treated without the infarction. Two months later, a Conductance catheter was inserted into the left ventricle. The ventricular pressure and volume were measured and the $E_n(t_n)$ derived. Preload recruitable stroke work (PRSW), ejection fraction (EF), end diastolic pressure (EDP), minimum (V_{min}) and maximum (V_{max}) LV volumes, relaxation

constant (tau), slope of the $E_n(t_n)$ during the Pre Ejection Period (PEP), Ejection time (ET) and Isovolumic relaxation (IVR) period and normalized minimum elastance (E^*_{min}) were analyzed and compared between the two groups.

Contraction and relaxation times were compromised in the MI group ($p<0.05$). PRSW and EF were reduced in the MI group ($p<0.05$). The EDP, V_{min} and V_{max} were enlarged in the MI group due to diastolic dysfunction and chamber dilatation ($p<0.05$). Tau increased in the MI group ($p<0.05$). The slope of the $E_n(t_n)$ curve during ET, IVR and the complete diastolic phase were different ($p<0.05$). Further, E^*_{min} was significantly augmented in the MI group.

We conclude that the $E_n(t_n)$ although similar in shape, differs quantitatively between normal and failing hearts provoked by MI.

Keyword: compliance, ischemia, contractility, ventricular function, hemodynamics, conductance volumetry

Introduction

Heart failure is the condition in which the heart cannot pump sufficient amounts of blood to sustain the body's metabolic needs and perfusion of vital organs [14]. It is therefore important to know what the pump function of the heart is in health and diseased states. One description of the heart's pump function is with the use of the End-Systolic Pressure-Volume Relation (ESPVR). At the basis of the ESPVR stands the varying elastance concept, whereby the time varying elastance, E(t), gives a time-domain description of the heart pump function [19].

The shape of the normalized time varying elastance curve ($E_n(t_n)$) has been shown to be similar in different animal species [4]. It has been reported that when E(t) is normalized with respect to peak value and peak time, the shape (wave form) of the $E_n(t_n)$ is independent of different cardiac pathologies, afterload, preload, and contractility [17]. We went about

testing whether the $E_n(t_n)$ is indeed independent of cardiac diseased state. For this purpose, we studied the infarcted rodent in terms of pressure-volume relation and derived the $E_n(t_n)$ for control (sham operated) rats and rats where failure is provoked by coronary artery ligation. To test this hypothesis, the normalized elastance values are compared between the control and MI group.

Materials and methods

Animals. Male Sprague-Dawley rats were purchased from Charles River Breeding Laboratories (France). They were maintained in temperature and humidity controlled rooms with typical light-dark cycle and given standard chow and tap water ad libitum. All rats were handled in accordance with the Guide for the Care and Use of Laboratory Animals published by the US National Institutes of Health (NIH Publication No. 85-23, revised 1996) and our Institutional Animal Care and Use Committee approved the protocol.

Experimental MI. The myocardially infarcted group (MI) consisted of Sprague-Dawley rats (n=7) with a body weight of 254±19g. The rodents were anesthetized with 3% Isofluorane (Forene, Abbott AG, Baar, Switzerland), intubated then ventilated with 100% oxygen at 60 cycles per minute with a tidal volume of 2ml (Harvard Apparatus Inc model 683, Holliston, Ma, USA) before the surgical procedure was performed. The rats were placed on a heating pad to maintain body temperature and disinfection performed of the thorax. A left thoracotomy was performed at the 3rd intercostal space to gain access to the heart. The pericardium was opened and the left anterior descending coronary artery was located, between the left atrium and the pulmonary artery, ligated with a 4.0 Polypropylene (Ethicon Somerville, NJ, USA) to provoke the MI. This was confirmed by a change of color of the left ventricle from red to a purplish/grey distal to the ligation.

The ribs were closed with 2-3 ligatures, a chest drained inserted to avoid any pneumothorax

and the muscles surrounding the rib cage were closed before the skin was closed. Analgesia was given (Pro-Dafalgan) in order to attenuate any pain ensued by the rodents due to the MI (20mg, Upsamedica SA, Baar, Switzerland). The anesthesia was gradually weaned and when the rat began to awaken and spontaneous breathing resumed, the intubation tube was removed. The rats were then returned to the animal house once complete recovery was observed. A similar sham operated control group (CTRL) (n=9) with the rodents weighing 238±7g was performed without the myocardial infarction.

Hemodynamic measurements and pressure-volume curves. Eight weeks after the initial operation the rats were again anaesthetized and intubated. The right neck region was disinfected to provide access to the carotid artery. The skin was opened and the right jugular vein and carotid artery were isolated. A conductance catheter (Aria®, Millar Instruments Inc, Texas, USA) was inserted into the left ventricle via the right carotid artery. Parallel conductance was measured after injection of 10% saline into the jugular vein using a 1ml syringe (20µL Natrium chloratum, Sintetica SA, Mendrisio, Switzerland) in accordance to the method by Baan et al [1]. Alpha was validated with trans-thoracic echocardiography and was found to be 3. An occlusion analysis was performed by temporarily occluding the inferior vena cava below the diaphragm via a mini laparotomy. Figure 1 (left) shows pressure-volume loops recorded during such an inferior vena cava occlusion for a control rat.

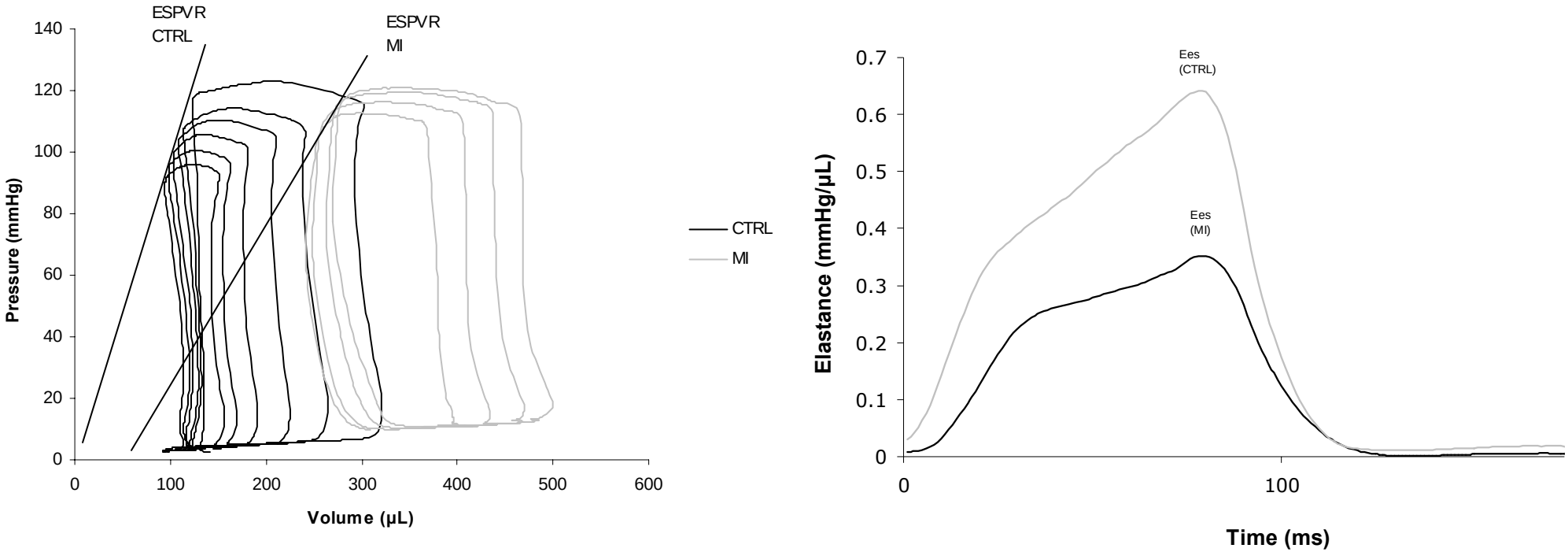

Figure 1 (left). Occlusion analysis compared between the CTRL (grey) and the MI group (black) showing elevated E_{min} (EDPVR) evident of raised EDP and a reduced SV because of HF with maintained E_{max} (ESPVR).

Figure 1 (right). The TVEC extrapolated from the occlusion analysis is visible above taken from a CTRL (grey) and MI (black) rat.

On the same graph are shown the End-Systolic Pressure-Volume Relationship (ESPVR) and End-Diastolic Pressure-Volume Relationship (EDPVR), which are assumed to be linear and whose slopes define the maximum (E_{max}) and minimum (E_{min}) elastance, respectively. E^*_{max} and E^*_{min} denote normalized values. The linear ESPVR intercepts the volume axis at V_0. Assuming that V_0 does not change during the heart cycle, we can define the instantaneous elastance, E(t) or TVEC as $E(t) = P_v/(V(t)-V_0)$. A typical waveform for the TVEC is shown in Figure 1 (right).

From steady state pressure-volume recordings we derived the following parameters: heart rate (HR), stroke volume (SV), cardiac output (CO), end systolic pressure (ESP), end diastolic pressure (EDP), end systolic volume (ESV), end diastolic volume (EDV), ejection fraction (EF), contraction time (duration of the isovolumic contraction), contraction index (maximum dP/dt divided by pressure at this point), and relaxation time (duration of the isovolumic relaxation) and Tau defined as the time required for LV pressure to decline 1/e or 37% of its value at dP/dt_{min}.

The following parameters were also derived from the pressure and volume data: Preload-Recruitable Stroke Work (PRSW), defined as the slope of the area of the pressure-volume loop vs. end diastolic volume (EDV), dP/dt_{max} and the preload adjusted dP/dt_{max} (dP/dt_{max} vs EDV), both used in the literature as indices of contractility [16].

Normalized time varying elastance curve. The normalized time varying elastance curve, $E_n(t_n)$, was obtained by way of $E^* = E/E_{max}$ and $t^* = t/t_{max}$ (*= normalized). A typical $E_n(t_n)$ is represented in Figure 2.

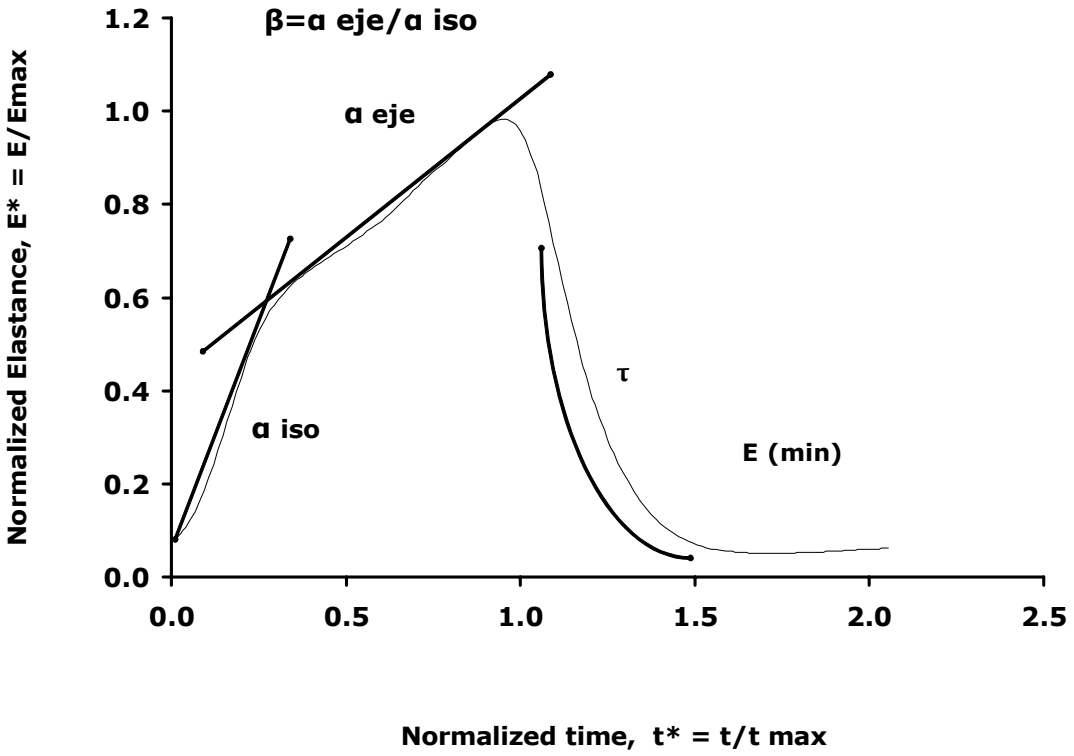

Figure 2. The $E_n(t_n)$ with the relevant slopes used for calculating α (iso), α (eje), the exponential decay time ($e^{-t/\tau}$) and E_{min}. The exponential decay time is not the same as tau calculated by the CC.

Comparison of the $E_n(t_n)$ curve between the CTRL and MI group is done at two levels. First, on a point-by-point basis, by comparing the values of the E* at the same nondimensional time t*, t* varying over the entire cardiac cycle at 0.1 intervals. Second, by comparing four different parameters characterizing the $E_n(t_n)$, namely a) the slope of the pre-ejection period (PEP), b) the slope of the ejection period (EP), c) the characteristic time of the exponential decay during early diastole and d) its end-diastolic value, E^*_{min}. These parameters are shown schematically in Figure 2. The PEP slope is denoted as α_{iso} and the ET slope as α_{eje}. The exponential decay time during early diastole ($e^{-t^*/\tau}$, $1.1 \leq t^* \geq 1.5$) was used to find the constant τ. The start of the PEP being the moment when LV dP/dt exceeds 30% of positive dP/dt_{max} to focus the linear part of E(t) during the isovolumic contraction phase. The end of

the PEP is defined as the moment when the steep rise of the aortic pressure begins. The end of the ET is defined as the time when dP/dt decreases to 20% of dP/dt_{min}.

Beta (β) was also derived and defined as the ratio of the two systolic slopes (α_{eje} /α_{iso}). The mean and SEM were calculated for each group and compared using an two tailed Student's t-test. Statistical significance considered when $p<0.05$(*) or $p<0.01$(†).

Results

Hemodynamic parameters. Hemodynamic parameters for the CTRL group and the MI group are shown in Table 1. Statistical significance at $p<0.05$ (*) and $p < 0.01$ (†) is also shown. Heart failure has caused the EDP to double and EDV increased by 33%, indicative of chamber dilation ($p<0.05$). SV decreased by approximately 30% ($p<0.05$) and ESV doubled ($p<0.01$). Ejection fraction decreased significantly, from 60% to 36% ($p<0.01$). Cardiac output decreased by 33% ($p<0.05$).

Heart rate, E_{max} and E_{min} were not different between the CTRL and the MI group (Table 1). Due to dilation, the intercept volume V_0 increased significantly ($p <0.01$) (Table 1). Despite a 10% decrease in the average value, dP/dt_{max} did not change significantly between the two groups. The slope of the dP/dt_{max}-EDV curve as well as Preload Recruitable Stroke Work, however, did decrease significantly in the MI group (Table 1). Contraction and relaxation times were prolonged and contractility index was reduced in the MI group by 21% as compared to the CTRL group ($p<0.01$ for all, Table 1).

Table 1.*Cardiac and arterial functional parameters processed from the conductance catheter. CTRL (Control group) and MI (Myocardial infarction group) with statistical significance considered when p<0.05* and p<0.01†.*

Contractile parameters

	E_{es} (mmHg/µL)	E_{min} (mmHg/µL)	E^*_{es} LV mass (mmHg/(µL/g))	E^*_{es} EDV (mmHg)	E^*_{es} BW (mmHg/µL/kg)	E^*_{min} LV mass (mmHg/µL/g)	E^*_{min} ESV (mmHg)	dP/dt max-EDV (mmHg/ms/µL)	PRSW (mmHg)	Contractility index (s^{-1})	dP/dt max (mmHg/ms)	dP/dt min (mmHg/ms)
CTRL	0.96±0.2	0.05±0.03	0.85±0.19	0.57±0.17	490±140	0.04±0.03	5.6±2.8	26.8±10.9	70±17	95.7±6.7	5128±1241	-4722±725
MI	0.99±0.2	0.08±0.12	1.10±0.24*	0.78±0.24*	490±240	0.07±0.09	18±15*	18.9±6.9*	50±17†	76.3±11.6†	4606±1407	-4406±1200

Volumetric parameters

Timing parameters

	SV (µL)	CO (ml/min)	EDV (µL)	ESV (µL)	EF (%)	Vo (µL)	SEP (ms)	DFP (ms)	ICT (ms)	IRT (ms)	Tau (ms)
CTRL	300±120	108±45	450±90	180±30	60.3±2.6	-76±74	51.3±8.2	60.9±12.7	17.4±1.0	46.4±0.6	6.0±0.3
MI	210±90*	72±33*	600±150*	390±180†	35.9±16.6†	54±92†	51.4±7.8	57.8±13.8	20.1±2.0†	53.6±5.1†	14.6±5.6†

Physiological parameters

Coupling parameters

	Body weight (kg)	LV mass (g)	LV mass/Body weight (g/kg)	Lung weight (g)	Heart weight (g)	P_{sys} (mmHg)	LVEDP (mmHg)	HR (bpm)	Ea	Ea/Ees
CTRL	0.48±0.03	0.85± 0.12	1.75±0.21	0.76±0.26	1.44±0.07	74.8±9.6	3.33±1.3	350±35	0.86±0.44	0.86±0.36
MI	0.42±0.03†	1.03±0.15†	2.51±0.52†	0.79±0.29	1.82±0.35†	79.1±12.2	7.14±3.2†	335±25	1.49±0.93*	1.37±0.85*

Normalized time varying elastance curve. The mean $E_n(t_n)$ for the two groups were compared at 10 time intervals over the cardiac cycle and statistical significance found at the intervals marked with an asterisk or a cross (Figure 3). Significant differences were found at the following points: start of PEP (*p<0.05), the main part of the Ejection period (*p<0.05), the end of the IVR phase (*p<0.05) and the complete diastolic period (†p<0.01) (Figure 3).

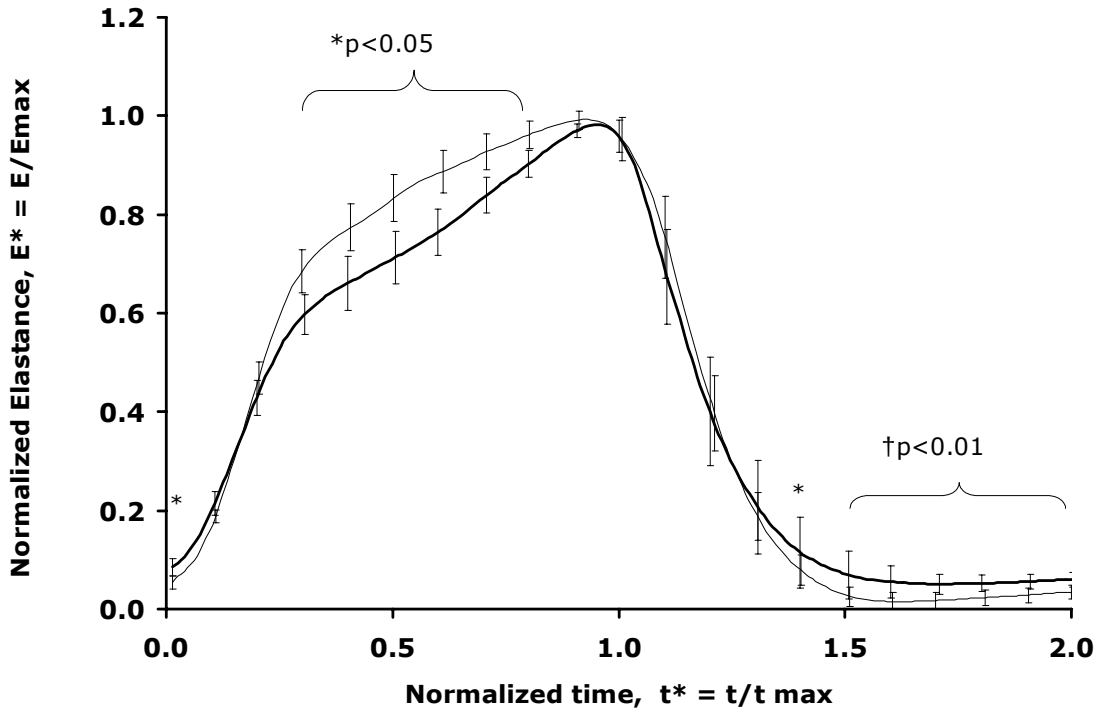

Figure 3. The $E_n(t_n)$ for the CTRL (fine line) and the MI (dark line) groups. Statistical significance of p<0.05 was observed at the start of the PEP, during the Ejection phase and at the 1,4 time interval. Statistical significance of p<0.01 was found during the complete diastolic period.

The slopes of the $E_n(t_n)$ during the pre-ejection period, $\alpha_{iso,}$ were 2.31±0.38 vs 1.84±0.28 for the CTRL and MI group, respectively, and are statistically significant (p<0.05) (Figure 4A). This suggests a reduced contractility in the early systolic phase in the MI group. The α_{eje} compared between the CTRL and the MI group was 0.40±0.17 vs 0.47±0.19, respectively, with no evidence of statistical significance (Figure 4B).

The τ constant derived from the exponential decay time ($e^{-t/\tau}$) was found to be 8.33±1.70ms vs 6.07±1.58msec for the CTRL and the MI group, respectively, the difference being statistically significant ($p<0.05$, Figure 4C). This indicates a quicker relaxation time in the CTRL group.

The normalized E_{min} for the CTRL and the MI group was 0.05±0.03 and 0.09±0.04, respectively, the difference being significant ($p<0.05$, Figure 4D).

Beta (β) was found to be 0.15±0.08 and 0.31±0.11 for the CTRL group and the MI group, respectively, with $p<0.05$* (Figure 4E).

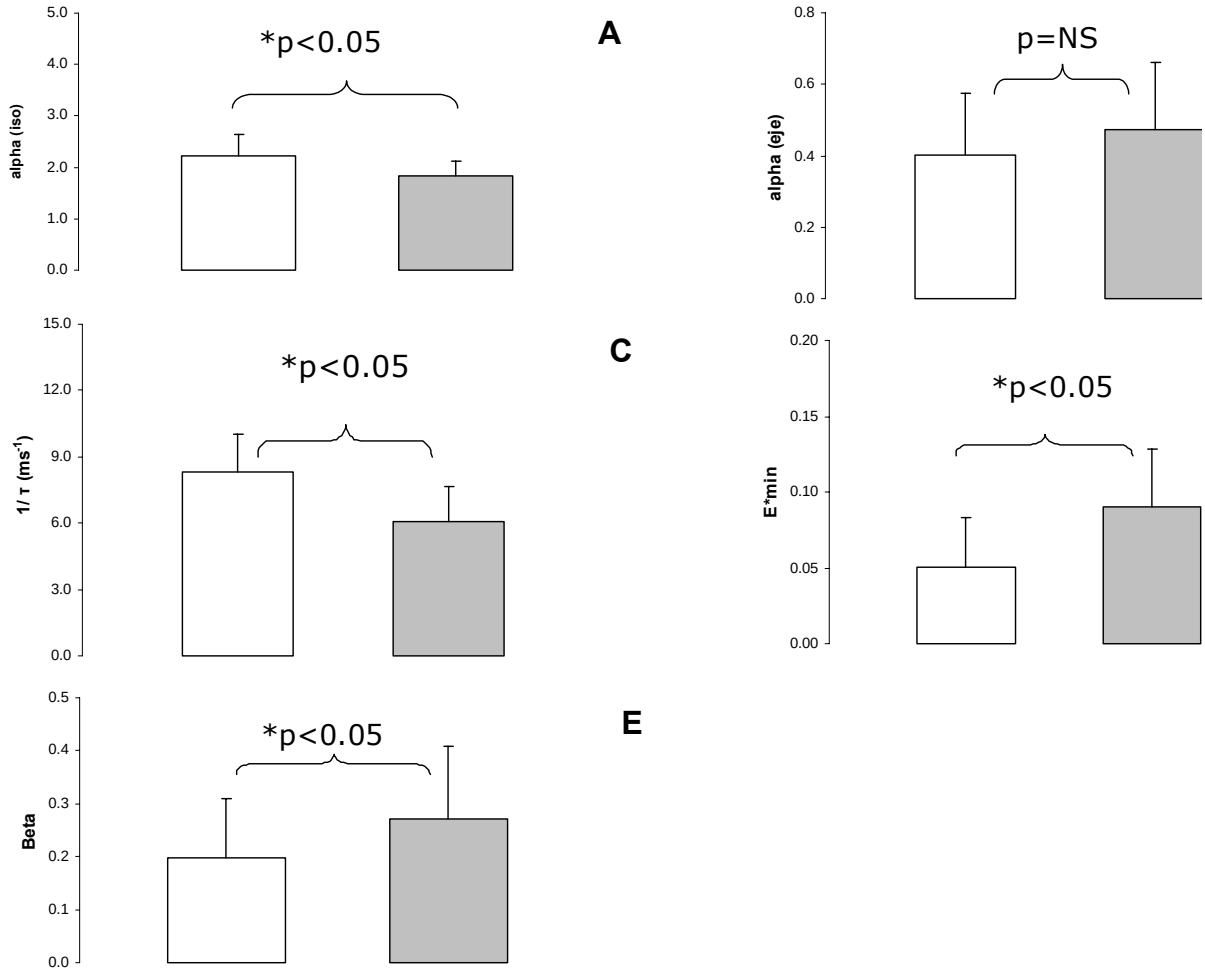

Figure 4. Comparison made between the CTRL (white) and the MI group (grey) with p<0.05.* ***Panel A*** *α (iso),* ***B*** *α (eje),* ***C*** *1/τ,* ***D*** E^*_{min} *and* ***E*** *Beta (β).*

Discussion

Main findings

We have found that the $E_n(t_n)$ although similar in shape, differs quantitatively between normal and failing rat hearts, after induced myocardial infarction. Differences in $E_n(t_n)$ were found during ejection, isovolumic relaxation and at end diastole (Figure 3). Also, there is a difference in the slope of the $E_n(t_n)$ at the PEP ($\alpha_{iso,}$ Figure 4A), in the decay of $E_n(t_n)$during the IVR phase (τ, Figure 4C), and at the ratio of PEP/ET slopes (ß, Figure 4E). The functional and dimensional parameters representative of cardiac function are altered due to the MI (Table 1).

The use of time-varying elastance for assessing cardiac function in health and disease

Cardiac function has here been evaluated using the Conductance catheter (CC)). The CC was first used by Baan in 1980 and has gained popularity as an accepted method to establish indices of cardiac contraction in rodent models and derived in the present study and as mentioned above [3,7,15]. Suga and colleagues have shown that the TVEC is fairly independent of loading conditions, contractile state and heart rate [19] However, subsequent studies revealed limitations to this simplified theory, such as ESPVR curvilinearity, afterload dependence under certain conditions and that V_o may change during contraction [10,15,18]. Further, the ESPVR has been reported to be influenced by regional ischemia in acute and chronic animal models of heart failure [6,13] and augmented in spontaneously hypertensive rats [2].

Uniqueness of the normalized time-varying elastance curve

Senzaki et al. have reported on human data and showed that the shape of the $E_n(t_n)$ is independent of different cardiac pathologies, afterload, preload, and contractility [17]. In a later study by the same group, Georgakopoulos et al. showed that the shape of the $E_n(t_n)$ is

identical in different animal species, the similarity in $E_n(t_n)$being attributed to small differences in myofibril protein isoforms and protein kinetics among species [4].

Assuming a unique $E_n(t_n)$, Senzaki et al. advocated the use of such a global $E_n(t_n)$ to derive ESPVR values from non-invasive single-beat recordings of ventricular pressures and volumes [17]. This could have potentially important clinical implications, because echocardiography could be used to estimate ventricular volume and peripheral arterial pressure for intraventricular systolic pressure, thereby providing a clinically feasible noninvasive estimate of cardiac contractility. Several other groups pursued this technique due to the fact that no vena cava occlusion is required and which makes feasible clinical applications [9,11]. A number of subsequent studies have shown, however, that the method proposed by Senzaki is not accurate or non-applicable. For example, Shisido et al. used a bilinear approximation for the time-varying elastance focusing primarily on the shape of the $E_n(t_n)$. The ratio of the two slopes, Beta, supposedly constant in a global $E_n(t_n)$, was found to correlate to EF, E_{max} and E_a [18]. Kjorstad et al. also found the concept of a global $E_n(t_n)$ inaccurate and the single-beat based method for deriving ESPVR imprecise and incapable of showing anticipated changes in contractility [8]. When scrutinizing Senzaki et al's results, one reveals large differences (standard deviations) on the $E_n(t_n)$, especially during the ejection and diastolic phases in the presence of aneurysms, dilated cardiomyopathy and coronary artery diseased (with conserved LV function) groups [17].

A more sensitive comparison of the $E_n(t_n)$ under different conditions and pathologies is obtained by looking at variations in the slope (time derivatives) of the $E_n(t_n)$ during different phases of the heart cycle (α_{iso} and α_{eje}). Obviously, time derivatives of the $E_n(t_n)$ (dE^*/dt) relate in a straightforward manner to time derivatives of the pressure (dP/dt) during the isovolumic contraction and relaxation phases, but the relation becomes more complex during ejection. The slope of $E_n(t_n)$ during the PEP phase (α_{iso}) decreased significantly in MI rats (Figure 4A).

In consequence, β rose in the MI group (Figure 4E). Shisido et al., who found that β was significantly attenuated during reduced contractility and vasoconstriction but augmented during vasodilatation [18]. Kjorstad et al. showed significant differences in β values between controls and postischemic groups. In the same study, during the administration of methoxamine, to augment afterload, the $E_n(t_n)$ was altered in shape especially during the ET and diastolic phases which we also found in the MI group (Figure 4) [18]. Hayashi et al used β and found the ratio E_{es}/E_a, proposed by Sunagawa, to correlate significantly and positively under various contractile and loading conditions [5,20]. The ratio E_a/E_{es} in our study was effectively >1 for the MI group (1.36±0.73) and < 1 for the Co group (0.92±0.36) though not statistically significant when compared between the two groups.

Validation of the MI-induced HF model

We have based our study on the $E_n(t_n)$ on a comparison between a CTRL and a MI-induced failing heart model. A number of parameters relating to cardiac geometry, systolic and diastolic function were measured to validate our heart failure model and similar geometrical findings were presented using MRI in a study by Nahrendorf et al. [12]. The failing hearts are dilated as seen by the increased V_{min} and V_{max} values ($p<0.05$ and 0.01 respectively, Table 1). SV is compromised while HR is maintained resulting in reduced CO, decreased EF, SV and PRSW also representative in our HF model (Table 1). In addition, there are changes in the diastolic portion of the pressure-volume relationship, namely an elevated EDP (Table 1), indicating the presence of combined systolic and diastolic heart failure [21].

dP/dt_{max} is compromised during HF which we advocate though not statistically significantly (Table 1). Nevertheless, when dP/dt_{max}–EDV is compared, a significant difference is established (Table 1).

PRSW is sensitive to contractility changes, such as those induced by MI, but insensitive to preload and afterload alterations. Thus, PRSW when compared to E_{max}, is more sensitive to

inotropic state, remains linear under most conditions and is independent of HR. When comparing the CTRL and MI groups, E_{max} was comparable but PRSW showed a significant difference with $p<0.01$ (Table 1). The HF model is also validated by a compromised contraction time and contractility index (Table 1).

During diastole, E^*_{min} was significantly greater in the MI group (Figure 4D) and therefore EDP rises as the ventricle goes into failure ($p<0.01$ and Table 1). Tau, the index of time constant of isovolumic LV pressure decline being an indicator of diastolic function is prolonged during MI (Table 1, $p<0.05$*) and advocated with our exponential decay time seen in Figure 4C. Tau and relaxation time are also significantly prolonged which supports the diastolic HF model ($p<0.01$, Table 1).

In conclusion, in our model of MI, cardiac function is compromised. The overall features of the $E_n(t_n)$ are qualitatively comparable between the CTRL and MI groups, however, when $E_n(t_n)$ is compared quantitatively between the two groups, statistical significance is found at the ejection phase and during diastole. Also, there is a difference in the slope of the $E_n(t_n)$ at the PEP (α_{iso}), at the IVR phase (τ), and at the ratio of PEP/ET slopes (β). These differences need to be taken into account when assessing cardiac contractility based on a generalized TVEC in different animal models or in the human in different physiological or pathological states.

Grants

This work was supported by an award from the Swiss National Research Foundation (3100AO-104257/1), Cardiovascular Scientific Foundation (Fonds Scientifique Cardiovasculaire), Swiss Life Anniversary Foundation for Public Health and Medical Research, Novartis Foundation for Medico-Biological Research.

References

1. Baan J, van der Velde ET, de Bruin HG, Smeenk GJ, Koops J, van Dijk AD, Temmerman D, Senden J, Buis B. Continuous measurement of left ventricular volume in animals and humans by conductance catheter. *Circulation* 1984;70:812-823.
2. Cingolani OH, Yang XP, Cavasin MA, Carretero OA. Increased Systolic Performance with diastolic dysfunction in adult spontaneously hypertensive rats. *Hypertension* 2003;41:249-254.
3. Feldman MD, Mao Y, Valvano JW, Pearce JA, Freeman GL. Development of a multifrequency conductance catheter based system to determine LV function in mice. *Am J Physiol Heart Circ Physiol* 2000;279:H1411-1420.
4. Georgakopoulos D, Mitzner WA, Chen CH, Byrne BJ, Millar HD, Hare JM, Kass D. In vivo murine left ventricular pressure-volume relations by miniaturized conductance micrometer. *Am J Physiol Heart Circ Physiol* 1998;274:H1416-H1422.
5. Hayashi K, Shigemi K, Shisido T, Sugimachi M, Sunagawa K. Single-beat estimation of ventricular end-systolic elastance-effective arterial elastance as an index of ventricular mechanoenergetic performance. *Anesthesiology* 2000;92:1769-76.
6. Huang Y, Hunyor SN, Jiang L, Kawaguchi O, Shirota K, Ikeda Y, Yuasa T, Gallagher G, Zeng B, Zheng X. Remodelling of the chronic severely failing ischemic sheep heart after coronary microembolization: functional, energetic, structural, and cellular responses. *Am J Physiol Heart Circ Physiol* 2004;286:H2141-H2150.
7. Ito H, Takaki M, Yamaguchi H, Tachibana H, Suga H. Left ventricular volumetric conductance catheter for rats. *Am J Physiol Heart Circ Physiol* 1996;39:H1509-1514.
8. Kjorstad KE, Korvald C, Myrmel T. Pressure-volume-based single-beat estimations cannot predict left ventricular contractility in vivo. *Am J Physiol Heart Circ Physiol* 2002;282:H1739-H1750.

9. Lee W-S, Nakayama M, Huang W-P, Chiou K-R, Wu C-C, Nevo E, Fetics B, Kass DA, Ding P Y-A, Chen C-H. Assessment of left ventricular end-systolic elastance from aortic pressure-left ventricular volume relations. *Heart Vessels* 2002;16:99-104.
10. Little WC, Freeman GL. Description of LV pressure-volume relationships by time-varying elastance and source resistance. *Am J Physiol Heart Circ Physiol* 1987;253:H83-90.
11. McKay RG, Aroesty JM, Heller GV, Royal HD, Warren SE, Grossmann W. Assessment of the end-systolic pressure-volume relationship in human beings with the use of a time-varying elastance model. *Circulation* 1986;74:97-104.
12. Nahrendorf M, Hu K, Fraccarollo D, Hiller K-H, Haase A, Bauer WR, Ert G. Time course of right ventricular remodeling in rats with experimental myocardial infarction. *Am J Physiol Heart Circ Physiol* 2003;284: H241–H248.
13. Nordhaug D, Steensrud T, korvald C, Aghajani E, Myrmel T. Preserved myocardial energetics in acute ischemic left ventricular failure – studies in an experimental pig model. *Eur J Cardiothorac Surg* 2002 ;22 :135-142.
14. Opie LH, Perlroth MG. Ventricular function. In: Opie LH, editor. Heart Physiology-from cell to circulation Lippincott Williams & Wilkins, 2004: 355-401.
15. Sato T, Shisido T, Hayashi K, Kawada T, Miyano H, Miyashita H, Inagaki M, Sugimachi M, Sunagawa K. ESPVR of in situ rat left ventricle shows contractility-dependent curvilinearity. *Am J Physiol Heart Circ Physiol* 1998;274:H1429-1434.
16. Schertel ER. Assessment of left-ventricular function. *Thorac Cardiovasc Surg* 1998;46:248-254.
17. Senzaki H; Chen C-H, Kass D. Single-Beat Estimation of End-Systolic Pressure-Volume Relation in Humans. *Circulation.* 1996;94:2497-2506.

18. Shisido T, Hayashi K, Shigemi K, Sato T, Sugimachi M, Sunagawa K. Single-Beat Estimation of End-Systolic elastance Using Bilinearly Approximated Time-Varying Elastance Curve. *Circulation* 2000;102:1983-1989.
19. Suga H. Paul Dudley White International Lecture: Cardiac Performance as viewed through the Pressure-volume window. *Jpn Heart J* 1994;35:263-280.
20. Sunagawa K, Maughan WL, Sagawa K. Effect of regional ischemia on the left ventricular end-systolic pressure-volume relationship of isolated canine hearts. *Circ Res* 1983;52:170-178.
21. Zile M, Baicu CF. Alterations in ventricular function: diastolic heart failure In: Mann DL, editor. Heart Failure: A companion to Braunwald's Heart disease. Saunders, 2004: 209-227.

PAPER 2

Noninvasive Doppler-derived myocardial performance index in rats with myocardial infarction: validation and correlation by conductance catheter.

David Jegger[1,2], Xavier Jeanrenaud[4], Mohammad Nasratullah[4], Pierre-Guy Chassot[5], Ajit Mallik[1], Hendrik Tevaearai[3], Ludwig K. von Segesser[2], Patrick Segers[6], Nikolaos Stergiopulos [1].

Laboratory of Haemodynamics and Cardiovascular Technology, EPFL, 1015 Lausanne, Switzerland[1]; Department of Cardiovascular Surgery, CHUV, 1011 Lausanne, Switzerland[2]; Department of Cardiovascular Surgery, Inselspital, 3000 Bern, Switzerland[3] ; Department of Cardiology, CHUV, 1011 Lausanne, Switzerland[4]; Department of Anaesthesiology, CHUV, 1011 Lausanne, Switzerland[5]; Hydraulics Laboratory, Institute of Biomedical Technology, Ghent University, 9000 Gent, Belgium[6].

Running head: Echocardiographic correlation with conductance catheter

***Am J Physiol Heart Circ Physiol* 290: H1540–H1548, 2006.**

Abstract

The rodent model of myocardial infarction (MI) is extensively used in heart failure (HF) studies. However, long term follow-up of echocardiographic left ventricular (LV) function parameters such as the myocardial performance index (MPI) and its ratio with the fractional shortening (LVFS/MPI), has not been validated in conjunction with invasive indices, such as those derived from the conductance catheter (CC).

Sprague-Dawley rats with LAD coronary artery ligation (MI group, n=9) were compared to a sham operated control group (CTRL group, n=10) without MI. TTE was performed every 2

weeks over an 8 week period, after which classical TTE parameters, specially MPI and LVFS/MPI were compared to invasive indexes obtained using a CC.

Serial TTE data showed significant alterations in the majority of the noninvasive functional and structural parameters (classic and novel) studied in the presence of MI. Both MPI and LVFS/MPI significantly (all reported values $p<0.05$) correlated with body weight ($r=-0.58$ and 0.76 for MPI and LVFS/MPI, respectively), preload recruitable stroke work ($r=-0.61$ and 0.63), LV end-diastolic pressure (LVEDP) ($r=0.82$ and -0.80), end-diastolic volume ($r=0.61$ and -0.58) and end-systolic volume ($r=0.46$ and -0.48). Forward stepwise linear regression analysis revealed that, of all variables tested, LVEDP was the only independent determinant of MPI ($r=0.84$) and LVFS/MPI ($r=0.83$).

We conclude that MPI and LVFS/MPI correlate strongly and better, than the classic noninvasive TTE parameters, with established invasively assessed indexes of contractility, preload and volumetry. These findings support the use of these two new noninvasive indexes for long-term analysis of the post-MI LV remodeling.

Keywords: echocardiography, heart failure, hemodynamics, infarction, ventricular function

Introduction

The understanding of the progressive structural and molecular cardiac changes following myocardial infarction (MI) is of major interest to the cardiovascular research community [11,24]. It may indeed contribute to the development of new therapeutic modalities for heart failure (HF) [17]. The changes in cardiac structure and function in the follow-up of MI can be assessed using different techniques, including both invasive (conductance catheter, CC) and non-invasive approaches (tran thoracic echocardiography, TTE) [2,27]. Among other advantages, the non-invasive echocardiographic methodologies are certainly appealing for long term follow-up protocols. In addition TTE is an established clinical diagnostic tool [22].

Several structural and functional parameters can be assessed using TTE such as myocardial wall thickness, end systolic and diastolic volumes, left ventricular (LV) mass, ejection fraction (EF), fractional shortening and velocity of circumferential fibre shortening. The myocardial performance index (MPI) is a relatively recent parameter combining both systolic and diastolic functions. MPI is the ratio of total time spent in isovolumic activity (isovolumic contraction and relaxation times) to the ejection time and is measured from the mitral inflow and LV outflow time intervals. Recently, in a clinical setting, the MPI has been described as a predictor of cardiovascular mortality, independent of other measurements of cardiac function (EF, wall motion score index) and of traditional cardiovascular risk factors (smoking, diabetes, hyperlipidemia and hypertension) in elderly men [1]. Additionally, it correlates to plasma Brain Natriuretic Peptide (BNP) in patients with hypertrophic cardiomyopathy [15]. It is an attractive parameter as it appears to be independent of the LV shape. Indeed, the measurement of the LV dimensions is not mandatory. It has been reported that MPI correlates with dP/dt_{max} and tau and is affected by the pre- and afterloads [3,13,14,29]. However, the MPI's preload-dependency reported by Moller et al. in patients without MI [13] could not be reproduced by Cheung et al. in a porcine model [6]. Nevertheless, its reliability has been proven clinically [18,19] as well as in large [12] and in small animal models of MI [14]. Furthermore, despite its increasing use, MPI has never been validated against established indices of systolic and diastolic function as assessed from pressure-volume data in chronic rodent models of MI. Only volumetric comparisons were reported [5,8] and only one study correlated MPI with certain CC parameters in a porcine model [12]. In a clinical setting, compared to other TTE parameters such as EF and E/A ratio (peak early diastolic filling velocity over peak filling velocity at atrial contraction), the MPI appears more representative and sensitive to functional changes provoked post MI [18,19]. Therefore, we thought it would be instructive to analyze in a follow-up study the possible

interest of this parameter to capture the LV structural and functional alterations occurring during the post-MI remodeling period.

Also, because the LV fractional shortening (LVFS) is an ejection phase index [3], we hypothesized that the ratio of these two parameters (LVFS/MPI) would be more sensitive to MI induced alterations of cardiac function as compared to MPI alone. Therefore, the aim of this study was to assess changes in MPI and the LVFS/MPI ratio in a rodent MI model and to correlate MPI as well as the related LVFS/MPI index to other invasive indices obtained by CC.

Material and methods

Animals. Male Sprague-Dawley rats were purchased from Charles River Breeding Laboratories (Lyon, France). They were maintained in temperature and humidity controlled rooms with typical light-dark cycle and given standard chow and tap water ad libitum. The investigation conforms to Guide for the Care and Use of Laboratory Animals published by the US National Institutes of Health (NIH Publication No. 85-23, revised 1996).

Experimental protocol. The rats in the MI group (n=9) had a body weight of 254±19g (mean ± standard deviation) and were anesthetized with Isofluorane (Forene, Abbott AG, Baar, Switzerland), intubated and ventilated with 100% oxygen at 60 cycles per minute with a tidal volume of 2ml (Harvard Apparatus Inc model 683, Holliston, Ma, USA) before the surgical procedure was performed. The rats were placed on a heating pad to maintain body temperature and disinfection was performed of the thorax. A left thoracotomy was performed at the 3rd intercostal space to gain access to the heart. The pericardium was opened and the left anterior descending coronary artery was located (between the left atrium and the pulmonary artery) and ligated with a 4.0 Polypropylene suture (Ethicon Somerville, NJ, USA) to provoke the MI, which was visually confirmed by a change of color of the left ventricle (LV) from red

to a purplish/grey distal to the ligation site. The ribs were closed with 2-3 ligatures, a chest drain inserted to avoid any pneumothorax and the muscles surrounding the rib cage were sutured together before the skin was closed. Analgesia was given (Pro-Dafalgan) in order to attenuate any pain ensued by the rodents due to the MI (Upsamedica SA, Baar, Switzerland). The anesthesia was gradually weaned and when the rat began to awaken and spontaneous breathing resumed, the intubation tube was removed. The rats were then returned to the animal house once complete recovery was observed. A sham operation was performed on a similar control group (CTRL) (n=10) with the rodents weighing 238±7g (mean ± standard deviation).

Invasive cardiac measurements with the conductance catheter. Eight weeks after the initial operation the rats were again anaesthetized and intubated. The right neck region was disinfected to provide access to the carotid artery. The skin was opened and the right jugular vein and carotid artery were isolated. A 2Fr conductance catheter (SPR 838 Aria®, Millar Instruments Inc, Texas, USA) was inserted into the left ventricle via the right carotid artery. Parallel conductance was measured after injection of 10% saline into the jugular vein using a 1ml syringe (20µL Natrium chloratum, Sintetica SA, Mendrisio, Switzerland) in accordance to the method by Baan et al. [2]. An occlusion analysis was performed by temporarily occluding the inferior vena cava below the diaphragm via a mini laparotomy. For each animal, the CC calibration correction factor alpha was assessed with the use of an ultrasonic flowmeter (Transonic, Ithaca NY, USA) placed around the ascending aorta.

From the simultaneous measurement of LV pressure and volume during steady state conditions, the following parameters were derived: Stroke Volume (SV_c), end-systolic volume (ESV_c), end-diastolic volume (EDV_c), ejection fraction ($EF_c = SV_c/EDV_c$), isovolumetric contraction time (ICT, duration of the isovolumic contraction), peak positive (dP/dt_{max}) and peak negative (dP/dt_{min}) value of the time-derivative of LV pressure, contractility index

(dP/dt_{max} divided by the pressure at this point), isovolumetric relaxation time (IRT, duration of the isovolumic relaxation), time constant of relaxation derived from the peak systolic pressure to the next begin of diastolic pressure (Tau), heart rate (HR), left ventricular end-diastolic (LVEDP) and begin diastolic pressures (LVBDP), taken as the pressures associated with the bottom left and right corner of the pressure-volume loop, respectively, systolic (LVSP) and end-systolic pressure (LVESP), systolic ejection period (SEP) and diastolic filling period (DFP). Cardiac output (CO_c) was calculated from HR multiplied by SV_c. The subscript 'c' refers to data measured with the conductance catheter in order to differentiate between the same parameters measured with TTE.

From the occlusion data, we calculated the slope (E_{es}) and volume axis intercept (V_0) of the end-systolic pressure-volume relationship (ESPVR), the slope of the end-diastolic pressure-volume relationship (EDPVR), preload-recruitable stroke work (PRSW) (with stroke work assessed from the area enclosed by the pressure-volume loop), preload adjusted dP/dt_{max} (slope of the relation between dP/dt_{max} and end diastolic volume (EDV_c)).

Echocardiographic measurements. TTE was performed at baseline and every two weeks for an eight week period with a commercially available echocardiographic system (C256 Sequoia, Acuson, Mountain View, CA, USA) with the animal in the left lateral decubitus position. Light anesthesia was used during the analysis with Isofluorane ventilated inside a nose-cone at 0.5l/min with 100% oxygen (Forene, Abbott AG, Baar, Switzerland). Once asleep, the rat was shaven with an electrical razor (Surgical clipper 9661, 3M health care, MN, USA). Ultrasound transonic blue gel (Tyco healthcare/Kendall, Mallinckrodt Dar, MO, Italy) was placed on the thorax to optimize visibility of the cardiac chambers. A 15MHz linear array transducer (15L8) was used with a frame rate of 100Hz using bidimensional and color Doppler imaging. The probe was placed to obtain short and long axis and four chamber views. From the long axis view, an M-mode trace of the LV was obtained, and LV end-

diastolic diameter (LVDed), LV systolic diameter (LVDes), and posterior and septal wall diastolic wall thickness (PWth and SWth) were measured. LV fractional shortening (LVFS) was calculated according to = (LVDed-LVDes)/LVDed x100. Ejection fraction was calculated from a long axis view using planimetry (EF_e) = 100*($LVDed^3$ –$LVDes^3$)/$LVDed^3$. Velocity of circumferential fiber shortening (Vcf) was calculated using the following formula (LVDed-LVDes)/(ET x LVDed). The subscript 'e' refers to data assessed with echocardiography. End diastolic volume (EDV_e) and end systolic volume (ESV_e) were calculated using the Simpson's method, and stroke volume SV_e was calculated as EDV_e-ESV_e. Aortic flow or cardiac output (CO_e) was recorded and calculated using pulse Doppler imaging, with the smallest possible sample volume placed at the level of the aortic annulus. Doppler yields the velocity profile (aortic velocity time integral (VTI)) which is multiplied with the cross sectional area of the outflow tract to obtain flow. Integration of the velocity profile yields the aortic velocity time integral. LV mass was calculated as = (((LVDed+SWth+PWth)^3 –$LVDed^3$)*1.04)*0.8+0.14 (in grams, with LV dimensions expressed in mm) [20]. Relative wall thickness was assessed as RWT = (PWth+SWth)/(LVDed). LV ejection time (ET) was measured as the time from the beginning to the end of the aortic flow wave (Figure 1). Isovolumic relaxation time (IRT) was measured as the interval between the aortic closure click and the start of mitral flow, while isovolumic contraction time (ICT) was obtained as the time delay between the cessation of mitral inflow and the onset of aortic ejection. Additionally, the mitral valve closure time (MCO) was measured. MPI is then defined as (MCO-ET)/ET = (ICT+IRT)/ET (Figure 1). A newer index of LV function, proposed by Broberg et al., LVFS/MPI, was also assessed [3].

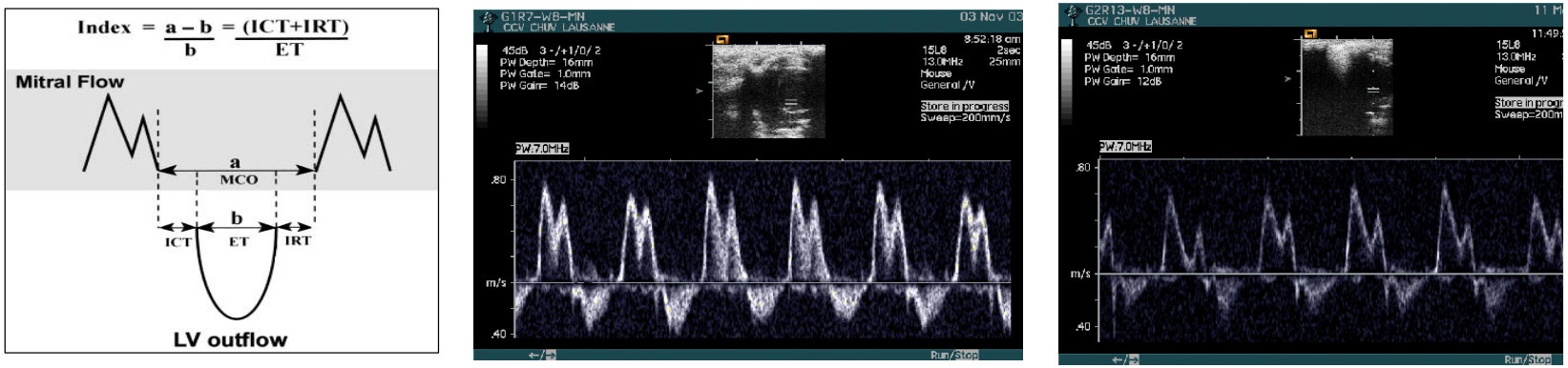

A B C

Figure 1. Panel A shows schematic representation of mitral inflow and left ventricular (LV) outflow obtained from pulsed-wave Doppler and used to calculate the myocardial performance index whose formula is shown on the top of Panel A. ICT, isovolumic contraction time; IRT, isovolumic relaxation time; ET, ejection time; MCO, time from closure until opening of the mitral valve; a, the sum of the isovolumic contraction time, ejection time, and isovolumic relaxation time; b, ejection time. Panels B and C show typical transmitral flow images in control (B) and MI (C).

Statistical analysis. TTE was performed three times on each rat and measurements were averaged. Values are reported as means ± SD. Echocardiographic follow-up data were analyzed using a general linear model of repeated measurements ANOVA, with time as within-subjects factor, and group (MI or control) as between subject's factor. At each instant in time, values were considered different between groups if statistical significance reached $p<0.05$. If the ANOVA test indicated an effect of time within one of the groups, paired t-tests were performed, with baseline data as fixed control. P-values <0.05 were considered significant. The MPI and LVFS/MPI were correlated with TTE and the CC measurements of LV systolic and diastolic function using a Pearson product moment correlation, in as much as data were normally distributed, with relations considered significant when reaching $*p<0.05$. Correlations were performed with the pooled data and then with the two groups separated. Forward stepwise regression analysis was performed for MPI and LVFS/MPI (dependent variable) with all aforementioned conductance catheter and TTE derived parameters as independent variables. All analysis was done in SPSS (SPSS 11.5, SPSS Inc, Chicago, IL, USA). A Bland-Altman analysis was performed between the CC and TTE data for SV, ESV, EDV, EF and MPI, using the data measured at week 8, to compare the compatibility in ventricular volumes as measured by the noninvasive (TTE) and invasive (CC) techniques.

Results

Hemodynamics assessed with the Conductance Catheter (volumetric data with subscript c). ESV_c and EDV_c rose significantly in the MI group as compared to the CTRL group. V_0 also increased significantly. The evolution of the heart failure caused the LVEDP to rise significantly (Table 1).

*Table 1. Comparison between the two groups for different invasive indices analyzed at sacrifice with the conductance catheter. Ejection fraction (EF_c), preload recruitable stroke work (PRSW), left ventricular end-diastolic pressure (LVEDP), left ventricular begin diastolic pressure (LVBDP), volume axis intercept (V_0), isovolumic relaxation time (IRT), isovolumic contraction time (ICT), contractility index (CI), left ventricular end-systolic pressure (LVESP), end systolic elastance normalized to LV mass (E^*_{es} LV mass) and cardiac output (CO_c). See Figure 3 legends for other abbreviations. *p<0.05, †p<0.01 CTRL vs MI at same age.*

	Parameters	Control Group	MI Group
LV pressures and volumes	EDV_c (ml)	0.52±0.10	0.75±0.15*
	ESV_c (ml)	0.15±0.07	0.56±0.14*
	SV_c (ml)	0.35±0.07	0.25±0.05
	V_0 (mL)	0.155±0.039	0.254±0.092*
	LVESP (mmHg)	90±20	93±16
	LVEDP (mmHg)	5.7±2.1	9.8±1.9†
	LVBDP (mmHg)	6.4±14.2	8.6±4.9
Isovolumic contraction phase indices	dP/dt_{max} (mmHg/ms)	5128±1241	4606±1407
	dP/dt_{max} - EDV_c (mmHg/s/µL)	25.8±11.2	20.5±7.0*
	CI (s^{-1})	95.7±6.7	76.3±11.6*
	ICT (ms)	17.6±2.4	20.2±1.8*
Contractile indices	E^*_{es} LV mass (mmHg/(µL/g))	0.85±0.19	1.10±0.24*
	PRSW (mmHg)	69.8±17.2	50.1±16.6*
Ejection phase indices	EF_c (%)	54.2±15.4	36.1±14.3*
	CO_c (ml/min)	108±45	72±33*
Active phase of relaxation indices	Tau (ms)	12.2±11.3	17.3±6.8*
	dP/dt_{min} (mmHg/ms)	-4722±475	-4406±1200
	IRT (ms)	46.4±4.7	53.6±5.1*

The $dP/dt_{max,}$ dP/dt_{max}-$EDV_{c,}$ contractility index and contraction time were all altered in the MI group. The slope of the ESPVR, E_{es}, was similar in both groups, though the ESPVR in the MI group did shift notably to the right thus raising the V_0 values. However, E_{es} normalized to LV mass decreased in the MI group. Also, the PRSW and SV_c were compromised in the MI group. EF_c and CO_c decreased significantly in the MI group (Table 1). Tau increased in the MI group. The IRT was significantly prolonged in the MI group. dP/dt_{min} was augmented by 10% in the MI group (p=NS, Table 1).

Echocardiography (volumetric data with subscript e) and serial follow-up data.

Body weight increased with age in both groups but remained significantly lower in the MI group (Figure 2A). LV mass increased with age in both groups however, after 8 weeks absolute LV mass was higher in the MI group (0.98±0.11g (CTRL) vs 1.29±0.10g (MI), $p<0.01$). The same applied for LV weight/body weight ratio being 1.70±0.20g/kg (CTRL) vs 2.45±0.45g/kg (MI) ($p<0.01$). The HR was comparable between the CTRL and MI groups being 318±29 beats/min and 319±29 beats/min, respectively, at week 8.

The EF_e was comparable at baseline but decreased significantly in the MI group (Figure 2H). The DV_e and ESV_e were significantly greater in the MI group versus the CTRL group (Figure 2B, C). The SV_e decreased significantly in the MI group (Figure 3D).

RWT and LVFS attenuated in the MI group but remained stable in the CTRL group (Figure 2E,). Vcf rose slightly in the CTRL group but was conserved in the MI group (Figure 2G). CO_e was significantly less in the MI group ($p<0.05$) at week 8 (89±14ml/min (MI) vs 112±20ml/min (CTRL)).

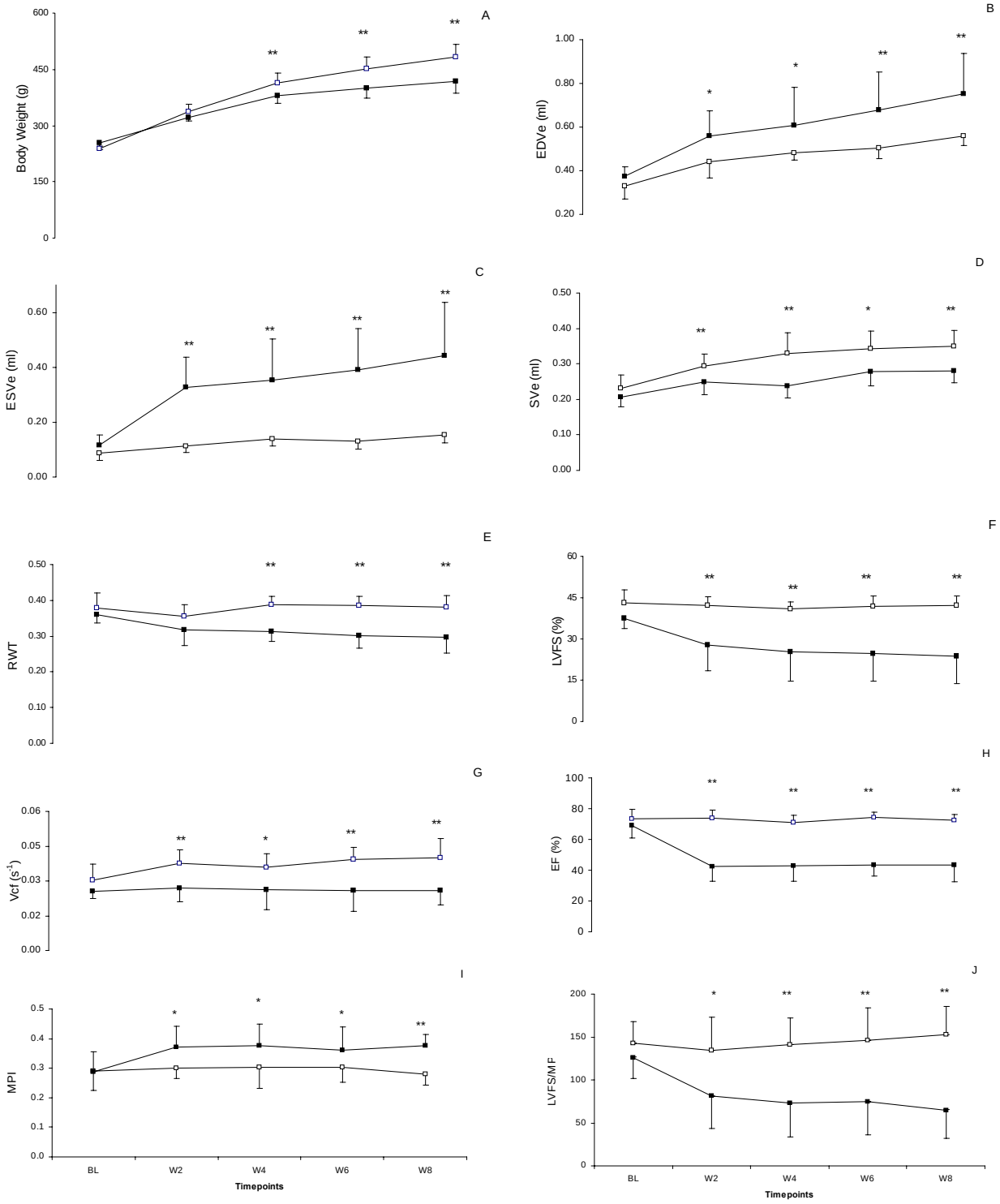

*Figure 2. Echocardiographic measurements from baseline (BL) to week (W) eight with ■ = MI and □ = control. Panel A: Body weight (BW, Panel A), End-diastolic volume (EDV_e, Panel B), end-systolic volume (ESV_e, Panel C), stroke volume (SV_e, Panel D), Relative wall thickness (RWT, Panel E), Left ventricular fractional shortening (LVFS in %, Panel F), Velocity of circumferential fibre shortening (Vcf in s^{-1}, Panel G:), Ejection fraction (EF in %, Panel H), Myocardial performance index (MPI, Panel I:), LVFS/MPI (Panel J). Statistical significance expressed as *p<0.05 and **p<0.001.*

MPI and valve opening and closure timing parameters. The ICT was stable in the CTRL group but was prolonged in the MI group. The IRT was not different between groups but did rise in the MI group when compared to baseline at week 6 and 8 ($p<0.001$). ET remained stable over time without any relevant difference between the groups. Consequently, the MPI increased significantly in the MI group when compared to the CTRL group (Figure 2I). LVFS/MPI decreased significantly in the MI group as compared to the CTRL group (Figure 2J).

Correlation of invasive parameters versus MPI and LVFS/MPI (pooled data). In the univariate correlation analysis, both MPI and LVFS/MPI were significantly correlated with body weight, LVEDP, PRSW, EDV and ESV (Table 2).

*Table 2. Correlation coefficients (r) and statistical significance (expressed as *p<0.05 and †p<0.01) of MPI, LVFS/MPI, LVFS, EF, Vcf and RWT versus CC parameters for the combined groups using univariate regression analysis. See Figure 2 and Table 1 legends for abbreviations.*

		TTE Parameters					
		MPI	LVFS/MPI	LVFS	EF	Vcf	RWT
	Body Weight	-0.58†	0.76†	0.82†	0.79†	0.86†	0.54*
CC parameters	PRSW	-0.61†	0.63†	0.54*	0.58*		0.58*
	LVEDP	0.82†	-0.80†	-0.68†	-0.67*	-0.46*	-0.78†
	EDV	0.61†	-0.58†	-0.55*	-0.64*		-0.62*
	ESV	0.46*	-0.48*	-0.58*	-0.70†		-0.76†

Forward stepwise linear regression analysis revealed that, of all the variables tested, LVEDP was the only independent determinant of MPI (R^2=0.70, p<0.0001) and of LVFS/MPI (R^2=0.68, p<0.0001).

Correlation of invasive parameters versus MPI and LVFS/MPI (groups separated). From the above pooled data, the two groups were separated and univariate regression analysis was applied. The corresponding graphs, with the linear regressions and correlation coefficients are shown in Figure 3. For the majority of the parameters, the regression lines of the pooled data and of the separated groups are almost identical or similar. Overall, the correlation coefficients based on the pooled data were comparable to those derived from the separate groups (Figure 3 and Table 2).

Invasive versus non-invasive assessment of ventricular volume, MPI and EF (Bland-Altman analysis). The average difference found for the EDV was 0.03±0.05ml (Figure 4 A), for ESV was -0.04±0.03ml (Figure 4 B), for SV was 0.003±0.02ml (Figure 4 C), for EF was 5.8±5.4% (Figure 4 D) and for MPI was 0.007±0.02 (Figure 4E). The correlation coefficients for ESV, EDV, SV, EF and MPI when absolute values were compared between TTE and CC were found to be 0.92, 0.98, 0.92, 0.95, and 0.85 respectively (all p<0.05). The mean alpha value used for the volume correction was 2.5±0.8.

Intra- and interobserver variability. Intra- and interobserver differences were 5.1±2.1% and 4.4±7.7% for LVFS, 6.5±5.8% and 5.8±7.7% for EF, 6.8±3.6% and 6.8±8.8% for Vcf, and 9.6±1.9% and 7.0±5.0% for MPI, respectively.

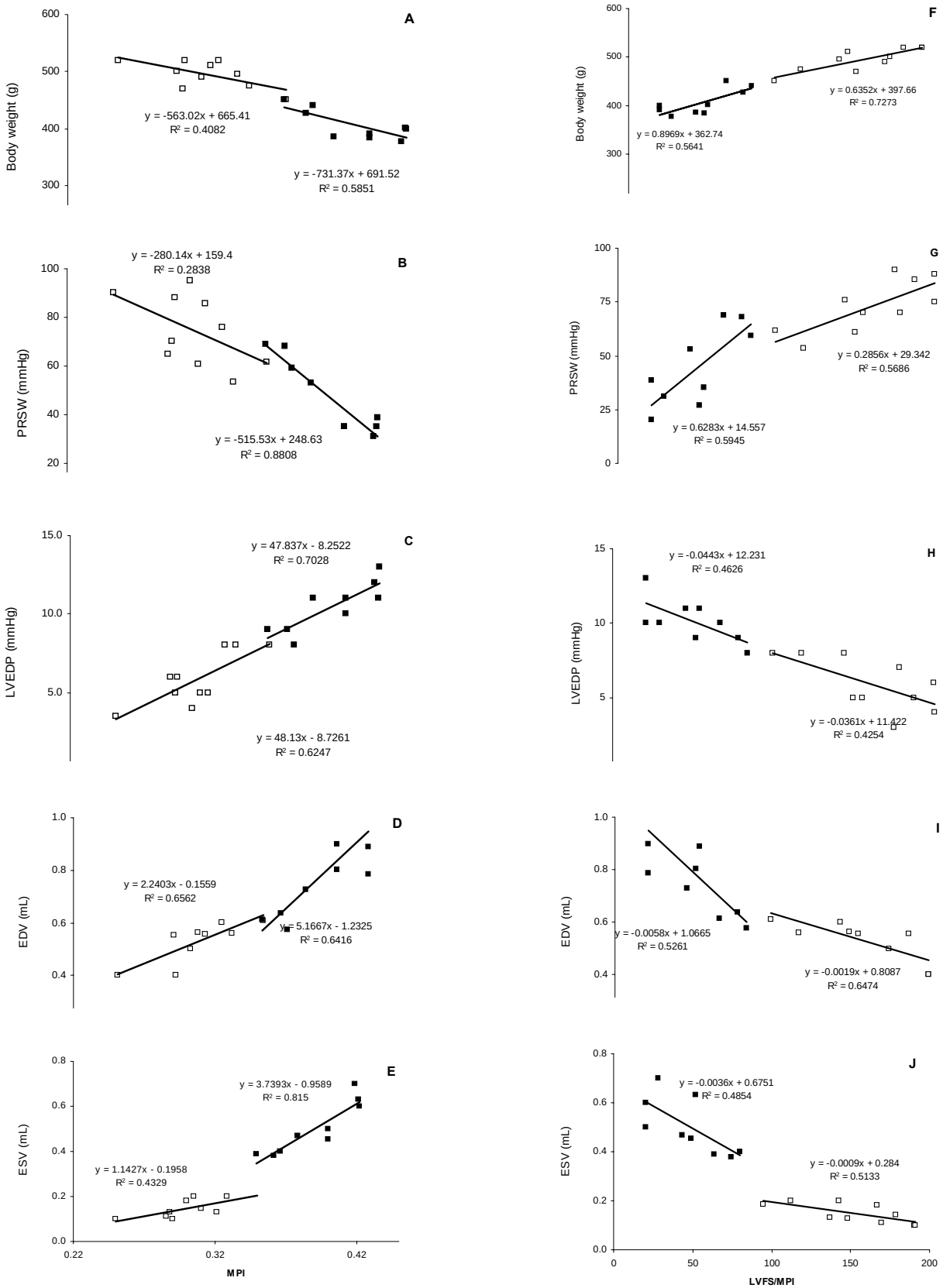

Figure 3. Correlation coefficients (R^2) of CC parameters versus MPI, LVFS/MPI for the CTRL and MI groups using univariate regression analysis. See Figure 2 and Table 1 legends for abbreviations.

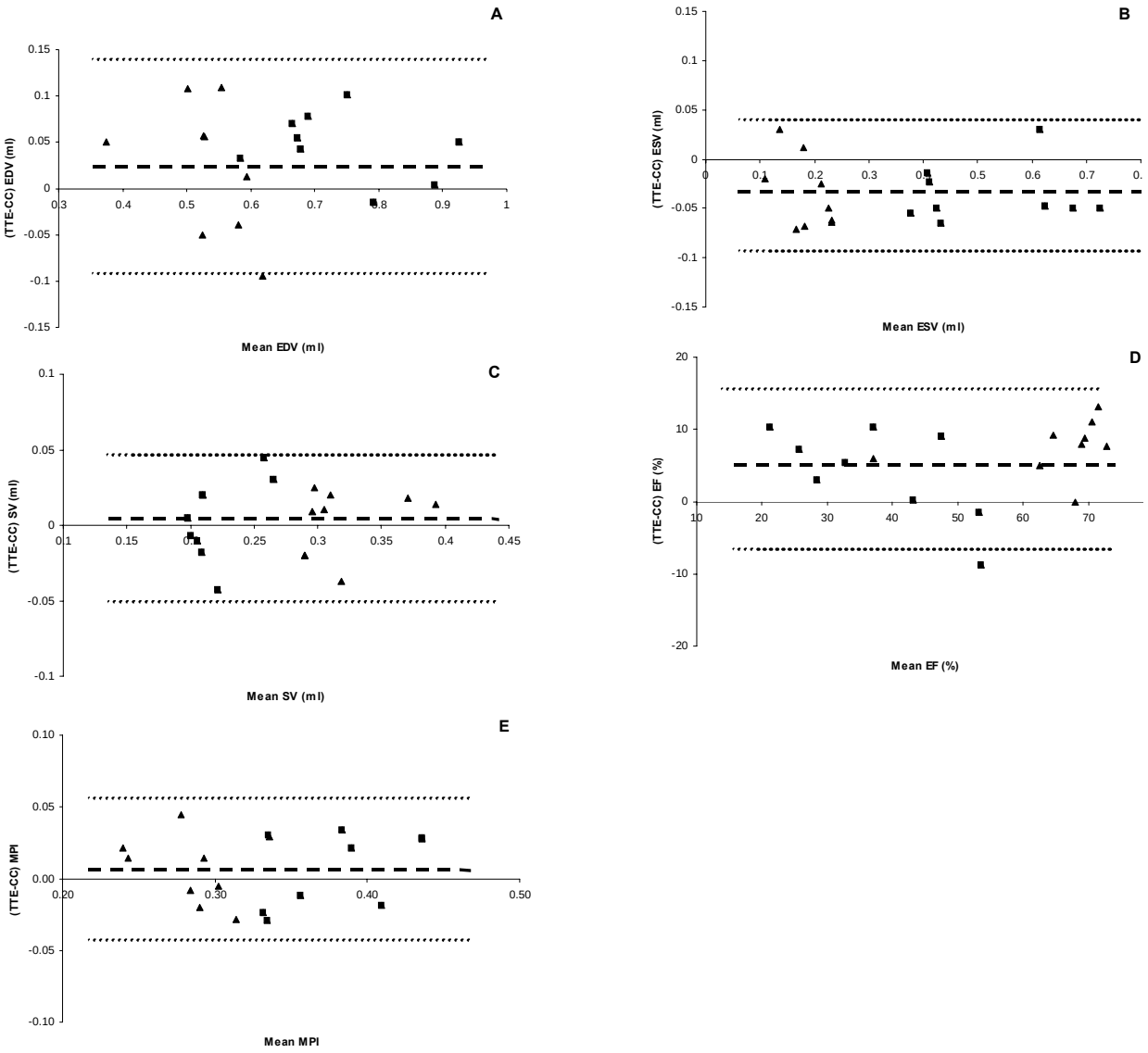

Figure 4. Bland-Altman analysis of EDV (A), ESV (B), SV (C), EF (D) and MPI (E), measured by TTE and CC at week 8 for the control and MI groups. CTRL rats represented by black triangles and MI rats by black squares. The y-axis presents the differences between the two measuring techniques. The x-axis represents the mean values of the two measuring techniques. Dashed lines indicate mean differences; dotted lines indicate boundaries of two standard deviations of the differences.

Discussion

We evaluated the adaptation response and long term effects of MI on cardiac function using TTE in rodents and after 8 weeks compared these data with invasively measured indices

of ventricular function. A number of classic and newly proposed parameters (MPI and LVFS/MPI) derived noninvasively from TTE were computed and reported. These changes post MI were profound and easily detectable by the different noninvasive indices, including the two newly proposed ones. More so, significant correlations were established between the new and classic noninvasive and established invasive parameters (PRSW, LVEDP, EDV and ESV) of ventricular function. The best and most significant correlation coefficients were established between the two new parameters and PRSW and LVEDP. EDV expressed similar correlation coefficients compared to the classic TTE parameters while ESV showed the lowest correlation, however still significant. Therefore, MPI and LVFS/MPI reflect well the changes post MI in contractility (PRSW), preload (LVEDP) and volumetry (EDV, ESV).

Serial assessment of cardiac function. Classically, EF, RWT, LVFS and Vcf are used to evaluate systolic function with TTE in rat models of pressure and volume overload [4,10,26]. In a rodent study with MI by Sjaarstad et al., body weight, LVFS, Vcf and CO were all compromised due to MI [24]. Gao et al. performed TTE in mice, demonstrating that the LVFS remains constant over time in control mice but attenuates with time in a model of MI [9]. In our study, all of the above parameters and MPI and LVFS/MPI were significantly compromised over time due to the MI (Figure 2A, F and G). However, some of the above parameters have certain limitations; LVFS and Vcf are preload and afterload dependent and are limited by spatial resolution; while EF is frame rate dependent and assumes symmetrical contraction, which is not the case in aneurysmal and MI hearts. RWT is only useful in studies measuring myocardial wall adaptations due to hypertensive response [10]. If used in MI models with an apical infarction present, but M-mode measured at the papillary muscle level, values will be falsely positive as the MI would cause wall thinning at the apex. However, in our study all MI's were antero-apical precluding this phenomenon. Therefore, the MPI and recently LVFS/MPI [3], were introduced as they have been reported to be independent of load

and LV geometry [3,29]. Slama and Salemi et al. have reported the MPI in conjunction with serial studies, but only in hypertensive models [23,26]. In our study, these two novel parameters fair well compared to the classic TTE parameters reported above (Figure 2). More so, the LVFS/MPI seems to visually express alterations in cardiac function post MI more clearly, compared to the classic ones, in spite of the large standard deviations (Figure 2J). These deviations are as a result of the fact that the infarct size in the MI model is difficult to homogenize and vary between 37±7%, not forgetting the variations of intra and inter observer variability. Also, it should be acknowledged that MPI is highly dependent on timing intervals and temporal resolution and hence susceptible to interpretation errors in cases when heart rate changes over time during the experimental procedure.

Noninvasive versus invasive assessment of cardiac function. We measured cardiac function using both TTE echocardiography and CC in the same animal, allowing us to correlate findings from both techniques. Hence, the relation between classic (EF, LVFS, Vcf and RWT) and novel indices such as MPI and LVFS/MPI, and established invasive cardiac function parameters, could be derived (Table 2). The MPI and LVFS/MPI express the largest correlation coefficients and most significant for PRSW and LVEDP compared to the classic ones. Similar coefficient values are found between classic and novel indices with respect to EDV. However, ESV shows the smallest relationship for the novel indices, none the less still significantly comparable. LVFS correlated well to the invasive indices but not as well as MPI and LVFS/MPI (Table 2). LVFS has also been shown to be related to dP/dt_{max} (and is modified with contractility and afterload manipulations) [3,16] and dP/dt_{min} [9]. Therefore, LVFS could be considered as a good marker to represent serial and endpoint cardiac function. However, Vcf has been shown to be dependent on dP/dt_{max} and is modified with contractility, preload and afterload manipulations [3]. In our study, Vcf could not correlate to invasive indices except for LVEDP.

Concerning the MPI, it has been reported that the MPI correlates with dP/dt_{max}, $dP/dt_{min,}$ LVEDP and tau and that it is dependent on contractility yet also affected by preload and afterload [3,14,25]. The dependence of MPI on preload was also reported by Moller et al. in patients without MI [13]. However, in a recent publication by Cheung et al., this phenomenon could not be reproduced in a porcine model [6]. In our study, MPI correlated with PRSW, a measure of contractility, and with LVEDP and LV volumes. Tei et al. also found correlations of MPI with dP/dt_{max} and tau when using cardiac catheterization in larger mammals [29], but we could not confirm this finding using our data. In an acute MI setting, Morgan et al. also showed the MPI to correlate to end-systolic and end-diastolic TTE dimensional values [14]. We advocate this by expressing a relationship between MPI and ESV and EDV (Table 2). Furthermore, it must be stipulated that the MPI is LV geometry independent, thus ideal for studying the course of a disease associated with chamber remodeling, typically elaborated during MI [29].

Concerning the LVFS/MPI, it was shown by Broberg et al. that this ratio correlated strongly with dP/dt_{max} in mice and was dependent on contractility and afterload variations, but not on preload variations [3]. However, in our study, the above ratio correlated to the load-independent contractile parameter PRSW, to LVEDP (preload) and volumetric ones (Table 2) but not to dP/dt_{max}. Therefore, the ratio is also affected by preload as LVEDP varies with MI. In our study of chronic MI, LVFS/MPI was the most sensitive to changes in contractility (PRSW) and filling (LVEDP) compared to classic TTE parameters. In multiple linear regression analysis, LVEDP appeared as the strongest predictor of MPI and LVFS/MPI, suggesting that these indices are potentially useful non-invasive indicators of filling pressure in the rat, at least in the setting of cardiac remodeling following MI.

It is to be emphasized that the reported data was obtained in a pooled analysis, including both control and MI data. When comparing EDV, ESV, EF, MPI and SV as

assessed by CC with TTE using the Bland-Altman analysis, the mean difference is close to zero for all parameters validating the coherence of the two methods. Slight discrepancies exist between the two methods, as the TTE accuracy is frame rate dependent and the CC accuracy depends on initial calibration, alpha estimation and the calculation of parallel conductance [8]. With this in mind, both methods are representative and suitable for evaluating changes in cardiac function. EF_c correlates well to EF_e ($r=0.80$ with $p<0.01$) and the differences in EF that are visible between the two groups are similar between the two methods (bias 6%) as seen in Table 1 and Figure 4 respectively. Similar correlations between CC and TTE have been demonstrated as the ones we found for ESV and EDV [5]. Also, MPI_e has been correlated to MPI_c with a bias of only 0.007 (roughly 2%). Due to the fact that at week 8, acceptable concordance was achieved between methods, one can assume that during the time course of the study, similar relations can be established. Thus, validating not just endpoints, but also the cardiac structural (EDV, ESV, SV) and functional (EF, MPI) variations from the study's baseline.

Study limitations. The number of animals in each of the subgroups was comparable to other studies, justifying detailed analysis of the MPI and LVFS/MPI within each subgroup. When compared to other research groups, between 6 and 12 rats are used per group [7,9,26] and all correlations are performed by pooling the analyzed data [14,25]. Therefore, after a detailed literature review, no other group has demonstrated acceptable correlations using subgroup analysis techniques. Another limitation arises from the use of anesthetics which might influence the data due to its effect on inotropy and chronotropy. However, following previous reports, we used Isoflurane during the complete study period as it seems to be the most appropriate technique for repeated and prolonged studies necessitating stable haemodynamic conditions [21]. In addition, the simultaneous measurement of the TTE and CC parameters is technically challenging as the rat is small and the positioning of the TTE probe in performed

with the animal in the lateral decubitus position.

In conclusion, we were able to follow serial changes in cardiac function post MI with these novel parameters (MPI or LVFS/MPI) with success and as efficiently as classic TTE parameters. More so, LVFS/MPI visually expressed better the serial modifications in cardiac function. Both novel parameters were correlated to the load-independent contractile parameter, PRSW, and to the preload parameter, LVEDP, being pertinent in following preload changes post MI. Finally, chamber remodeling post MI can successfully be followed due to the fact that ESV and EDV both correlate to MPI and LVFS/MPI

Grants

This work was supported by an award from the Swiss National Research Foundation (3100AO-104257/1), Cardiovascular Scientific Foundation (Fonds Scientifique Cardiovasculaire), Swiss Life Anniversary Foundation for Public Health and Medical Research, Novartis Foundation for Medico-Biological Research.

References

1. Arnlov J, Lind L, Andren B, Riserus U, Berglund L, Lithell H. A Doppler-derived index of combined left ventricular systolic and diastolic function is an independent predictor of cardiovascular mortality in elderly men. *Am Heart J* 2005;149:902-7.
2. Baan J, van der Velde ET, de Bruin HG, Smeenk GJ, Koops J, van Dijk AD et al. Continuous measurement of left ventricular volume in animals and humans by conductance catheter. *Circulation* 1984;70:812-823.
3. Broberg CS, Pantely GA, Barber BJ, Mack GK, Lee K, Thigpen T et al. Validation of the myocardial performance index by echocardiography in mice: a noninvasive measure of left ventricular function. *J Am Soc Echocardiography* 2003;16:814-23.
4. Cantor EJF, Babick AP, Vasanji Z, Dhalla NS, Netticadan T. A comparative serial echocardiographic analysis of cardiac structure and function in rats subjected to pressure and volume overload. *J Mol Cell Cardiol* 2005;38:777-786.
5. Chen C-H, Nevo E, Fetics B, Nakayama M, Pak PH, Maughan WL et al. Comparison of continuous left ventricular volumes by transthoracic two-dimensional digital echo quantification with simultaneous conductance catheter measurements in patients with cardiac disease. *Am J Cardiol* 1997;80:756-761.
6. Cheung MMH, Smallhorn JF, Redington AN, Vogel M. The effects of changes in loading conditions and modulation of inotropic state on the myocardial performance index: comparison with conductance catheter measurements. *Eur Heart J* 2004;25:2238-2242.
7. Derumeaux G, Mulder P, Richard V, Chagraoui A, Nafeh C, Bauer F et al. Tissue Doppler imaging differentiates physiological from pathological pressure-overload left ventricular hypertrophy in rats. *Circulation* 2002;105:1602-1608.

8. Feldman MD, Erikson JM, Mao Y, Korcarz CE, Lang RM, Freeman GL. Validation of a mouse conductance system to determine LV volume: comparison to echocardiography and crystals. *Am J Physiol Heart Circ Physiol* 2000;279:H1698-H1707.
9. Gao X-M, Dart AM, Dewar E, Jennings G, Du X-J. Serial echocardiographic assessment of left ventricular dimensions and function after myocardial infarction in mice. *Cardiovasc Res* 2000;45:330-338.
10. Heyen JRR, Blasi ER, Nikula K, Rocha R, Daust HA, Frierdich G et al. Structural, functional, and molecular characterization of the SHHF model of heart failure. *Am J Physiol Heart Circ Physiol* 2002;283:H1775-H1784.
11. Iwanaga Y, Hoshijima M, Gu Y, Iwatate M, Dieterle T, Ikeda Y et al. Chronic phospholambin inhibition prevents progressive cardiac dysfunction and pathological remodeling after infarction in rats. *J Clin Invest* 2004;113:727-736.
12. LaCorte JC, Cabreriza SE, Rabkin DG, Printz BF, Coku L, Weinberg A et al. Correlation of the Tei index with invasive measurements of ventricular function in a porcine model. *J Am Soc Echocardiogr* 2003;16:442-7.
13. Moller JE, Puolsen SH, Egstrup K. Effect of preload alterations on a new Doppler echocardiographic index of combined systolic and diastolic performance. *J Am Soc Echocardiogr* 1999;12:1065-72.
14. Morgan EE, Faulx MD, McElfresh TA, Kung TA, Zawaneh MS, Stanley WC et al. Validation of echocardiographic methods for assessing left ventricular dysfunction in rats with myocardial infarction. *Am J Physiol Heart Circ Physiol* 2004;287:H2049-2053.
15. Okawa M, Kitaoka H, Matsumura Y, Kubo T, Yamasaki N, Furuno T et al. Functional assessment of myocardial performance index (tei index) correlates with plasma brain

natriuretic peptide concentrations in patients with hypertrophic cardiomyopathy. *Circ J 2005*;69:951-957.

16. Ono K, Masuyama T, Yamamoto K, Doi R, Sakat Y, Nishikawa N et al. Echo Doppler assessment in rats with hypertensive hypertrophy. *J Am Soc Echocardiogr* 2002;15:109-17.
17. Palojoki E, Saraste A, Eriksson A, Pulkki K, Kallajoki M, Voipio-Pulkki L-M et al. Cardiomyocyte apoptosis and ventricular remodeling after myocardial infarction in rats. *Am J Physiol Heart Circ Physiol* 2001;280:H2726-H2731.
18. Poulsen SH, Jensen SE, Nielsen JC, Moller JE, Egstrup K. Serial changes and prognostic implications of a Doppler-derived index of combined left ventricular systolic and diastolic myocardial performance in acute myocardial infarction. *Am J Cardiol* 2000;85:19-25.
19. Poulsen SH, Jensen SE, Tei C, Seward JB, Egstrup K. Value of the Doppler index of myocardial performance in the early phase of acute myocardial infarction. *J Am Soc Echocardiogr* 2000;13:723-30.
20. Reffelmann T, Kloner RA. Transthoracic echocardiography in rats. *Basic Res Cardiol* 2003;98:275-284.
21. Roth DM, Swaney JS, Dalton ND, Gilpin EA, Ross J Jr. Impact of anesthesia on cardiac function during echocardiography in mice. *Am J Physiol Heart Circ Physiol* 2002 ;282 :H2134-H2140.
22. Sahn DJ, DeMaria A, Kisslo J, Weyman A. Recommendations regarding quantification in M-mode echocardiography: results of a survey of echocardiographic measurements. *Circulation* 1978;58:1072-83.

23. Salemi VMC, Pires MD, Cestari IN, Cestari IA, Picard MH, Leirner AA et al. Echocardiographic Assessment of Global Ventricular Function Using the Myocardial Performance Index in Rats with Hypertrophy. *Artificial Organs* 2000;28:332–337.
24. Sjaarstad I, Sejersted OM, Ilebekk A, Bjornerheim R. Echocardiographic criteria for detection of postinfarction congestive heart failure in rats. *J Appl Physiol* 2000;89:1445-1454.
25. Slama M, Ahn J, Peltier M, Maizel J, Chemla D, Varagic J et al. Validation of echocardiographic and Doppler indexes of left ventricular relaxation in adult hypertensive and normotensive rats. *Am J Physiol Heart Circ Physiol* 2005;289:H1131-H1136.
26. Slama M, Ahn J, Varagic J, Susic D, Frohlich ED. Long-term left ventricular echocardiographic follow-up of SHR and WKY rats: effects of hypertension and age. *Am J Physiol Heart Circ Physiol* 2004 ;286 :H181-185.
27. Tanaka N, Dalton N, Rockman HA, Pterson KL, Gottshall KR, Hunter JJ et al. Transthoracic echocardiography in models of cardiac disease in the mouse. *Circulation* 1996;94:1109-17.
28. Tei C. New non-invasive index for combined systolic and diastolic ventricular function. *J Cardiol* 1995;26:135.
29. Tei C, Nishimura RA, Seward JB, Tajik AJ. Noninvasive Doppler-derived myocardial performance index: correlation with simultaneous measurements of cardiac catheterization measurements. *J Am Soc Echocardiogr* 1997;10:169-78.

PAPER 3

Ventricular-arterial coupling in a rat model of reduced arterial compliance provoked by hypervitaminosis D and nicotine.

David Jegger[1,2], Rafaela da Silva[1], Xavier Jeanrenaud[4], Mohammad Nasratullah[4], Hendrik Tevaearai[3], Ludwig K. von Segesser[2], Patrick Segers[6], Virginie Gaillard[5], Jeffrey Atkinson[5], Isabelle Lartaud[5], Nikolaos Stergiopulos [1].

Laboratory of Haemodynamics and Cardiovascular Technology, EPFL, 1015 Lausanne, Switzerland[1]; Department of Cardiovascular Surgery, CHUV, 1011 Lausanne, Switzerland[2]; Department of Cardiovascular Surgery, Inselspital, 3000 Bern, Switzerland[3]; Department of Cardiology, CHUV, 1011 Lausanne, Switzerland[4]; Pharmacology Laboratory, Pharmacy Faculty, Henri Poincaré University 54000 Nancy, France[5]; Hydraulics Laboratory, Institute of Biomedical Technology, Ghent University, 9000 Gent, Belgium[6].

Running head: isolated systolic hypertension and ventricular-arterial coupling

Accepted in: *Am J Physiol Heart Circ Physiol* 2006 (in press).

Abstract

Objective: Rodent models of isolated systolic hypertension (ISH) are rare. One exception is the vitamin D_3 and nicotine (VDN) model, in which arterial calcification raises arterial stiffness and vascular impedance. Although several aspects of the effects of VDN treatment on arterial or cardiac hemodynamics have been investigated, a complete analysis of the effect of VDN on ventricular-arterial interaction has not yet been performed.

Methods: Wistar rats were treated with VDN (VDN group, n=9) and a control group (CTRL, n=10) was included without the VDN treatment. At week 8, invasive indexes of cardiac function were obtained using a conductance catheter. At the same time, aortic pressure and flow were measured to derive vascular impedance and characterize ventricular-vascular interaction.

Results: VDN caused significant increases in systolic (138±6 mmHg vs. 116±13 mmHg, $p<0.01$; mean ± stdev) and pulse pressures (42±10 mmHg vs. 26±4 mmHg, $p<0.01$) with respect to control, whereas diastolic pressure, stroke volume and cardiac output remained unaltered. Total arterial compliance decreased (0.12±0.08 ml/mmHg vs. 0.21±0.04 ml/mmHg in control, $p<0.05$) and pulse wave velocity increased significantly (8.8±2.5 m/s vs. 5.1±2.0 m/s in control, $p<0.05$). The arterial elastance rose significantly in the VDN group ($p<0.05$). Preload recruitable stroke work and end-systolic elastance were both elevated in the VDN group thus decreasing the ratio of arterial elastance over end-systolic elastance and augmenting efficiency. Wave reflection was augmented in the VDN group, as reflected by the increase in the wave reflection coefficient, Γ (0.63±0.06 vs. 0.52±0.05 in control, $p<0.05$), and the amplitude of the reflected pressure wave (13.3±3.1 mmHg vs. 8.4±1.0 mmHg in control, $p<0.05$).

Conclusions: We studied ventricular-arterial coupling in a VDN-induced rat model of reduced arterial compliance. The VDN treatment lead to development of ISH and provoked alterations

in cardiac function, arterial impedance, arterial function and ventricular-arterial interaction, which in many aspects are similar to effects of an aged and stiffened arterial tree. The VDN model may thus prove to be a useful model to study the patho-physiological effects of increased arterial stiffness.

Keywords: blood flow, calcium, hypertension, hemodynamics, ventricular function.

Introduction

Epidemiological studies have emphasized the close relationship between elevated blood pressure and the incidence of cardiovascular disease [44]. Systolic blood pressure and pulse pressure (PP), in particular, have been demonstrated to be strong independent predictors of cardiovascular mortality [10,33]. PP is on one hand determined by heart-related parameters such as heart rate and stroke volume (also related to arterial load), but also by the cushioning capacity of arteries (total arterial compliance) and the timing and intensity of wave reflections [28,41]. The former is influenced by arterial stiffness, which is usually expressed as the inverse of stiffness, i.e., as compliance or distensibility. The latter results from the summation of all backward running waves i.e., waves returning towards the heart after reflection at peripheral sites. In a recent review, aortic stiffness (measured from aortic pulse wave velocity, PWV) and an early return of reflected waves to the heart have been established as independent predictors of cardiovascular risk [35].

During aging, alterations in aortic structure and function occur, leading to a decrease in aortic compliance. In particular, the arterial extracellular matrix undergoes many profound age-related changes responsible for wall stiffening. Age-dependent medial degeneration, including phenomena such as elastocalcinosis (calcification followed by degeneration and fragmentation of elastic fibers) is probably the most important element in increased arterial stiffness [2]. More than 6 decades ago, Blumenthal et al. have noted that the time course of

the decrease of elasticity with age closely paralleled the curve of the intensity of medial calcification with age [5]. Another interesting case is provided by patients suffering from end-stage renal disease, in which aortic pulse wave velocity is related to aortic calcification [23].

To study the effects of arterial stiffening on arterial and cardiac function, many experimental animal models have been used, ranging from acute animal models where the aorta was either replaced by a stiff tube [18,30] or wrapped with a non-compliant Dacron band [15], to chronic models, where aortic stiffness is increased by inbreeding [14], as a result of hypertension-induced remodeling [16] through some chemical or biological treatment or old age [2,7,25]. Of particular importance is a model of aortic elastocalcinosis induced by the administration of vitamin D_3 and nicotine (VDN), developed originally by Hass et al. [11]. The VDN model leads to arterial stiffening by decimation of the arterial wall elastic fibre network [29]. Earlier studies on the effects of VDN on arterial hemodynamics showed that arterial stiffening caused by VDN decreased compliance and increased wave speed, aortic characteristic impedance, and wave reflections leading to isolated systolic hypertension (ISH) and the development of compensatory LV hypertrophy [20,21,25].

To date, however, no data have been reported on the effects of VDN on cardiac dimensions using trans-thoracic echocardiography (TTE) and conductance catheter (CC), contractility, and on the resulting changes in the interaction between the heart and the vessels i.e. ventricular-arterial coupling. The primary goal of this work, therefore, is to assess the changes occurring at the arterial and cardiac levels after aortic stiffening with VDN, and comprehensively quantify the resulting changes in arterial hemodynamics, cardiac function and ventricular-arterial coupling.

Material and methods

Animals. Male Wistar rats were purchased from Charles River Breeding Laboratories (Lyon, France). They were maintained in temperature and humidity controlled rooms with a

typical light-dark cycle and given standard chow and mineral water (Mont Roucous, France) *ad libitum*. The investigation conforms with the Guide for the Care and Use of Laboratory Animals published by the US National Institutes of Health (NIH Publication No. 85-23, revised 1996).

Experimental protocol for the VDN treatment. The procedure for preparing the calcification model was described previously by Lartaud et al [20]. Briefly, on day 1, 15 rats were injected (300 000 IU/kg hind leg muscle) with vitamin D_3 (Duphafral D_3 1000, Duphar BV, Weesp, The Netherlands) at 9AM and given nicotine (Nicotine hydrogen tartrate, Sigma Chemical Company, MO, USA) 25mg/kg. Nicotine was given orally by gavaging in 5ml/kg sterile water twice, at 9AM and 5PM (vitamin plus nicotine group, VDN). The VDN is a one-day only treatment. Another 10 rats received an injection with normal saline intramuscularly and underwent two gavages of distilled water (control placebo group, CTRL).

The VDN rats were two months old with a body weight of 226±8g (mean ± standard deviation). Four rats died within the first two weeks and two died at week 5 thus leaving n=9. The control group had the same age and similar body weight (BW) of 226±7g. No deaths occurred. The two groups were housed for an 8 week period and were then sacrificed, after analyzing cardiac and vascular function.

Assessment of arterial structure and function. Aortic flow (Figure 1A) was measured using a transit-time ultrasonic flow meter (Transonic, Thaca NY, USA) with the flow probe placed around the ascending aorta and filled with conducting gel. Aortic pressure (Figure 1A) was measured by retracting the CC from the LV into the ascending aorta. As soon as the trace changed from an LV one to an aortic one, the CC was withdrawn 0.5cm in order to ensure that the CC and flow meter were positioned on the same spot. From the pressure signal, mean arterial pressure (MAP), systolic (SBP), diastolic (DBP) and pulse pressure were derived (PP). Steady state measurements containing 10 cycles were averaged to construct a

representative steady-state beat of aortic pressure (P_{ao}) and flow (Q_{ao}). Discrete Fourier transform (Mathematica 5.2®, Wolfram Research Inc., IL, USA), was applied to obtain pressure and flow in the frequency domain.

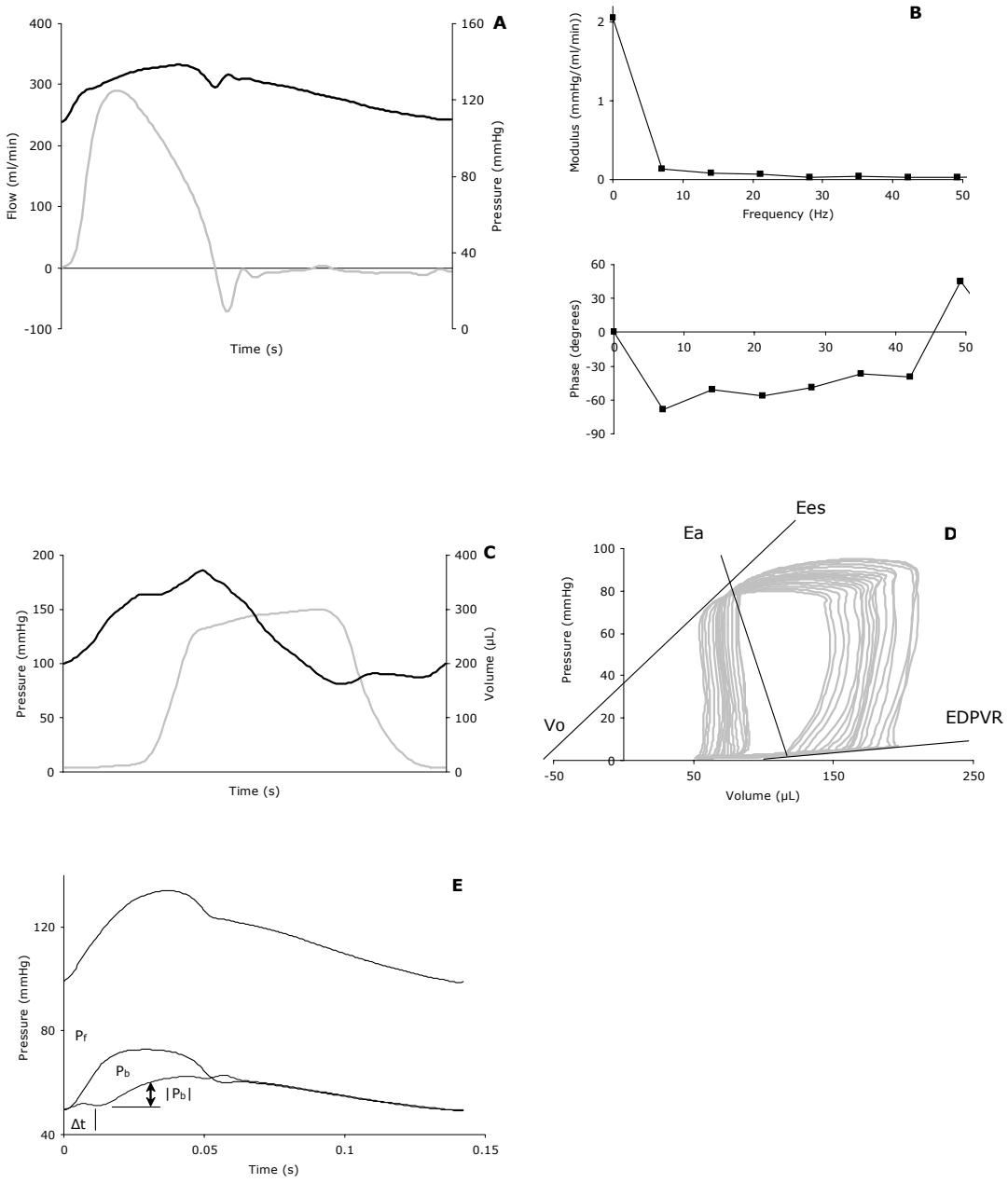

Figure 1. Panel A: aortic pressure (black) and flow (grey) measured during steady state conditions. From these, input impedance is derived (Panel B) as well as the forward (P_f) and backward (P_b) running pressure wave components (Panel E). □t is the time interval between the foot of the forward running and the foot of the reflected wave; $|P_b|$ is the amplitude of the reflected wave. Panel C: left ventricular pressure (grey) and volume (black) as measured by the conductance catheter. Panel D: pressure-volume loops after partial vena cava occlusion; E_a, is effective arterial elastance; E_{es}, end-systolic elastance, slope of the end-systolic pressure-volume relation; V_o, the intercept of the end-systolic pressure-volume relation; EDPVR, is end-diastolic pressure-volume relationship.

The ratio of mean P_{ao} and Q_{ao} (DC component of Z_{in}) is systemic vascular resistance (R). Input impedance being a complex quantity, is expressed in terms of its modulus and phase as a function of frequency (Figure 1B). The accuracy of the phase estimations may, however, be somewhat compromized by a non-precise co-localization of the pressure and flow measurements in the aorta. The characteristic impedance of the aorta, Z_c, was estimated as the average of the impedance modulus between the 5^{th} and the 10^{th} harmonic. The frequency response of the Millar pressure catheter is flat up to 100 Hz, and flow signals with filter cut-off settings of 100 Hz were used. The frequency contents of the signals are thus high enough to allow for computation of the 10^{th} harmonic (approximately 60 Hz) [36]. Because heart rate differed from animal to animal, impedance values were averaged per harmonic, with mean values and standard deviations of modulus, phase and frequency computed and plotted. Total arterial compliance (C) was estimated using the Pulse Pressure Method [40]. Pulse wave velocity (PWV) was estimated indirectly from the characteristic impedance and ascending aorta dimensions as $PWV= Z_c*A/\rho$, where $A=\pi r^2$ is the luminal cross-sectional area of the ascending aorta measured with echocardiography and ρ being the density of blood.

After euthanasia of the rat, the aorta was excised and a 5mm sample of the descending aorta was dehydrated in graded ethanol solutions and embedded in paraffin. Three 20μm thick sections were stained with hematoxylin-eosin for measurements of internal diameter (Di) and medial thickness (h) (Saisam, Microvision Instruments)[20]. Elastic modulus (EM; 10^6 dyne/cm^2) was calculated according to the Moens-Korteweg equation: $EM =(PWV^2 \times D_i \times \rho)/h$, where PWV (cm/s) is pulse wave velocity and ρ =1.05g/ml (blood density). Wall stress (WS; 10^6 dyne/cm^2) was calculated from the Lamé equation: $WS= (MAP \times 1333 \times D_i)/2h$. The ratio h/D_i was also calculated.

Assessment of cardiac function. Eight weeks after the initial treatment (VDN or placebo), the rats were anaesthetized and intubated. The right neck region was disinfected and the skin opened. The right jugular vein and right carotid artery were isolated. A 2Fr conductance catheter (CC) (SPR 838 Aria®, Millar Instruments Inc, Texas, USA) was inserted into the left ventricle via the right carotid artery. Parallel conductance (V_p) was measured after injection of 10% saline into the jugular vein using a 1ml syringe (20μL Natrium chloratum, Sintetica SA, Mendrisio, Switzerland), in accordance to the method by Baan et al. [3]. An occlusion analysis was performed by temporarily occluding the inferior vena cava through a small window made in the diaphragm via a mini laparotomy. For each animal, the CC calibration factor, α, was assessed as the ratio of stroke volume (SV) over CC-derived SV. SV was derived from aortic flow, which was measured simultaneously by means of an ultrasonic flowmeter (Transonic, Ithaca NY, USA) placed around the ascending aorta.

From the simultaneous measurement of LV pressure and volume during steady state conditions (Figure 1C), the following parameters were derived: Stroke Volume (SV), end-diastolic volume (EDV), ejection fraction (EF = SV/EDV), peak positive (dP/dt_{max}) and peak negative (dP/dt_{min}) value of the time-derivative of LV pressure, heart rate (HR), left ventricular end-diastolic (LVEDP) and end-systolic pressure (P_{es}). Cardiac output (CO) was calculated from HR multiplied by SV.

From the occlusion analysis, we calculated the slope (E_{es}) and volume axis intercept (V_0) of the end-systolic pressure-volume relationship (ESPVR, Figure 1D). We derived also the slope of the end-diastolic pressure-volume relationship (EDPVR), the preload-recruitable stroke work (PRSW), with stroke work assessed from the area enclosed by the pressure-volume loop, as well as the preload adjusted dP/dt_{max} expressed as the slope of the relation between dP/dt_{max} and end diastolic volume. Data acquisition was provided at a sampling rate of 1kHz and analyzed using IOX (EMKA, Paris, France).

Assessment of cardiac structure. For the histology, heart tissue samples were fixed in 4% formaldehyde, mounted in paraffin block and slices were obtained with a microtom. After deparaffinization and hydratation the samples were treated with either periodic acid Schiff (PAS) staining (Sigma) protocol (to discriminate cell borders) or 0.1% picrosirius red (for collagen, Sigma). The mean of the cardiomyocyte cross-sectional area and diameter were calculated by photomicrographs of 100 cells/specimen with a computer assisted image analysis system (Metamorph analysis).

*Assessment of cardiac structure using echocardiographic measurements***.** TTE was performed as previously described [17]. In brief, at baseline and every two weeks for an eight week period with a commercially available echocardiographic system (C256 Sequoia, Acuson, Mountain View, CA, USA) with the animal in the left lateral decubitus position. Light anesthesia was used during the analysis with Isofluorane ventilated inside a nose-cone at 0.5l/min with 100% oxygen (Forene, Abbott AG, Baar, Switzerland). Once asleep, the rat was shaven with an electrical razor (Surgical clipper 9661, 3M health care, MN, USA). Ultrasound transonic blue gel (Tyco healthcare/Kendall, Mallinckrodt Dar, MO, Italy) was placed on the thorax to optimize visibility of the cardiac chambers. A 15MHz linear array transducer (15L8) was used with a frame rate of 100Hz using bidimensional and color Doppler imaging. The probe was placed to obtain short and long axis and four chamber views. From the long axis view, an M-mode trace of the LV was obtained, and LV end-diastolic diameter (LVDed), LV systolic diameter (LVDes), and posterior and septal wall diastolic wall thickness (PWth and SWth) were measured. LV mass was calculated as = $(((LVDed+SWth+PWth)^3 - LVDed^3)*1.04)*0.8+0.14$ (in grams, with LV dimensions expressed in mm). Relative wall thickness was assessed as RWT = (PWth+SWth)/(LVDed).

Wave reflection analysis. Aortic pressure, $P_{ao,}$ was separated into its forward (P_f) and backward (P_b) running components using the linear wave separation method [45]:

$$P_f = (P_{ao} + Z_c * Q_{ao})/2 \text{ and } P_b = (P_{ao} - Z_c * Q_{ao})/2$$

An example of the aortic pressure wave and its forward and backward (reflected) components is shown in Figure 1E. The backward component is the sum of all reflected waves travelling towards the heart [45]. To characterize wave reflections, the reflection coefficient (□) was computed as [45]:

$$\Gamma = (Z_{in} - Z_c)/(Z_{in} + Z_c)$$

Γ is a frequency-dependent complex quantity. In order to facilitate comparison between the groups we computed and compared the modulus of the reflection coefficient at the 1st harmonic, $|\Gamma_1|$, which is assumed to be representative of the general wave reflection properties of the arterial tree. The time of the arrival of the foot of the reflected wave was defined as Δt (Figure 1E). The shorter the Δt, the stronger the systolic pressure augmentation resulting from wave reflections.

Coupling parameters. Arterial elastance (E_a) was calculated as the ratio of P_{es} divided by SV and the coupling parameter E_a/E_{es} computed [42]. Efficiency, defined as the ratio of stroke work over pressure-volume area (PVA; stroke work plus potential energy) was calculated. In addition to the "conventional" coupling parameter, we also calculated two recently proposed ventricular-arterial coupling parameters [41]. The first one is the "Compliance Coupling Index, CCI" expressed as the product of characteristic chamber elastance (E_{es}xC), E_{es} being the inverse of ventricular compliance at end systole and C arterial compliance. Second, the "Temporal Coupling Index, TCI", expressed as the ratio of characteristic times (RC/T), T being the heart period and RC the characteristic diastolic pressure decay time which is a combination of the capacitive-resistive properties of the arterial tree [40].

Tissue calcium content. A 10mm sample of the descending thoracic aorta as well as the cardiac apex were removed, and tissue calcium content (μmol/g dry wt) was determined

by atomic absorption spectrophotometry (AA10;Varian) after mineralization and acid digestion of the tissue [13].

Statistical analysis. Values are given as mean ± SD. Differences were determined by the unpaired Student's *t*-test, and the null hypothesis was rejected at $p<0.05$. A linear regression analysis was also performed between calcium and all other parameters. All analysis was done using SPSS (SPSS 11.5, SPSS Inc, Chicago, IL, USA).

Results

Basic hemodynamic parameters. At eight weeks post VDN treatment (sacrifice), the heart weight (HW) and HW/BW ratio were both significantly greater in the VDN group ($p<0.05$, Table 1). Systolic and pulse pressures were both higher in the VDN group ($p<0.01$, Table 1). P_{es} rose significantly in the VDN group ($p<0.05$, Table 1), however, LVEDP remained unaltered. P_{es} values were higher than SBP due to the fact that P_{es} was measured at the beginning of the experiment whereas SBP at the end of the occlusion analysis, when pressures were overall lower.

*Table 1. Values are mean ± SD. Comparison between the two groups for different invasive indices analyzed at sacrifice with the conductance catheter. HR, heart rate; SBP, systolic blood pressure; DBP, diastolic blood pressure; MAP, mean arterial pressure; PP, pulse pressure; P_{es}, LV end-systolic pressure; LVEDP, left ventricular end-diastolic pressure; V_0, slope and intercept of the end-systolic pressure-volume (PV) relation; HW/BW, heart weight ratio over body weight. *p<0.05, †p<0.01 CTRL vs VDN at same age.*

	Parameters	Control Group	VDN Group
Hemodynamics	HR (bpm)	360±25	390±27*
	Body weight (g)	463±47	421±62
	Heart weight (g)	1.04±0.16	1.23±0.08†
	Heart/body weight	2.16±0.32	2.46±25*
	SBP (mmHg)	110±9	136±7†
	DBP (mmHg)	80±6	91±8
	MAP (mmHg)	90±7	102±7
	PP (mmHg)	29±5	47±9*
	P_{es} (mmHg)	128±15	148±15*
	LVEDP (mmHg)	8.6±2.4	7.4±3.9

Arterial alterations. Aortic internal diameter was higher in the VDN group ($p<0.05$) but medial thickness remained unchanged (Figure 2).

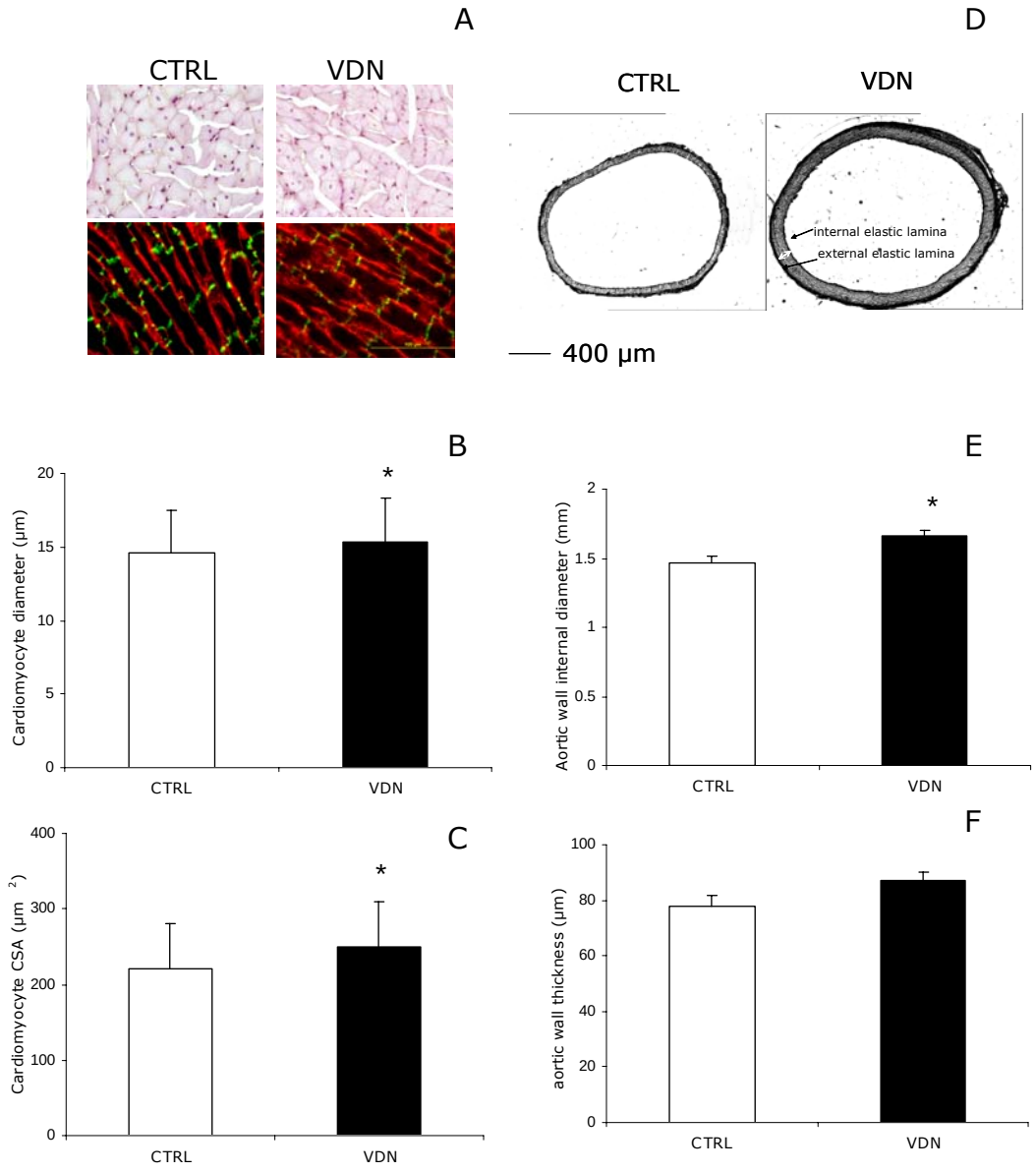

Figure 2. Panel A: Cardiomyocyte hypertrophy was estimated from LV section from control and VDN treated groups. Upper panels show representative cardiomyocyte cross-sectional and diameter as revealed by histology using periodic acid schiff. Below, show cardiomyocyte length as visualized by immuhistochemistry using double staining with antibodies against laminin (red) and connexin 43 (green). Panel B: The two groups representing cardiomyocyte diameter and Panel C: cross sectional area (CSA). Panel D: Aortic sections of the thoracic aorta in representative rats from the CTRL and VDN groups. The first cm of the descending thoracic aorta was removed, fixed in formaldehyde (10% in phosphate buffered saline) and embedded in paraffin for histomorphometric analyses. For each rat, three sections (thickness 20 µm) were cut and stained with hematoxylin-eosin for the measurement in a double-blind fashion of mean internal diameter and medial thickness (h, mean of 4 measurements of the distance (double white arrow) between the external and the internal elastic laminae (black arrows)). Panel E: The two groups representing aorta internal diameter (D_i) and Panel F: medial thickness (h).

However, their ratio (h/D_i) remained unchanged (Table 2). Arterial WS was similar in control and in VDN rats, but the EM was significantly higher in VDN ($p<0.05$, Table 2). The ratio, EM/WS was significantly elevated in the VDN rats ($p<0.05$, Table 2). There was a substantial (-43%, $p<0.05$) decrease in C and increase in PWV ($p<0.05$, Table 2) in the VDN group. Systemic vascular resistance, R, was similar between the groups (Table 2). There was a trend towards elevated aortic characteristic impedance, Z_c (Table 2).

*Table 2. Values are mean ± SD. Comparison between the two groups for arterial indices analyzed at sacrifice with the conductance catheter. R, total systemic vascular resistance; C, total arterial compliance; Z_c frequency domain estimate of Z_c; PWV, pulse-wave velocity; D_i, internal diameter; h, wall thickness; EM, elastic modulus and WS, wall stress. *p<0.05, †p<0.01 CTRL vs VDN at same age.*

	Parameters	Control Group	VDN Group
Arterial structure, function and composition	D_i (mm)	1.46±0.05	1.66±0.04*
	h (μm)	78±11	87±10
	h/D_i	0.053±0.004	0.053±0.008
	R (mmHg/(ml/s))	1.67±0.48	1.87±0.88
	C (ml/mmHg)	0.21±0.04	0.12±0.08*
	Z_c (mmHg/(ml/s))	0.06±0.01	0.08±0.02
	PWV (m/s)	5.1±2.0	8.8±2.5*
	EM (10^6 dyne/cm^2)	6±5	19±8*
	WS (10^6 dyne/cm^2)	1.2±0.2	1.4±0.3
	Calcium (μmol/g dry wt)	17±1	442±174*

Figure 3 displays the averaged Z_{in} spectra in terms of modulus and phase angle. The mean values of the modulus of the input impedance of the VDN group were consistently higher than that of the control for all frequencies, indicating the loss of compliance in the VDN group (Figure 3). The phase angle crossed the frequency axis at about 30Hz for the CTRL and 43Hz for the VDN. This shift of the zero phase cross over towards higher frequencies is also indicative of higher wave velocity in the VDN group (Figure 3). Calcium in the aorta increased by a factor of 28 in the VDN group compared to controls (Table 2).

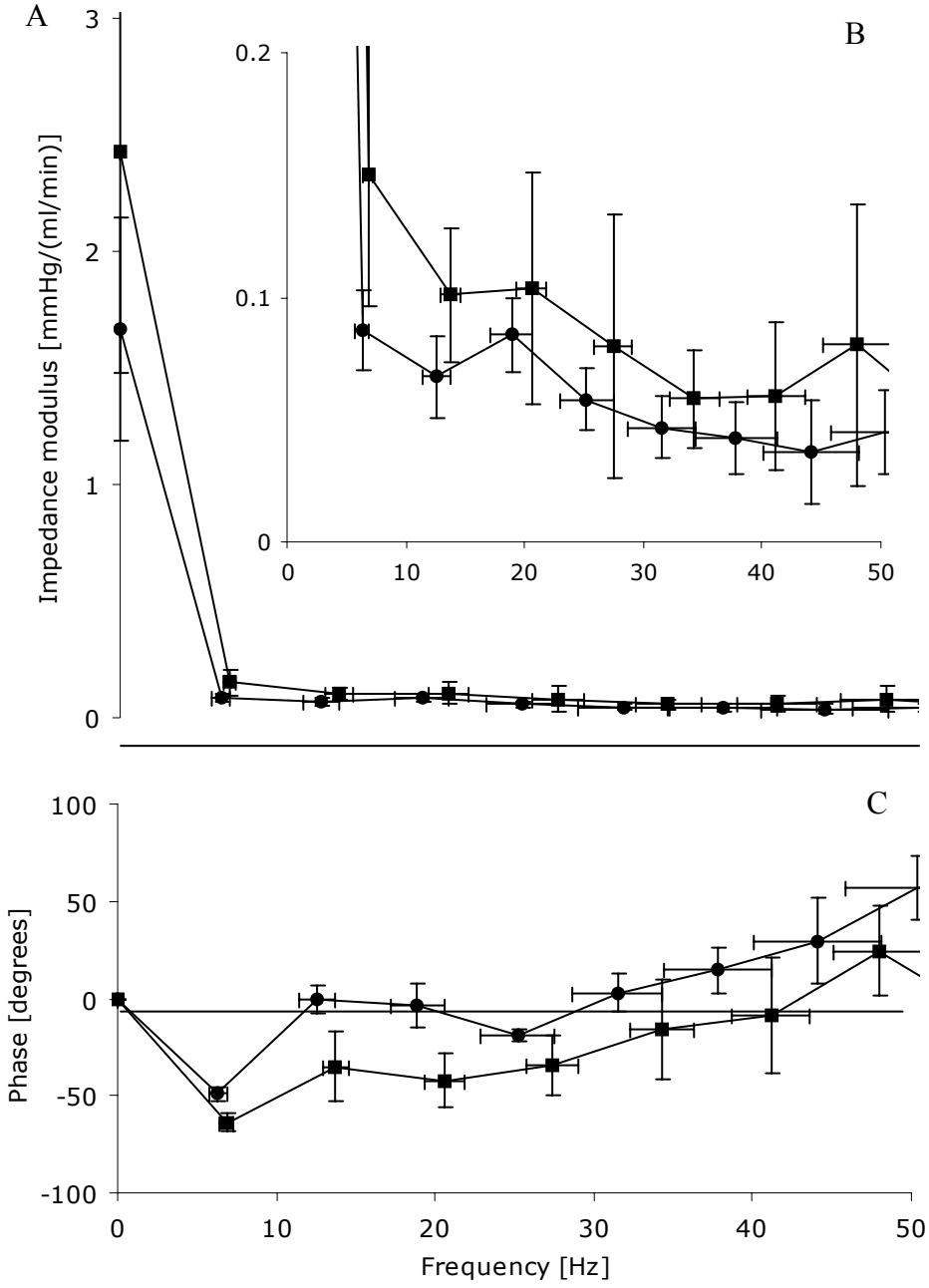

Figure 3. Modulus (A), modulus magnified at 0.1mmHg/(ml/min) in order to emphasize the difference between the two groups (B) and phase (C) of the input impedance (Z_{in}) spectra. Solid line gives the calculated average and the error bars are SD. ♦ represents the CTRL group and ■ the VDN one.

Cardiac alterations. SV was significantly lower in the VDN group, but cardiac output was maintained due to the significantly higher HR in this group (Table 1 and 3). There was slight LV chamber shrinkage in the VDN group, reflected by significantly smaller EDV and ESV's (Table 3). The volume intercept of the ESPVR, V_0, increased significantly in the VDN group ($p<0.05$, Table 3). Contractility was significantly augmented in VDN rats, and this is reflected by a substantial increase in all related indices: E_{es} increased by 71%, PRSW by 34%, and the slope of the dP/dtmax-EDV relation increased by 100% ($p<0.05$, Table 3). EDPVR remained the same. As a consequence of identical EDPVR and augmented E_{es}, there was a tendency for higher EF in the VDN group (Table 3).

Table 3. Values are mean ± SD. Comparison between the two groups for cardiac structure, function and composition analyzed at sacrifice with the conductance catheter. dP/dt_{max} (preload dependent) and the preload adjusted dP/dt_{max} (dP/dt_{max} vs EDV); EF, ejection fraction; PRSW, preload recruitable stroke work; E_{es}, end-systolic elastance; EDPVR, end-diastolic pressure-volume relationship; CO, cardiac output; SV, stroke volume;

	Parameters	Control Group	VDN Group
Cardiac structure, function and composition	SV (ml)	0.15±0.03	0.11±0.03*
	EDV (ml)	0.27±0.05	0.18±0.04*
	ESV (ml)	0.11±0.04	0.07±0.04*
	dP/dt_{max} (mmHg/ms)	7100±1300	7900±700
	dP/dt_{min} (mmHg/ms)	-7600±1300	-8500±900
	dP/dt_{max} - EDV (mmHg/s/µL)	21±7	42±26*
	PRSW (mmHg)	77±22	103±18*
	EF (%)	59±8	64±12
	E_{es} (mmHg/µL)	1.27±0.60	2.07±0.90*
	Vo (µL)	-114±66	-41±77*
	EDPVR (mmHg/µL)	0.03±0.01	0.03±0.02
	PVA (Joules)	36±18	20±10*
	CO (ml/min)	55±11	56±26
	Calcium (µmol/g dry wt)	6.3±0.9	9.8±1.1*

*EDV, end-diastolic volume; ESV, end-systolic volume; PVA, pressure-volume area; *p<0.05, †p<0.01 CTRL vs VDN at same age.*

RWT increased significantly in the VDN group, as did the LV mass measured with TTE (Figure 4). Calcium in the myocardium increased by a factor of 1.6 in the VDN group (Table 3). Cardiomyocyte diameter and CSA were both significantly augmented in the VDN group (Figure 2). The significance is related to the high numbers of counted myocytes during the analysis procedure.

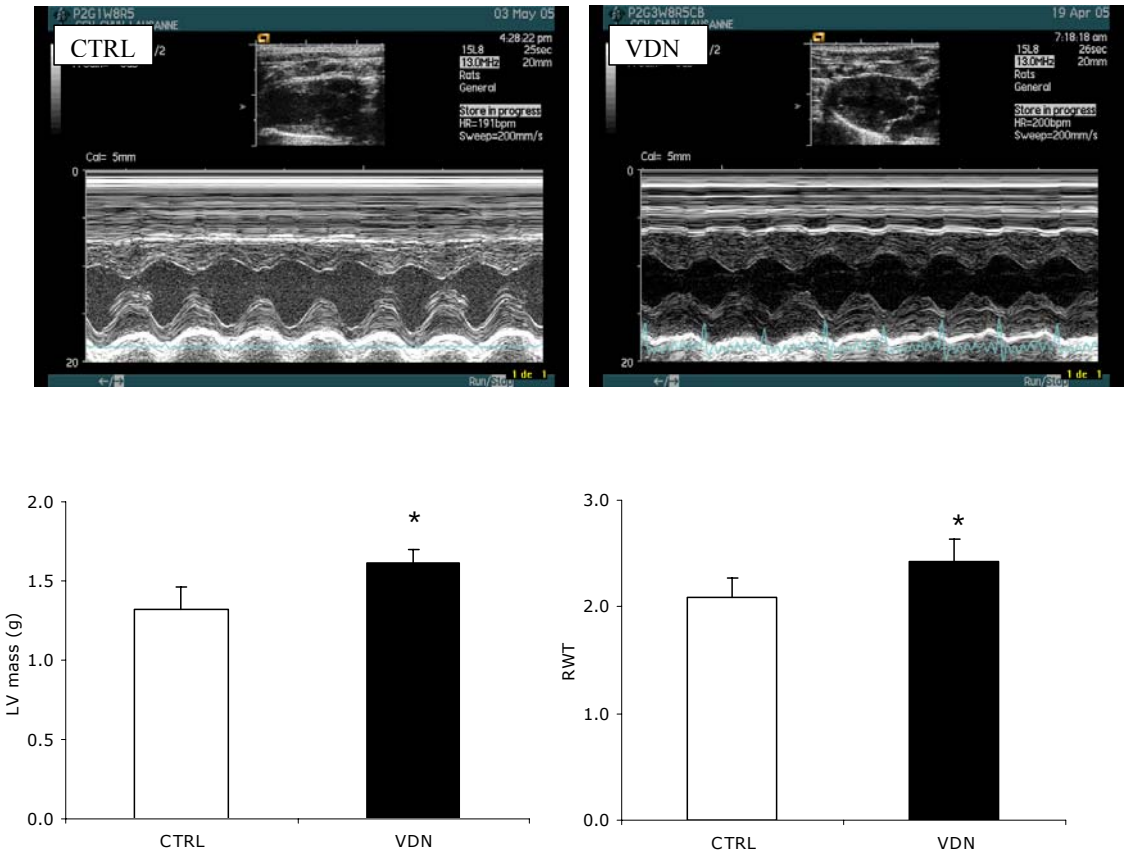

Figure 4. TTE M-mode of the CTRL and VDN rats showing hypertrophy of the posterior and septal walls of the long axis LV view in the VDN rat.

Wave analysis. A typical set of aortic pressure and flow waves for control and VDN rats is given in Figure 5.

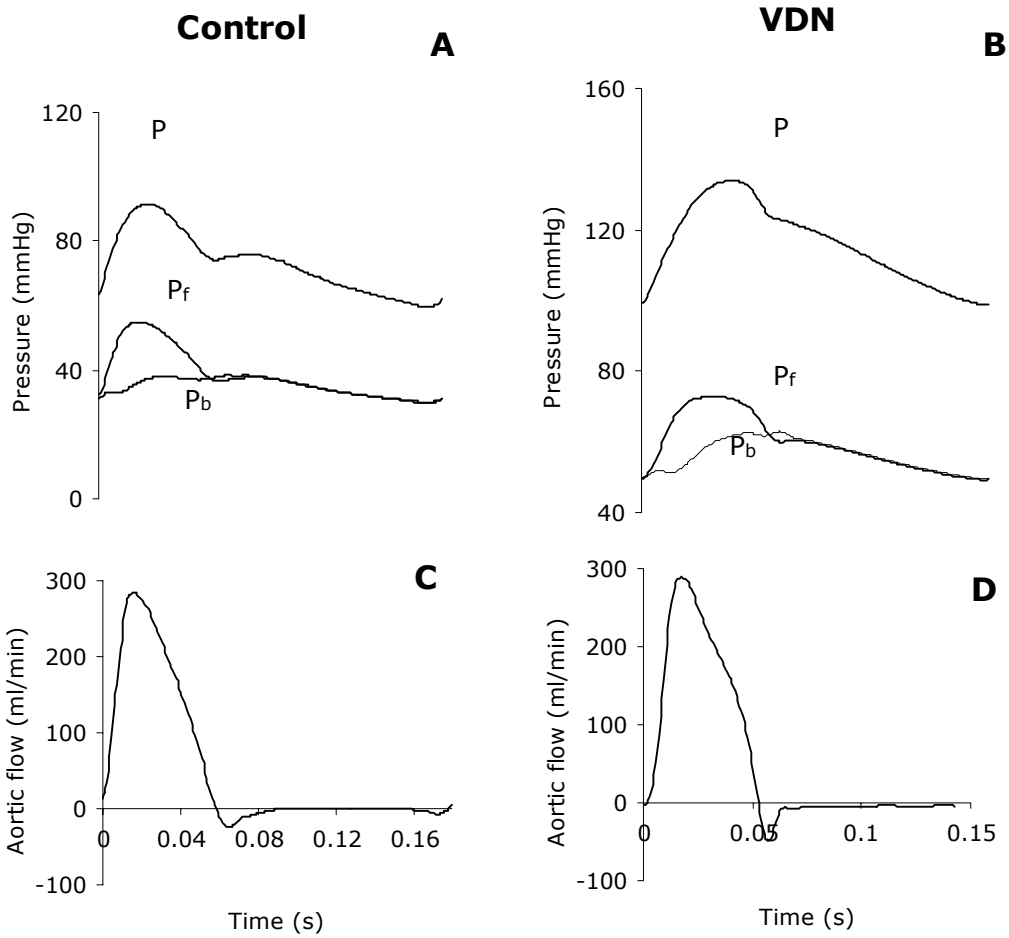

Figure 5. Pressure (A, CTRL and B, VDN) and flow (C, CTRL and D, VDN) measured in the aorta of control (left) and VDN-treated rats (right). Pressure is separated into its forward running wave component (P_f) and the reflected wave component (P_b).

It also shows the forward running and reflected waves, as obtained by the linear wave separation method. A significant difference in the shape of the pressure waves is observed. For the control group, the aortic pressure wave is of Type C, typical of the form of aortic pressure in young adults, characterized by the absence of reflected waves during systole [Murgo et al.]. This absence of significant wave reflection during systole is reconfirmed by

the existence of a very shallow reflected wave (Figure 5 A). For the VDN group, the aortic wave is of Type A, typical of that of an aged individual with a stiff arterial tree, characterized by a late systolic augmentation in the pressure wave. This augmentation is related to the arrival of a relatively strong wave reflection in mid-systole, as seen in Figure 5B. The amplitude of the reflected wave, $|P_b|$, increased by almost 40% in the VDN group ($p<0.05$, Table 4) and this is concurrent with an increase in the modulus of reflection coefficient ($p<0.05$, Table 4). The time of arrival of the reflected wave, Δt, was somewhat shorter in the VDN group (p=ns).

Ventricular-arterial coupling. E_a rose insignificantly in the VDN group (Table 4). E_a /E_{es} dropped in the VDN group reflecting alterations caused by the VDN diet (Table 4). The compliance coupling index, CCI=E_{es} x C, remained practically unaltered (Table 4). On the contrary, the temporal coupling index, TCI= RC/T, was significantly reduced in the VDN group (-26%, $p<0.05$, Table 4). Efficiency augmented significantly in the VDN group due to the reduction of the PVA ($p<0.05$, Table 3 and 4).

Table 4. Values are mean ± SD. Comparison between the two groups for coupling and wave analysis indices analyzed at sacrifice with the conductance catheter. E_a, effective arterial elastance; E_a/E_{es}, effective arterial elastance over end-systolic elastance; E_{es} x C, end-systolic elastance product compliance; RC/T, resistance-

	Parameters	Control Group	VDN Group
Coupling parameters	E_a (mmHg/µL)	0.89±0.24	1.41±0.46*
	E_a/E_{es}	0.70±0.53	0.60±0.17
	E_{es} x C	0.34±0.14	0.32±0.08
	RC/T	2.3±0.6	1.7±0.4*
	Efficiency (%)	0.35±0.11	0.48±0.10*
Wave reflection analysis	P_b (mmHg)	8.4±1.0	13.3±3.1*
	Δt (ms)	0.015±0.002	0.013±0.003
	Γ	0.52±0.05	0.63±0.06*

*compliance product over time period; P_b, backward wave amplitude; t_r, time point at which the backward wave arrives and Γ, reflection coefficient. *p<0.05, CTRL vs VDN at same age.*

Discussion

We evaluated the long-term effects of VDN on arterial function, cardiac function and ventricular- arterial coupling in rats. Treatment with VDN lead to a stiffened arterial tree similar to aged-related arterial calcification, which is elucidated by reduced arterial compliance Arterial stiffening, had a significant effect on wave reflections and ventricular-arterial coupling. VDN also caused LV concentric hypertrophy and lead to augmented cardiac performance.

Arterial stiffness, hypertension and cardiovascular risk. Arterial stiffening, either as a result of aging or of pathological changes in the arterial wall, leads to increases in systolic and PP [27]. Systolic blood pressure and pulse pressure (PP), in particular, have been demonstrated to be strong independent predictors of cardiovascular mortality [10,33]. The mechanisms linking arterial stiffness to ISH have been clearly identified and discussed in detail [45]. It is thus suggested that one should not only monitor PP and SBP to assess cardiovascular risk, but also the hemodynamic factors influencing SBP and PP, namely ventricular ejection, aortic stiffness and wave reflections [9,33,35,37]. In a recent review, aortic stiffness (PWV) and an early return of reflected waves to the heart have been established as independent predictors of cardiovascular risk [35].

Models of stiff arterial trees. Various animal models of chronic arterial stiffness have been reported in the literature, such as young SHR rats [12], Dahl salt-sensitive rats [16], DOCA-salt hypertension rats [34], VDN rats [2] and others. In some of the above models, however, arterial stiffening is not the primary effect.

Effect of VDN on baseline hemodynamics and arterial function. In our study, treatment with

VDN leads to increases in systolic and PP (Table 1). This is in agreement with earlier studies in VDN-treated rats, where systolic pressure and pulse pressure was found to increase whereas mean pressure remained constant and diastolic pressure decreased [20].

In previous studies, increase in aortic stiffness was represented by increases in aortic characteristic impedance, PWV and elasticity modulus, and occurred in the absence of any changes in mean blood pressure, geometry, or wall stress [20,29]. Our study shows similar findings, except that we found a slight rise in D_i in the VDN group which has, however also been reported in a setting with 90 days VDN treatment [43]. However, this rise in D_i had no effect on wall stress and its influence on the elasticity modulus is minimal. Further the thickness to diameter ratio, h/D_i, is the same in the two groups, which leads to similar mean stresses in the arterial wall in control and VDN.

Lartaud-Idjouadienne et al. found, however, that VDN affected only the elastic and not the resistive properties of the arterial system, with aortic characteristic impedance being increased by 56% whereas total peripheral resistance remained unchanged [20]. We know from earlier studies in the human [24] and other mammals [30,31,36] that when cardiac output and peripheral resistance are maintained while compliance is decreased, this results in an increased systolic pressure and a decrease in diastolic pressure, which is consistent with the findings of Lartaud-Idjouadiene et al [20,21]. This is in agreement with our findings (Figure 3) showing that the modulus of the input impedance of VDN rats for the first 5 harmonics was typically 35% higher than controls, and this corresponds well with the increase in pulse pressure (+36%). Characteristic impedance, Z_c, estimated as the average impedance modulus, rose but not significantly, the significance been hindered by the large standard deviations in the impedance moduli of the VDN group (Table 2). The change in mean value of the characteristic impedance is, however, consistent with the decrease in compliance in the VDN rats (Table 2). Z_c is proportional to the inverse square root of aortic compliance and

aortic compliance is the main determinant of total systemic compliance. Indeed, the ratio of $Z_{c,CTRL}/Z_{c,VDN}$=0.060/0.082=0.73 is very close to the ratio $\sqrt{C_{VDN}/C_{CTRL}} = \sqrt{0.12/0.21} = 0.75$, demonstrating that changes in compliance and aortic characteristic impedance are consistent.

In our study, aortic calcium compared well to previous reports on the effect of VDN on aortic wall composition and that elastocalcinosis is the major determinant of the induction of aortic stiffness in the VDN model [20, 21, 25, 29, 43]. Also, when a subgroup analysis was performed separating low from high calcium levels in the aorta; the level of calcium was found to be directly proportional to the level of augmented SBP being 148±13mmHg (low) and 171±14mmHg (high). More so, a direct correlation could be established between aortic calcium and SBP (r=0.91, p=0.005). Furthermore, in the present study, as in previous ones, calcinosis was stronger in the aortic wall than in the myocardium in VDN rats, as calcium deposits occur preferentially inside tissues containing elastic fibers, with a gradient of calcium content as follows: thoracic aorta > abdominal aorta ≥ carotid artery > kidney > caudal artery > myocardium > mesenteric bed [13].

Effect of VDN on cardiac structure and function. Lartaud et al. and others studied the consequences of VDN-induced arterial stiffening on certain cardiac structure, composition and performance parameters [4,20,32]. Lartaud et al. found that following VDN treatment, heart rate, stroke volume, cardiac output and stroke work were maintained whereas LV weight/body weight increased, suggesting hypertrophy. In our study, contrary to the above, we found that SV was compromised and CO maintained probably due to the fact that HR (+8%) was elevated after VDN treatment. More so, heart weight and its ratio with body weight rose after VDN treatment as did our non-biochemical indicators of hypertrophy. This is also the first time cardiac volumes have been measured post VDN treatment using conductance catheter techniques and validation with TTE.

Lartaud-Idjouadiene et al., gave considerable information on LV tissue composition but they did not quantify diastolic and systolic cardiac function in detail [20]. We have found that diastolic filling pressure as well as EDPVR remained unchanged, meaning that the diastolic function of the heart is preserved in the VDN group (Tables 1 and 2). Cardiac contractility, however, is significantly enhanced in the VDN group, as this is reflected by a 100% increase in both E_{es}, and the slope of dP/dt_{max}- EDV relationship (Table 2). This is as expected from the previously published data from Lartaud et al. due to the LV hypertrophy and rise in β-MHC isoform [20]. The β-MHC isoform develops a slower, more efficient form of contraction. Another reason could be changes in LV stiffness due to the moderate but significant increase in myocardial collagen content, thus interstitial fibrosis could be involved in the mechanism as reported in earlier studies [20].

Effect of VDN on wave reflections. Arterial stiffening, such as in ageing and hypertension, increases the amplitude of the arterial pulse wave and PWV, causing early return of reflected waves to the aorta. This, in turn, results in an associated increase in systolic and PP [35,44]. There is a strong correlation between the early return of wave reflections in the aorta and left ventricular hypertrophy [22]. Our results are in agreement with the above and this is the first time comprehensive wave analysis was analyzed in the VDN model. Indeed, the decrease in compliance caused by VDN is associated with an increase in PWV (Table 2), an increase in the amplitude of the reflected wave and a decrease in time of arrival of the reflected wave (Table 4), which indicates stronger wave reflections arriving earlier in systole. The larger amplitude of the reflected wave is further corroborated by the increased reflection coefficient. More so, a direct correlation could be established between aortic calcium and the amplitude of the reflected wave P_b ($r=0.84$, $p=0.02$)

Effect of VDN on ventricular-arterial coupling. Ventricular-arterial coupling is often judged upon optimal cardiac energetics, i.e., the ability of the heart to deliver optimal power

or operate under maximal efficiency [46] characterized by the ratio of E_a/E_{es}. It has been suggested that the heart delivers maximum SW when E_a/E_{es} =1, whereas optimal efficiency is obtained when E_a/E_{es} =0.5 [6]. As the ratio augments above 1.3 and below 0.3, the SW and efficiency are both compromised [16] as observed in patients with severe cardiac dysfunction [1]. Changes in ventricular-arterial coupling due to arterial stiffening with VDN have not been reported so far. We found that after treatment with VDN both E_a and E_{es} increased significantly as seen in aging [18] (Table 2 and 3), thus the ratio E_a/E_{es} was relatively preserved (Table 3). Due to the fact that E_a/E_{es} approaches 0.5 in the VDN group, optimal efficiency is attained therefore rises significantly due to a reduction of PVA (Table 3). Optimal energetic coupling of the heart and the arterial system has been reported to be preserved in hypertension and aging [8,18,38]. Although widely used, E_a/E_{es} has been criticized for not being a true coupling index [38]. This is because E_a is approximately equal to R/T, therefore the effective arterial elastance is primarily a measure of peripheral resistance and does not reflect the elastic properties of large conduit arteries. Further, E_a includes the effects of heart period, which is a cardiac parameter; therefore E_a is not a pure arterial parameter. In that respect, we have computed two other non-dimensional coupling parameters: the CCI and the TCI [41]. We found that the CCI (E_{es}xC) was maintained in the VDN group (0.32±0.08 in VDN vs. 0.34±0.14 in CTRL, Table 4). This means that the stiffening of the arterial tree after VDN was followed by a proportional increase in systolic LV chamber stiffness. Although CCI has been identified as an important coupling parameter and independent determinant of SV and aortic pressure [41], there are no reports on how this index behaves in arterial or cardiac disease. To the best of our knowledge, this is the first report showing that CCI is maintained during development of isolated systolic hypertension after arterial stiffening. Contrary to CCI, the TCI (RC/T) was compromized after VDN

treatment. This is because the decrease in compliance in the VDN group was not fully compensated by the increase in peripheral resistance and the slight increase in heart rate.

Clinical implications, novelty and validity. The present work offers a comprehensive study of ventricular-arterial coupling in presence of VDN-induced systolic hypertension. The effects of VDN treatment were analyzed at both the arterial level and the cardiac level, as well as in the framework of ventricular-arterial interaction. Most of previous work focused on the effects of VDN treatment on heart and vessels, but there was neither a report on cardiac mechanics and energetics, nor on the effect on ventricular-arterial coupling [2,20]. The comprehensive character of the study, which offers a consistent set of arterial, cardiac and ventricular-arterial data on the same animal model may be valuable for the global understanding of the pathophysiological phenomena involved in the development of systolic hypertension in presence of a stiffened arterial system. Further research at a molecular level is encouraged in order to elucidate the effects of VDN on cardiac function [4].

In conclusion, we have studied hemodynamics, arterial function, cardiac function and ventricular-arterial coupling in a rat model of reduced arterial compliance. The results show that arterial stiffening after VDN treatment provokes important changes in vascular impedance and wave reflections due to isolated systolic hypertension and LV hypertrophy while ventricular-arterial coupling was also altered. The effects are quantitatively similar to those of arterial stiffening with age.

Acknowledgments

This work was supported by an award from the Swiss National Research Foundation (3100AO-104257/1), Cardiovascular Scientific Foundation (Fonds Scientifique Cardiovasculaire), Swiss Life Anniversary Foundation for Public Health and Medical Research, Novartis Foundation for Medico-Biological Research, the French Ministry of

Education and Research (EA3448) Paris, the Regional Development Committee (CPER 2000-2006, “Bioingéniérie Appliqué aux Régulations Cellulaires”, Metz, France), the greater Nancy Urban Council (Nancy, France) and the Pharmacolor Association (Nancy, France). The authors thank Patrick Liminaña (Pharmacology Laboratory, Pharmacy Faculty, UHP Nancy 1, France) for technical help with histomorphometric analysis preparation.

References

1. Asanoi H, Sasayama S, Kameyama T. Ventriculoarterial coupling in normal and failing heart in humans. *Circ Res* 1989;65:483-493.
2. Atkinson J. Arterial calcification: mechanisms, consequences and animal models. *Path Biol* 1999;47:677-684.
3. Baan J, van der Velde ET, de Bruin HG, Smeenk GJ, Koops J, van Dijk AD, Temmerman D, Senden J, Buis B. Continuous measurement of left ventricular volume in animals and humans by conductance catheter. *Circulation* 1984;70:812-823.
4. Bin G, Fen QY, Hua LX, Hong ZB, Zheng PY, Shu TC. Dysfunction of myocardial sarcoplasmic reticulum in rats with myocardial calcification. *Life Sciences* 2005;77:966-979.
5. Blumenthal HT, Lansing AI, Wheeler PA. Calcification of the media of the human aorta and its relation to intimal arteriosclerosis, ageing and disease. *Am J Pathol*. 1944;20:665-679.
6. Burkhoff D, Sagawa K. Ventricular efficiency predicted by an analytical model. *Am J Physiol Regulatory Integrative Comp Physiol* 1986;250:R1021-1027.

7. Cantini C, Kieffer P, Corman B, Limiñana P, Atkinson J, Lartaud-Idjouadiene I. Aminoguanidine and Aortic Wall Mechanics, Structure and Composition in Aged Rats. *Hypertension*. 2001;38:943-948.
8. Cohen-Solal A, Caviezel B, Himbert D, Gourgon R. Left ventricular-arterial coupling in systemic hypertension: analysis by means of arterial effective and left ventricular elastances. *J Hypertens* 1994;12:591-600.
9. De Simone G, Roman MJ, Koren MJ, Mensah GA, Ganau A, Devereux RB. Stroke volume/pulse pressure ratio and cardiovascular risk in arterial hypertension. *Hypertension* 1999;33:800-805.
10. Franklin SS, Khan SA, Wong ND, Larson MG, Levy D. Is pulse pressure useful in predicting risk of coronary heart disease? The Framington heart study. *Circulation* 1999;100:354-60.
11. Hass GM, Trueheart RE, Taylor CB, Stumpe M. An experimental histologic study of hypervitaminosis D. *Am J Pathol* 1958;34:395-431.
12. Hayoz D, Rutschmann B, Perret F, Niederberger M, Tardy Y, Mooser V, Nussberger J, Waeber B, Brunner HR. Conduit artery compliance and distensibility are not necessarily reduced in hypertension. *Hypertension* 1992;20:1-6.
13. Henrion D, Chillon JM, Godeau G, Muller F, Capdeville-Atkinson C, Hoffman M, Atkinson J. The consequences of aortic calcium overload following vitamin D_3 plus nicotine treatment in young rats. *J Hypertens* 1991;9:919-926.
14. Heyen JRR, Blasi ER, Nikula K, Rocha R, Daust HA, Frierdich G et al. Structural, functional, and molecular characterization of the SHHF model of heart failure. *Am J Physiol Heart Circ Physiol* 2002;283:H1775-H1784.

15. Ioannou CV, Stergiopulos N, Katsamouris AN, Startchik I, Kalangos A, Licker MJ, westerhof N, Morel DR. *Eur J Vasc Endovasc Surg* 2003;26:195-204.
16. Jaeckel M, Simon G. Altered structure and reduced distensibility of arteries in Dahl salt –sensitive rats. *J Hypertens* 2003;21:311-9.
17. Jegger D, Jeanrenaud X, Nasratullah M, Chassot P-G, Mallik A, Tevaearai HT, von Segesser LK, Segers P, Stergiopulos N. Noninvasive Doppler-derived myocardial performance index in rats with myocardial infarction: validation and correlation by conductance catheter. *Am J Physiol Heart Circ Physiol* 2006;290:H1540-8.
18. Kass DA. Age related changes in ventricular-arterial coupling: pathologic implications. *Heart Failure Reviews* 2002;7:51-62.
19. Kelly RP, Tunin R, Kass DA. Effect of reduced aortic compliance on cardiac efficiency and contractile function of in situ canine left ventricle. *Circ Res* 1992;71:490-502.
20. Lartaud-Idjouadiene I, Lompre A-M, Kieffer P, Colas T, Atkinson J. Cardiac consequences of prolonged exposure to an isolated increase in aortic stiffness. *Hypertension* 1999;34:63-69.
21. Lartaud-Idjouadiene I, Niederhoffer N, Debets JJM, Struijker-Boudier H, Atkinson J, Smits JFM. Cardiac function in a rat model of chronic aortic stiffness. *Am J Physiol Heart Circ Physiol* 1997;272:H2211-H2218.
22. London GM, Guerin AP. Influence of arterial pulse and reflected waves on blood pressure and cardiac function. *Am Heart J* 1999;138:S5220-S224.
23. London GM, Marchais SJ, Safar ME, Genest AF, Guerin AP, Metivier F, Chedid K, London AM. Aortic and large artery compliance in end-stage renal failure. *Kidney Int* 1990;37:137-142.

24. Maeta H, Hori M. Effects of a lack of aortic “Windkessel” properties on the left ventricle. *Circ Jap* 1985;49:232-237.
25. Marque V, van Essen H, Struijker-Boudier H, Atkinson J, Lartaud-Idjouadiene I. Determination of aortic elastic modulus by pulse wave velocity and wall tracking in a rat model of aortic stiffness. *J Vasc Res* 2001;38:546-550.
26. Murgo JP, Westerhof N, Giolma JP, Altobelli SA. Aortic input impedance in normal man: relationship to pressure wave forms. *Circulation* 1980;62:105–116.
27. Nichols WW, O’Rourke M. McDonald’s Blood flow in Arteries: Theoretical, experimental and clinical principles. 4th ed. London, Sydney, Auckland: Arnold, 1998:54-401.
28. Nichols WW, Singh BM. Augmentation index as a measure of peripheral vascular disease state. *Curr Opin Cardiol* 2002;17:543-551.
29. Niederhoffer N, Lartaud-Idjouadiene I, Giummelly P, Duvivier C, Peslin R, Atkinson J. Calcification of medial elastic fibres and aortic elasticity. *Hypertension* 1997;29:999-1006.
30. Randall OS, van den Bos GC, Westerhof N. Systemic compliance: does it play a role in the genesis of essential hypertension? *Cardiovasc Res* 1984;18:455-62.
31. Reddy AK, Li Y-H, Pham TT, Ochoa LN, Trevino MT, Hartley CJ, Michael LH, Entman ML, Taffet GE. Measurement of aortic input impedence in mice: effect of age on aortic stiffness. *Am J Physiol Heart Circ Physiol* 2003;285:H1464-H1470.
32. Roman MJ, Ganau A, Saba PS, Pini R, Pickering TG, Devereux RB. Impact of arterial stiffening on LV structure. *Hypertension* 2000;36:489-494.
33. Safar ME. Systolic blood pressure, pulse pressure and arterial stiffness as cardiovascular risk factors. *Curr Opin Nephrol Hypertens* 2001;10:257-261.

34. Safar ME, Laurent P. Pulse pressure and arterial stiffness in rats: comparison with humans. *Am J Physiol Heart Circ Physiol* 2003;285:H1363-H1369.

35. Safar ME, Levy BI, Struijker-Boudier H. Current perspectives on arterial stiffness and pulse pressure in hypertension and cardiovascular diseases. *Circulation* 2003;107:2864-2869.

36. Segers P, Georgakopoulos D, Afansyeva M, Champio HC, Judge DP, Millar HD, Verdonck P, Kass DA, Stergiopulos N, Westerhof N. Conductance catheter-based assessment of arterial input impedance, arterial function and ventricular-vascular interaction in mice. *Am J Physiol Heart Circ Physiol* 2005;288:H1157–H1164.

37. Segers P, Stergiopulos N, Westerhof N. Quantification of the contribution of cardiac and arterial remodelling to hypertension. *Hypertension* 2000;36:760-765.

38. Segers P, Stergiopulos N, Westerhof N. Relation of effective arterial elastance to arterial system properties. *Am J Physiol Heart Circ Physiol* 2002;282:H1041-1046.

39. Sergio Saba P, Ganau A, Devereux RB, Pini R, Pickering TG, Roman MJ. Impact of arterial elastance as a measure of vascular load on left ventricular geometry in hypertension. *J Hypertens* 1999;17:1007-1015.

40. Stergiopulos N, Meister JJ, Westerhof N. Simple and accurate way for estimating total and segmental arterial compliance: the pulse pressure method. *Ann Biomed Eng* 1994;22:392–397.

41. Stergiopulos N, Meister JJ, Westerhof N. Determinants of stroke volume and systolic and diastolic aortic pressure. *Am J Physiol Heart Circ Physiol* 1996;270:H2050-9.

42. Suga H. Paul Dudley White International Lecture: Cardiac Performance as viewed through the Pressure-volume window. *Jpn Heart J* 1994;35:263-280.

43. Tatchum-Talom R, Niederhoffer N, Amin F, Makki T, Tankosic P, Atkinson J. Aortic stiffness and left ventricular mass in a rat model of isolated systolic hypertension. *Hypertension* 1995;26:963-970.
44. Weber T, Auer J, O'Rourke MF, Kvas E, Lassnig E, Berent R, Eber B. Arterial stiffness , wave reflections, and the risk of coronary artery disease. *Circulation* 2004;109:184-189.
45. Westerhof N, Sipkema P, van den Bos CG, Elzinga G. Forward and backward waves in the arterial system. *Cardiovasc Res* 1972;6:648–656.
46. Westerhof N, Stergiopulos N, Noble M. Snapshots of Hemodynamics. Berlin: Springer, 2005:1-196.

PAPER 4

Cardiovascular structure and function in a combined model of myocardial infarction and isolated systolic hypertension in rats: a novel experimental heart failure model.

David Jegger[1,2], PhD; Rafaela da Silva[1], PhD; Isabelle Lartaud[5], PhD; Virginie Gaillard[5], PhD; Xavier Jeanrenaud[4], MD; Mohammad Nasratullah[4], MD; Ludwig K. von Segesser[2], MD; Jeffrey Atkinson[5], PhD; Patrick Segers[6], PhD; Hendrik Tevaearai[3], MD; Nikolaos Stergiopulos[1], PhD.

Laboratory of Haemodynamics and Cardiovascular Technology, EPFL, 1015 Lausanne, Switzerland[1]; Department of Cardiovascular Surgery, CHUV, 1011 Lausanne, Switzerland[2]; Department of Cardiovascular Surgery, Inselspital, 3000 Bern, Switzerland[3]; Department of Cardiology, CHUV, 1011 Lausanne, Switzerland[4]; Pharmacology Laboratory, Pharmacy Faculty, 54000 Nancy, France[5], Cardiovascular Mechanics and Biofluid Dynamics, Institute of Biomedical Technology, Ghent University, 9000 Gent, Belgium[6] .

Running head: infarction and isolated systolic hypertension

Address for correspondence:

David Jegger

Abstract

Background: Epidemiological studies have shown that coronary heart disease and hypertension independently influence the development of heart failure (HF). We therefore hypothesized that a model combining myocardial infarction (MI) and isolated systolic hypertension (ISH) by way of vitamin D_3 and nicotine (VDN) mediated aortic elastocalcinosis would be of particular interest in order to translate basic research findings into clinical

applications.

Methods and Results: Wistar rats were treated with VDN (VDN, n=9), subjected to myocardial infarction by coronary ligation (MI, n=10) or to a combination of both MI and VDN treatment (VDN/MI, n=14). A sham treated group served as control (CTRL, n=10). Trans-thoracic echocardiography was performed every 2 weeks whereas invasive indices (conductance catheter) were obtained at week 8 before sacrifice. Calcium, collagen and protein contents were measured in the heart and the aorta. The heart weight and lung weight to body weight ratios were highest in the VDN/MI group. Also the ejection phase indices (ejection fraction, cardiac output, stroke volume, fractional shortening) were most compromised in this group. Cellular hypertrophy was increased in the VDN/MI group as compared to other groups. Cardiac calcium and collagen were highest in both MI groups. Brain natriuretic peptide was greatest in the VDN/MI group.

Conclusions: The combination of ISH and MI demonstrates larger compromises in cardiac structure and function of heart failure as compared to other models of HF. This model mimics several clinical phenomenon and may thus serve to further study novel therapies.

Keywords: calcium, echocardiography, heart failure, hypertension, myocardial infarction.

Submitted to Circulation

Introduction

Epidemiological studies have shown that coronary heart disease (CHD) and arterial hypertension are independent predictors of congestive heart failure (HF), the occurrence being 40% when both pathologies are associated [1. However, most experimental models are based on a single cause. Therefore, the development of a model combining myocardial infarction (MI) and hypertension would be of particular interest.

Whereas MI models are relatively well developed, there are several possibilities to induce

arterial hypertension in small animals. Spontaneously hypertensive rats (SHR) [2], renal hypertensive models [3,4], and Dahl salt-sensitive and salt-resistant rats [5] are typical models of essential hypertension. In patients however, the aged-related alterations in aortic structure are common and include the degeneration and fragmentation of elastic fibers, progressively leading to a loss of compliance [6]. Today, the subsequent chronic early return of a reflected pressure wave to the heart is accepted as an independent cardiac risk factor [7,8]. This phenomenon could be reproduced and studied in dogs after replacement of the thoracic aorta by a plastic tube [9]. In small animals, calcinosis and stiffening of the aorta can be induced by administration of vitamin D_3 and nicotine (VDN) [10,11] and leads progressively to the development of isolated systolic hypertension (ISH) and compensatory left ventricular (LV) hypertrophy [12-15].

The combination of ISH together with MI has not yet been evaluated in small animal models. We therefore hypothesized that such a model would show aggravated signs of cardiac dysfunction and accelerated evolution toward HF as compared to either of the two pathologies, and would represent therefore a novel small animal model of HF better mimicking the patho-physiological alterations found in the clinical environment.

Material and methods

Animals. Male Wistar rats, 2 months old (Charles River, Lyon, France) were maintained in temperature and humidity controlled rooms with a typical light-dark cycle and given standard chow and mineral water (Mont Roucous, France) *ad libitum*. The investigation conforms to the Guide for the Care and Use of Laboratory Animals published by the US National Institutes of Health (NIH Publication No. 85-23, revised 1996). The protocol was approved by our local ethical committee.

Animals (n=64) were randomized into four age- and weight-matched groups as follows:

Control group (CTRL, n=10, 226±7g). At day 1, the animals received normal saline intramuscularly (volume equivalent to the VDN group below) and underwent two 5ml/kg gavages of distilled water at 9AM and 5PM. At week 3, animals were anesthetized with Isofluorane (Forene, Abbott AG, Baar, Switzerland), intubated, ventilated (100% oxygen, 60 cycles/minute, tidal volume of 2ml, Harvard Apparatus Inc model 683, Holliston, Ma, USA) and placed on a heating pad before a sham operation was performed (left thoracotomy in the 3rd intercostal space and opening of the pericardium). The thorax was closed .Analgesia was then administered IP (40mg/kg) and again 24 hours post surgery (Pro-Dafalgan, Upsamedica SA, Baar, Switzerland).

VDN group (VDN, n=15, 226±8g). The procedure was previously described in detail [Lartaud 1999]. Briefly, on day 1 at 9AM, 300'000 IU/kg of vitamin D_3 (Duphafral D_3 1000, Duphar BV, Weesp, The Netherlands) was injected in the hind leg muscle and 25mg/kg nicotine (Nicotine hydrogen tartrate, Sigma Chemical Company, MO, USA) in 5ml/kg sterile water was given orally by gavaging. Gavaging was repeated once at 5PM the same day. Three weeks later, the animals underwent a sham operation (see CTRL group for description).

Myocardial infarction group (MI, n=10, 243±7g). At day 1, the animals were treated similarly as animals of the CTRL group At week 3,.an MI was induced by ligation of the left anterior descending coronary.

Combined VDN and MI group (VDN / MI, n=29, 213±24g). The animals received the VDN treatment at day 1 and underwent a MI at week 3 according to the procedures detailed above.

Annexe concerning the therapy schedule for the four groups over the study period.

Group	Day 1	Week 2	Week 3	Week 4	Week 6	Week 8

CTRL	Placebo	TTE	Sham	TTE	TTE	TTE + CC
MI	Placebo	TTE	MI	TTE	TTE	TTE + CC
VDN	VDN	TTE	Sham	TTE	TTE	TTE + CC
VDN / MI	VDN	TTE	MI	TTE	TTE	TTE + CC

Invasive cardiac measurements (Conductance Catheter). At week 8, the animals were reanaesthetized, intubated and the right jugular vein and carotid artery were isolated. A 2Fr conductance catheter (SPR 838 Aria®, Millar Instruments Inc, Texas, USA) was inserted into the ascending aorta via the right carotid artery. The systolic (SBP), diastolic (DBP), mean (MBP) and pulse pressures (PP) were obtained. Thereafter, the CC was advanced into the LV. Parallel conductance was measured after injection of 20µL of 10% saline into the jugular vein in accordance to the method by Baan et al. [16]. An occlusion analysis was performed by temporarily occluding the inferior vena cava below the diaphragm via a mini laparotomy. For each animal, the CC calibration correction factor alpha was assessed with the use of an ultrasonic flowmeter (Transonic, Ithaca NY, USA) placed around the ascending aorta.

Regarding further parameter descriptions, the subscript ‘c’ refers to data measured with the conductance catheter in order to differentiate from the same parameters measured with TTE (denoted by the subscript “e”). The following parameters were derived: Stroke Volume (SV), end-systolic volume (ESV), end-diastolic volume (EDV), ejection fraction (EF_c = SV/EDV), isovolumetric contraction time (ICT), peak positive (dP/dt_{max}) and peak negative (dP/dt_{min}) value of the time-derivative of LV pressure, contractility index (dP/dt_{max} divided by the pressure at this point), isovolumetric relaxation time (IRT, duration of the isovolumic

relaxation), time constant of relaxation derived from the peak systolic pressure to the next begin of diastolic pressure (Tau), heart rate (HR) and left ventricular end-diastolic (LVEDP). Cardiac output (CO_c) was calculated as SV multiplied by HR.

From the occlusion data, we calculated the slope (E_{es}) and volume axis intercept (V_0) of the end-systolic pressure-volume relationship (ESPVR), the slope of the end-diastolic pressure-volume relationship (EDPVR), preload-recruitable stroke work (PRSW) (with stroke work assessed from the area enclosed by the pressure-volume loop), preload adjusted dP/dt_{max} (slope of the relation between dP/dt_{max} and end diastolic volume (EDV)), potential energy (PE) and pressure-volume area (PVA). The ratio of stroke work and PVA is a measure of efficiency.

Echocardiographic measurements. Trans-thoracic echocardiography (TTE) (C256 Sequoia echocardiographic system, Acuson, Mountain View, CA, USA) was performed at baseline in 15 arbitrary rats before they were randomized into the 4 groups. Thereafter, a new TTE was performed in each rat every second week until week 8. Animals were lightly anesthetized with Isoflurane (Forene, Abbott AG, Baar, Switzerland) ventilated inside a nose-cone (0.5l/min, 100% oxygen) and positioned on their left side. A 15MHz linear array transducer (15L8, Acuson, Mountain View, CA, USA) was used using bidimensional and color Doppler imaging. The probe was placed to obtain short and long axis and four chamber views. From the long axis view, an M-mode trace of the LV was obtained, and LV end-diastolic diameter (LVDed), LV systolic diameter (LVDes), and posterior and septal wall diastolic wall thickness (PWth and SWth) were measured. LV fractional shortening (LVFS) was calculated according to = (LVDed-LVDes)/LVDed x100. Ejection fraction was calculated from a long axis view using planimetry (EF_e) = 100 x ($LVDed^3$ –$LVDes^3$)/$LVDed^3$. Velocity of circumferential fiber shortening (Vcf) was calculated using the following formula (LVDed-LVDes)/(ET x LVDed). EDV and ESV were calculated using the Simpson's

method, and SV was calculated as EDV-ESV. Aortic flow or cardiac output (CO_e) was recorded and calculated using pulse Doppler imaging, with the smallest possible sample volume placed at the level of the aortic annulus. Doppler yields the velocity profile (aortic velocity time integral (VTI)) which is multiplied with the cross sectional area of the outflow tract to obtain flow. Integration of the velocity profile yields the aortic velocity time integral. LV mass was calculated as = $(((LVDed+SWth+PWth)^3 - LVDed^3)*1.04)*0.8+0.14$ (in grams, with LV dimensions expressed in mm). Relative wall thickness was assessed as RWT = (PWth+SWth)/(LVDed). LV ejection time (ET) was measured as the time from the beginning to the end of the aortic flow wave. IRT was measured as the interval between the aortic closure click and the start of mitral flow, while ICT was obtained as the time delay between the cessation of mitral inflow and the onset of aortic ejection. Additionally, the mitral valve closure time (MCO) was measured. The myocardial performance index (MPI) is then defined as (MCO-ET)/ET = (ICT+IRT)/ET.

Cardiac and vascular tissue calcium content. A 10mm sample of the descending thoracic aorta as well as the cardiac apex were removed, and tissue calcium content (μmol/g dry wt) was determined by atomic absorption spectrophotometry (AA10;Varian) after mineralization and acid digestion of the tissue [17].

Scleroprotein analysis. Collagen content was measured from hydroxyproline content using protein hydrolysis followed by colorimetric spectrophotometry.

Vascular histomorphometry. Aortic geometry, internal diameter and medial thickness were then determined by computer-directed color analysis (Quant'Image software, Talence, France).

Vascular function. Pulse wave velocity (PWV) was estimated indirectly from the characteristic impedance and ascending aorta dimensions as $PWV= Z_c*A/\square$, where $A=\square r^2$ is the luminal cross-sectional area of the ascending aorta measured with echocardiography and

 being the density of blood. After euthanasia, the aorta was excised and a 5mm sample of the descending aorta was dehydrated in graded ethanol solutions and embedded in paraffin. Three 20μm thick sections were stained with hematoxylin-eosin for measurements of internal diameter (Di) and medial thickness (h) (Saisam, Microvision Instruments)[12]. Elastic modulus (EM; 10^6 dyne/cm^2) was calculated according to the Moens-Korteweg equation: EM $=(PWV^2 \times D_i \times \rho)/h$, where PWV (cm/s) is pulse wave velocity and ρ =1.05g/ml (blood density). Wall stress (WS; 10^6 dyne/cm^2) was calculated from the Lamé equation: WS= (MAP x 1333 x D_i)/2h. The ratio h/D_i was also calculated.

Cardiac infarct size and histology. After completion of these measurements, LV was excised and weighed. The infarct size area (IS) was determined as a percentage of the entire LV area, as reported previously [18]. For the histology, heart tissue samples were fixed in 4% formaldehyde, mounted in paraffin block and slices were obtained with a microtom. After deparaffinization and hydratation the samples were treated with either periodic acid Schiff (PAS) staining (Sigma-Aldrich Chimie SARL, Epalinges, Switzerland) protocol (to discriminate cell borders) or 0.1% picrosirius red (for collagen, Sigma). The mean of the cardiomyocyte cross-sectional area and diameter were calculated by photomicrographs of 100 cells/specimen with a computer assisted image analysis system (Metamorph analysis).

Immunohistochemistry. The following primary antibodies were incubated for 2 h at room temperature: Mouse antibody against connexin 43 (BD Biosciences Pharmingen, Basel, Switzerland) and rabbit antibody against laminin (to discriminate the cell border, Sigma) used as primary antibodies were diluted (1:100) in PBS containing 4% of NGS whereas goat Alexa 488 anti-mouse and goat Alexa 555 anti-rabbit were used as secondary antibodies.

RNA extraction and quantitative real time-polymerase chain reaction (RT-PCR). At the end of each experiment at sacrifice, the heart was removed and the apex was immediately frozen in liquid nitrogen. Total tissue RNA was extracted by using the RNeasy Mini Kit

(Qiagen, Hilden, Germany) following the instructions of the manufacturer. Reverse transcriptase reaction was performed starting from 1μg of total RNA in presence of 0.5 μmol/L of dNTP (Amersham, Otelfingen, Switzerland), 1 μg oligo dT (Promega, Mannheim, Germany) and 200 U/μl Superscript II (Invitrogen, Basel, Switzerland) at 42°C for 1 hour. For each quantitative RT-PCR reaction 1/10 of the reverse transcriptase product was used. RT-PCR was performed on ABI PRISM 7700 (BD Biosciences, Heidelberg, Germany) using Absolute QPCR ROX mix (ABgene-Axon, Baden-Dättwil, Switzerland). PCR primers and probes sequences were synthesized by MWG Biotech (Ebersberg, Germany). Sequences were the following: i) rat brain natriuretic peptide precursor (BNP) forward 5'-CAGCTCTCAAAGGACCAAGG-3'and reverse 5'-AGAGCTGGGGAAAGAAGAGC-3' with an internal probe of 5'-FAM CGCCTTCCGGATCCAGGAGAGACTTCG-3'-TAMRA; ii) rat GAPDH forward 5'- CCATCACTGCCACTCAGAAGAC-3 and reverse 5'-TCATACTTGGCAGGTTTCTCCA-3' with an internal probe of probe GAPDH rat FAM-5'-CGTGTTCCTACCCCCAATGTATCCGT-3'-TAMRA. Expression level of mRNA was determined by gene-specific standard curves. Taqman results were expressed as a ratio of BNP over GAPDH mRNA level for each sample and normalized to the sham-operated controls. We verify all samples of each group and all were run in duplicate.

Statistical analysis. Values are reported as means ± SD. Each TTE analysis was repeated three times and averaged. Comparison of TTE evolution was analyzed by repeated-measures analysis of variance. If significance was found for a variable, pairwise comparisons have been performed using Bonferroni's adjustment for multiple tests. P-values <0.05 were considered significant. All analysis were done using the SPSS software (SPSS 11.5, SPSS Inc, Chicago, IL, USA).

Results

Early and late mortality.There were no deaths in the CTRL and MI groups whereas in the VDN group, 4/15 rats died within the first 2 weeks (early mortality rate of 27%) and 2 died at week 5 (total mortality of 40%). In the VDN/MI group, 15/29 rats died within the first 2 weeks (early mortality of 52%) and none died olater.

General characteristics. At week 8, body weight (BW) was the lowest in the VDN/MI group (Table 1). In this group, the heart weight (HW) was significantly increased as compared to the CTRL group but significantly lower than in the MI group ($p<0.05$, Table 1). Therefore, their ratio HW/BW, an indicator of cardiac hypertrophy, was found elevated in both MI and VDN/MI groups with the highest value in the VDN/MI group (Table 1). Both VDN treated groups of animals exhibited significantly elevated SBP and PP ($p<0.05$, Table 1). The infarct size area was largest in the VDN/MI group as compared to the MI group ($p<0.05$). The lung weight (LW) was also measured showing that the LW/BW, an indicator of congestive heart failure, was the highest in the VDN/MI group ($p<0.05$, Table 1).

*Table 1. General characteristics of the four groups. Values are mean ± SD. BW, body weight; HW, heart weight; HR, heart rate; SBP, systolic blood pressure; DBP, diastolic blood pressure; MAP, mean arterial pressure; PP, pulse pressure; IS, infarction size; LV, left ventricle; LW, lung weight; LW/BW, lung weight/body weight; * p<0.05 vs CTRL, † vs MI and § vs VDN.*

	Parameters	CTRL	MI	VDN	VDN/MI
Demographics	n	10	10	9	14
	BW (g)	463±47	481±45	421±62	402±39*†
	HW (g)	1.04±0.16	1.57±0.24*	1.23±0.08†	1.33±0.24*†
	HW/BW	2.16±0.32	2.94±0.33*	2.46±.25	3.62±0.70*†§
	HR (bpm)	360±25	377±33	390±27	403±40*
	SBP (mmHg)	110±10	112±10	138±6*†	141±10*†
	DBP (mmHg)	80±6	81±6	91±8	92±10
	MAP (mmHg)	90±7	92±7	102±6	103±9
	PP (mmHg)	28±5	28±6	47±8*†	52±1*†
	PP/MAP (%)	28±8	22±6	38±9*	29±11
	IS (% IS/LV surface area)	0	31±6*	0†	37±7*†§
	LW/BW	1.03±0.29	0.83±0.26	1.02±0.09	1.23±0.15†

Invasive cardiac structure and function (CC). At sacrifice, EDV and ESV values were augmented in the MI group as compared to the CTRL group. The SV and CO_c values thus remained within a normal range (Table 2). In contrast, in the VDN/MI group, only the ESV was increased and consequently SV and CO_c were compromised (Table 2). Contractility indices dP/dt_{max}-EDV and E_{es} were significantly elevated in both VDN treated groups. Consequently, the PE and PVA values were reduced (Table 2).

*Table 2. Invasive cardiac structure and function of the four groups (CC). Values are mean ± SD. EDV, end-diastolic volume; ESV, end-systolic volume; SV, stroke volume; LVEDP, left ventricular end-diastolic pressure; dP/dt_{max} (preload dependent) and the preload adjusted dP/dt_{max} (dP/dt_{max} vs EDV); isovolumetric contraction time, ICT; E_{es}, end-systolic elastance; potential energy, PE; pressure-volume area, PVA; PRSW, preload recruitable stroke work; EF_c, ejection fraction; ET, ejection time; CO_c, cardiac output; tau, time constant of relaxation; EDPVR, end-diastolic pressure-volume relationship; IRT, isovolumetric relaxation time; * $p<0.05$ vs CTRL, † vs MI and § vs VDN.*

	Parameters	CTRL	MI	VDN	VDN/MI
LV pressures and volumes	EDV (ml)	0.27±0.05	0.39±0.12	0.18±0.04†	0.29±0.10§
	ESV (ml)	0.11±0.04	0.22±0.08*	0.07±0.04†	0.19±0.10§
	SV (ml)	0.15±0.03	0.17±0.06	0.11±0.03†	0.10±0.03*†
	LVEDP (mmHg)	4.9±1.8	8.6±4.0	4.9±4.0	7.4±3.3
Isovolumic contraction phase indices	dP/dt_{max} (mmHg/ms)	7100±1300	7200±900	7900±700	8100±1500
	dP/dt_{max} - EDV (mmHg/s/µL)	20±6	15±6	42±26*†	35±17†
	ICT (ms)	21±1	24±3	23±4	25±4
Contractile indices	E_{es} (mmHg/µL)	0.66±0.30	0.34±0.11	1.23±0.54*†	0.84±0.50†
	PE (J)	19±14	33±13	10±4.6†	15±14†
	PVA (J)	36±18	44±17	21±11†	19±8.8†
	Efficiency (%)	0.37±0.13	0.28±0.07	0.48±0.10†	0.43±0.15
	PRSW (mmHg)	77±22	79±28	103±18	91±44
Ejection phase indices	EF_c (%)	59±8	44±8*	64±12†	33±7*§†
	ET (ms)	46±5	48±4	46±4	46±7
	CO_c (ml/min)	55±11	59±17	56±26	42±12†
Active phase of relaxation indices	Tau (ms)	13±3	16±3	11±3†	14±3
	dP/dt_{min} (mmHg/ms)	-7600±1300	-6300±1100	-8500±900†	-6900±1200§
	EDPVR (mmHg/µL)	0.03±0.01	0.03±0.03	0.03±0.02	0.03±0.02
	IRT (ms)	51±3	56±3*	52±2	56±4*

EF_c, which decreased in the MI group, is even more perturbed in the VDN/MI group (Table 2). LVEDP were highest in the MI groups but no statistical significance could be reached (Table 2). Also, minimal changes were observed with respect to timing parameters and those of diastolic function in all four groups (Table 2). Importantly, as clearly observed in the occlusion analysis curves, the MI, VDN and VDN/MI groups constitute completely different models of heart failure and arterial stiffening (Figure 1).

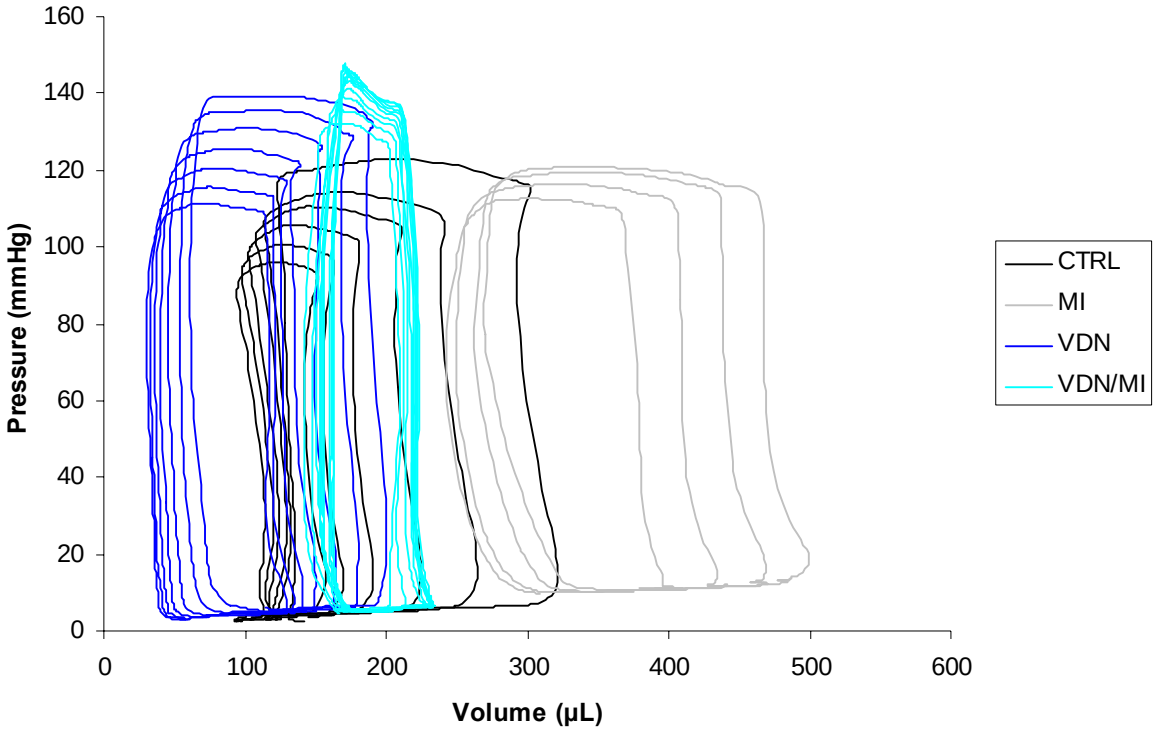

Figure 1. Pressure-Volume loops of the four groups showing relative ejection fractions for each group.

Non-invasive cardiac structure and function (TTE). Figure 2 represents the M-mode of the four groups. Notice the greater RWT in the VDN group while wall motion abnormalities occurred in the two infarcted groups.

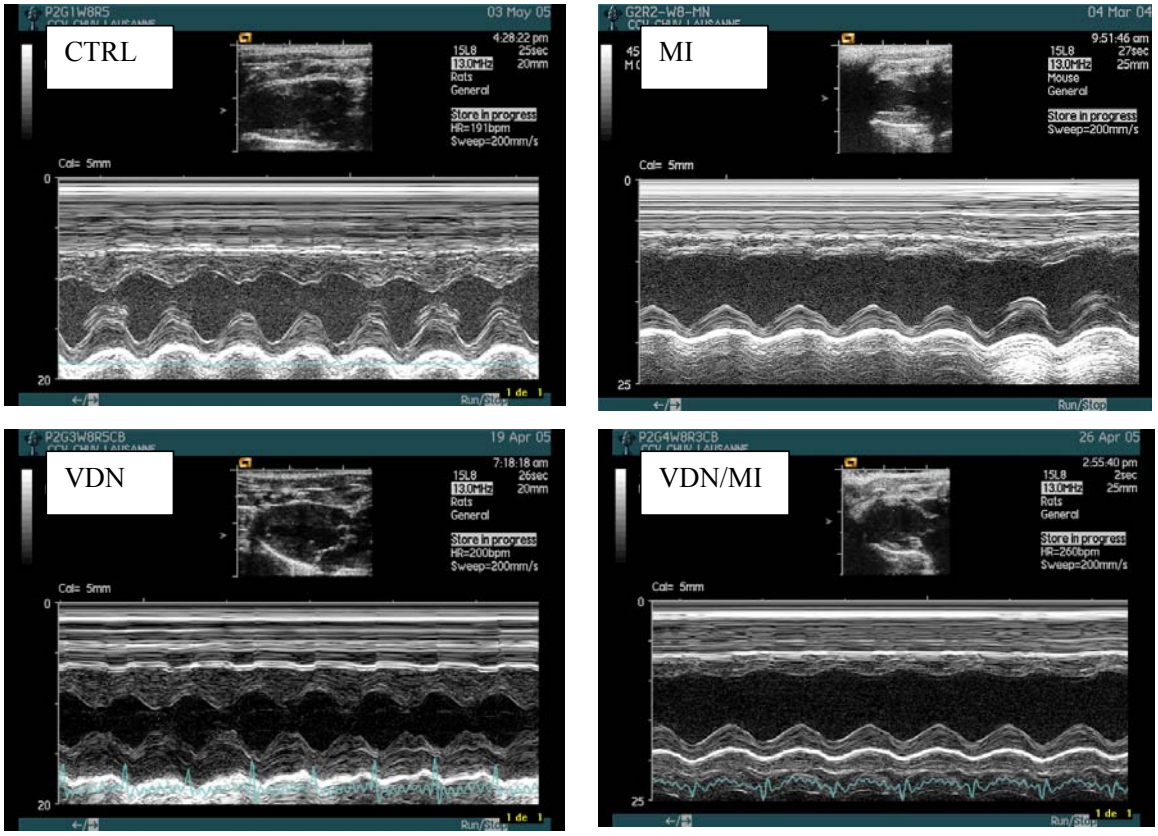

Figure 2. Representative TTE M-mode of the four groups at week 8. Posterior wall motion dyskinesia is visible in the MI and VDN/MI groups, whereas wall thickening is seen in the VDN group.

The two infarcted groups presented significantly reduced EF_e's at week 8 as compared to the CTRL and VDN groups (Figure 3A). Also, there was no negative effect of VDN on the EF_e. RWT is thinnest in the infarcted groups with MI group being significantly smaller vs CTRL. Additionally, the VDN group shows thickening compared to the CTRL group while significantly larger compared to the MI group (Figure 3B). The RWT is significantly affected by time in the combined group. The LVFS followed the trend of the EF_e in the two infarcted groups (Figure 3C). V_{cf} was most compromized in the two MI groups (Figure 3D).

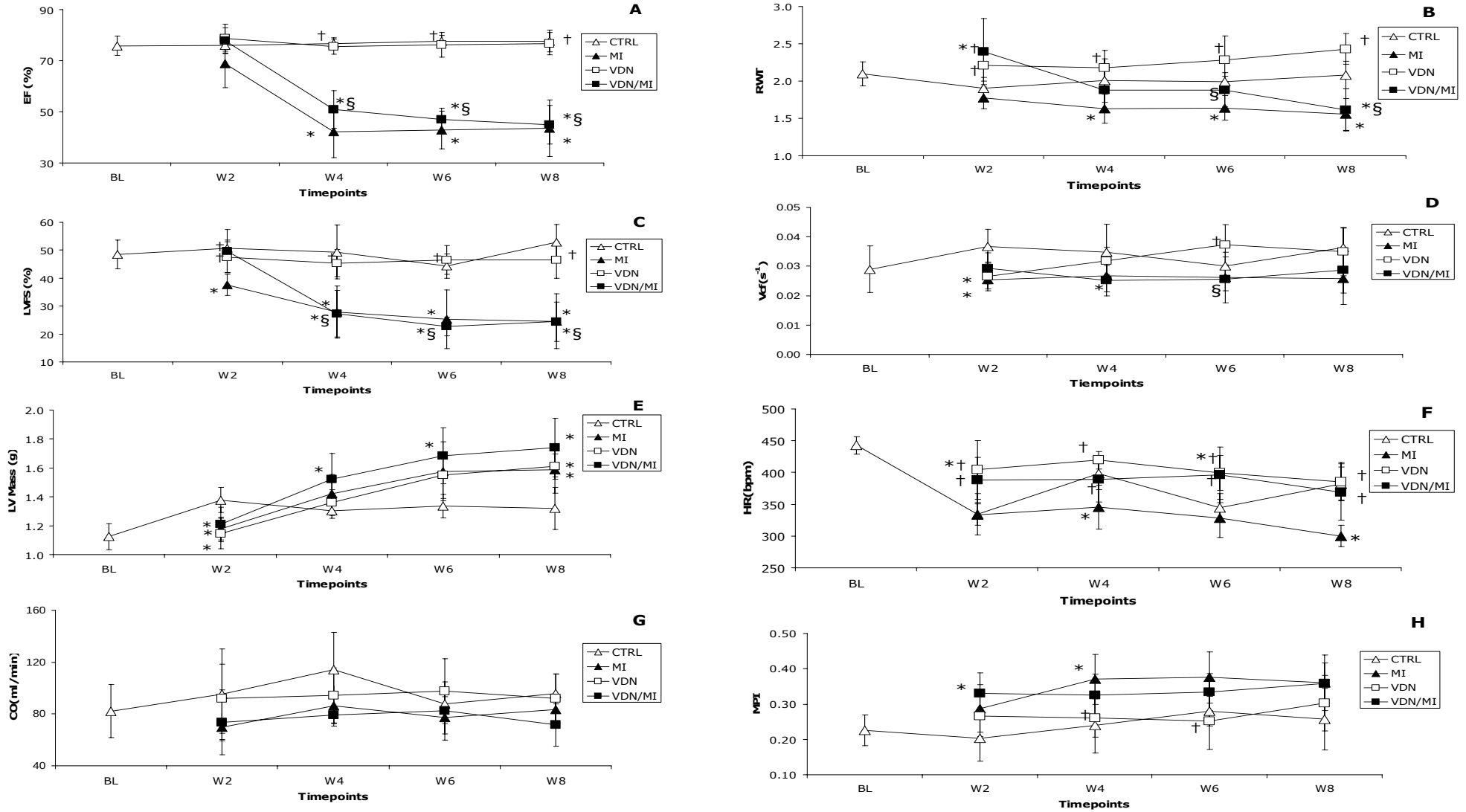

*Figure 3. Serial TTE of the four groups. EF_e, ejection fraction; RWT, relative wall thickness; LVFS, left ventricular fractional shortening; V_{cf}, velocity of circumferential fibre shortening; LV mass; HR, heart rate; CO_e, cardiac output; MPI, myocardial performance index; $p<0.05$ represented by an * vs CTRL, † vs MI and § vs VDN.*

LV mass increased in all three groups with respect to CTRL and were all significantly greater at week 8 (Figure 3E). HR was most compromized in the MI group (Figure 3F). CO_e was reduced in the two MI groups but no significance could be established (Figure 3G). MPI was highest in the MI groups but again no significance could be established (Figure 3H).

Cardiac composition. The various parameters that we measured were not affected by the VDN treatment (Table 3).

*Table 3. Cardiac composition of the four groups. Values are mean ± SD. CSA, cross sectional area; BNP, brain natriuretic peptide. * p<0.05 vs CTRL, † vs MI and § vs VDN.*

	Parameters	CTRL	MI	VDN	VDN/MI
Cardiac composition	Ca myocardial (µmol/g dry wt)	6.3±0.9	108±24	9.8±1.1*†	149±28*†
	Collagen (% dry weight)	6.9±0.8	15.1±1.9*	7.7±0.9†	13.2±0.8*§
	Proteins (mg/g dry weight)	88±8	95±6	103±11	106±6
	Collagen/Protein	8.3±0.6	16.2±2.1*	7.3±0.7†	13.0±1.1§
	Myocyte diameter (µm)	14.6±2.9	17.9±4.3*	15.3±2.9†	20.5±5.3*†§
	Myocyte CSA (μm^2)	221±59	346±120*	250±60†	439±164*†§
	BNP (pmol/L)	0.35±0.10	1.0±0.33*	0.56±0.13	1.71±0.57*†§

However, most alterations observed in the MI group were found to be exaggerated in the combined VDN/MI group of animals. Indeed, the cardiomyocyte diameter as well as the CSA were respectively 19% and 36 % higher in the MI group as in the CTRL group (P<0.05), whereas they were 29% and 50% higher in the VDN/MI group as compared to the CTRL group (Table 3, Figure 4).

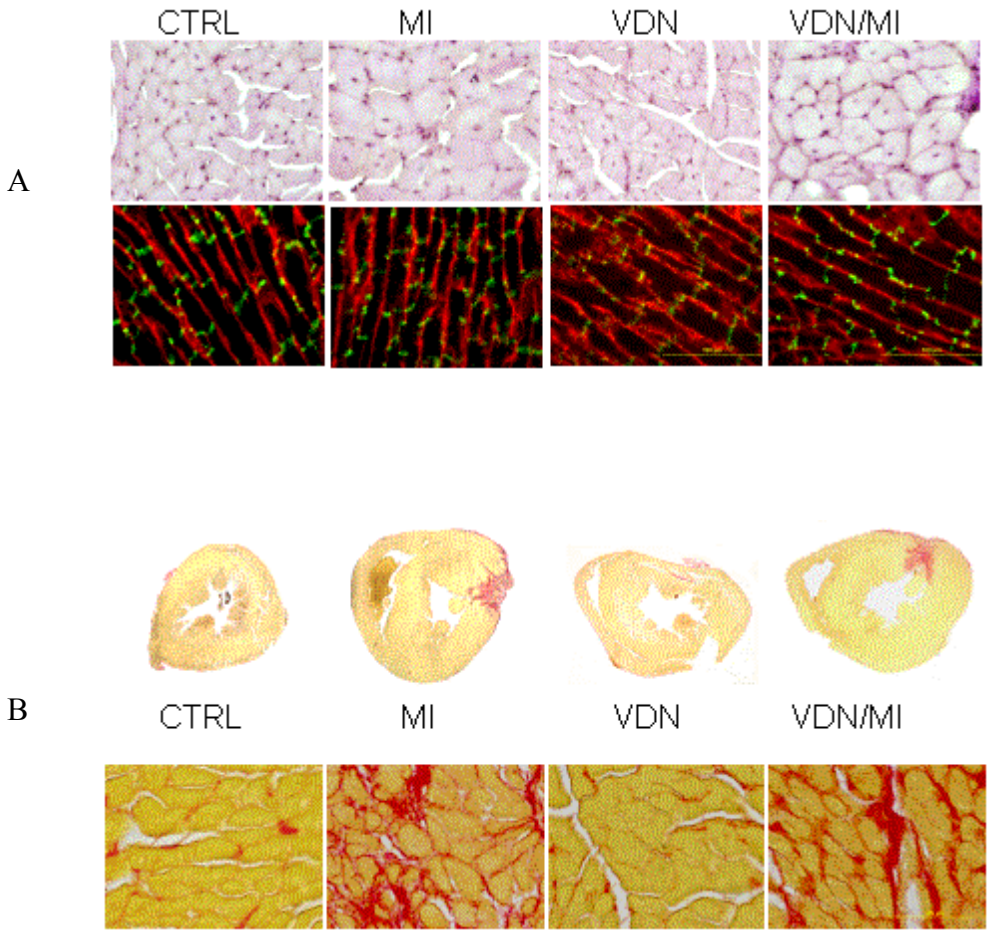

Figure 4. Panel A: Cardiomyocyte hypertrophy was estimated from left ventricle section for the 4 groups. Upper panels show representative cardiomyocyte cross-sectional and diameter as revealed by histology using periodic acid schiff. Below, show cardiomyocyte length as visualized by immuhistochemistry using double staining with antibodies against laminin (red) and connexin 43 (green).

Panel B: The extent of myocardial fibrosis was qualitatively visualized by picros-sirius red histological staining. Upper panel shows the entire cross-sectional area of the heart and downstream panel reveal same sections in a 40x magnification.

Similarly, collagen content was significantly elevated in both MI and VDN/MI groups. The protein levels were however comparable between all four groups (Table 3). Due to the infarct scar, the myocardial calcium content was, as expected, largely increased in both MI and VDN/MIgroups (Table 3). Although to a lesser extent, the myocardial calcium content was also significantly increased in the VDN group as compared to CTRL animals. Finally, the

mRNA expression of BNP was significantly increased in the MI group as compared to CTRL animals but was significantly more elevated in the combined VDN/MI group (Table 3).

Vascular structure, function and composition. Aortic structural parameters were comparable between the four groups (Table 4). However the aortic functional parameters were largely affected by the VDN treatment. Interestingly, the combination with an MI advocated these alterations (Table 4). Additionally, the PWV thus the EM were elevated in the combined group as observed in the VDN group (Table 4). However, statistical significance was hampered due to large standard deviations. As expected, the aortic calcium was found to be highly elevated in the VDN treated animals (Table 4). Biochemistry analysis revealed that collagen content was increased in all groups as compared to the CTRL group (Table 4). Protein level was not affected by the various treatments. Finally, fibrosis was clearly increased in both MI groups ($p<0.05$, Figure 4).

*Table 4. Aortic structure, function and composition of the four groups. Values are mean ± SD. D_i, internal diameter; h, wall thickness; MCSA, medial cross sectional area; PWV, pulse-wave velocity; EM, elastic modulus and WS, wall stress. * p<0.05 vs CTRL, † vs MI and § vs VDN.*

	Parameters	CTRL	MI	VDN	VDN/MI
Aortic structure	Di (mm)	1.46±0.05	1.53±0.05	1.66±0.04	1.52±0.06
	h (μm)	78±4	81±4	87±3	81±5
	h/Di	0.053±0.004	0.053±0.006	0.053±0.008	0.054±0.010
	MCSA (mm^2)	0.38±0.03	0.42±0.03	0.48±0.02	0.42±0.04
Aortic function	EM (10^6 dyne/cm^2)	5.6±4.7	5.1±2.7	19±7.9†	22±30
	WS (10^6 dyne/cm^2)	1.21±0.18	1.16±0.19	1.39±0.33	1.33±0.28
	EM/ WS	4.8±3.8	4.3±2.8	14±3.9	18±26
	PWV (m/s)	5.1±2.0	5.0±1.5	8.8±2.5	9.5±7.3
Aortic composition	Ca aortic (μmol/g dry wt)	17±1	15±1	442±174*†	329±143*†
	Collagen (% dry weight)	59±6	87±9*	75±10*	77±3*
	Proteins (mg/g dry weight)	155±13	186±16	187±9	194±7
	Collagen/Protein	39±3	47±3*	46±3	41±2

Discussion

We present a novel experimental model of HF combining MI and ISH in rats. This model not only confirms the presence of general critical signs of advanced HF but also demonstrates functional, structural and biochemical cardiac alterations that are, for the majority of them, augmented as compared to the standard MI or VDN models. Indeed, the combined VDN/MI model was the only one of the three we analyzed to show significant weight loss, increased LW/BW and increased HW/BW. Most importantly, the ejection phase indices (EF_c and CO_c) were the most compromised in this model. The systolic hypertension induced by the VDN treatment appears therefore to contribute substantially to the functional alterations provoked by the MI.

In the present study, the VDN treatment and the subsequent ISH influenced preferably the contractile parameters (dP/dt_{max}-EDV , PE, PVA, efficiency, PRSW, and E_{es}) while the MI affected more the diastolic function (LVEDP, IRT, dP/dt_{min} and tau). In addition, as opposed to the MI model where both EDV and ESV were increased, only the ESV parameter was augmented in the combined VDN/MI model. Consequently, the ejection phase indices (EF_c, CO_c, SV, LVFS) were dramatically altered in the VDN/MI group of animals. This is in accordance with results obtained using the combination of MI plus either renal hypertension [4] or aortic banding [19]. Some contradictions with other observations [3,9] may be explained by the discrepancies of the hypertensive models ontogeny as well as by the delay before certain structural and functional parameters are measured. Indeed, we chose to measure the parameters at week 8. However, the description would certainly have been different in animals were followed over a longer period as demonstrated by the progressive changes observed in the various TTE measurements. Indeed, the increased RWT observed 2 weeks after VDN treatment rapidly decreased after coronary ligation even though the LV mass remained the highest in the combined group. In clinical situations, the prevalence of eccentric

hypertrophy is also typically observed in patients suffering from hypertension and having CHD [20] or having had a MI [21,22].

Cardiac composition was altered by the MI and VDN treatment. Not surprisingly, both groups of infarcted animals showed the highest calcium content. However, VDN treatment further enhanced the cardiac calcium content both in the infarcted animals and in non-infarcted animals, confirming thus previous observation [23]. The extent of fibrosis and collagen levels was elevated in both infarcted groups, and was not influenced by VDN treatment, at least within this 8 weeks observation period. This was also observed in a model combining MI and SHR [24]. Finally, the cellular hypertrophy appeared to be significantly increased when the infarcted animals also had a VDN-induced ISH.

BNP is an attractive parameter to follow HF evolution as it is an independent predictor of long term survival [25], it reflects the remodeling process in hypertension [26,27] and is correlated with EF [28]. In our study, the expression of BNP was the highest in the group of animals combining ISH and MI. These findings were also reported in clinical studies [22], confirming therefore the interest of the VDN/MI model for translational applications to clinical implications.

In summary, the addition of hypertension on a MI model of HF largely compromises the cardiac function. Epidemiological studies have emphasized the close relationship between elevated blood pressure and the incidence of cardiovascular disease [29] and systolic blood pressure and pulse pressure (PP) in particular, have been demonstrated to be strong independent predictors of cardiovascular mortality [30,31]. Therefore, establishing an experimental model associating both pathologies could only be beneficial as a novel research tool in order to better elucidate the remodeling mechanisms involved in infarcted hearts with preexisting LV hypertrophy.

Our study may present some limitations. Combining two methods of inducing HF also

means combining the limitations of the two techniques. However, in the current study, the standard deviation observed in the VDN/MI group was in the same range as in the other groups. Interestingly, the infarcted surface (IS) was increased in the VDN/MI group as compared to the MI group even though the coronary ligation was performed in a randomized manner. It has indeed been proposed that the presence of LV hypertrophy is a necessary cofactor in the exacerbation of ischemic damage by chronic hypertension [32]. Hence, hypertension would augment the post-MI remodeling. Differing results might in fact have been obtained if the MI was performed before the VDN treatment [5]. Also, the EF which was lower after 4 weeks in the MI group as compared to the combined group appeared to rapidly stabilize in the MI group but progressively worsens in the VDN/MI group. Another limitation concerns the analysis of the TTE derived parameters which highly depend on the frame rate, resolution and intra-inter observer variability and may thus explain the differences between the EF_c and EF_e values. A difference of measurement of up to 10% between the 2 devices as well as a 10% intra-inter observer variability was recently reported [15].

In conclusion, the addition of MI on top of a raised afterload, confirms in this small animal model to substantially augment the severity of HF. Therefore, the VDN/MI combination appropriately mimics several clinical conditions and constitutes therefore an attractive model to study more in-depth the development of HF and subsequently the potential of novel therapeutic strategies.

Acknowledgements.

This work was supported by the Swiss National Research Foundation (3100AO-104257/1), Cardiovascular Scientific Foundation (Fonds Scientifique Cardiovasculaire), Swiss Life Anniversary Foundation for Public Health and Medical Research, Novartis Foundation for Medico-Biological Research, the Regional Development Committee (CPER 2000-2006,

"Bioingéniérie Appliqué aux Régulations Cellulaires", Metz, France), the greater Nancy Urban Council (Nancy, France) and the Pharmacolor Association (Nancy, France). The authors thank the assistance from the Bioimaging and optics – BIOP, Image Processing & Analysis Office of the EPFL and Patrick Liminaña (Pharmacology Laboratory, Pharmacy Faculty, UHP Nancy 1, France) for excellent technical help with histomorphometric analysis preparation.

References

1. Ho KKL, Pinsky JL, Kannell WB, Levy D. The epidemiology of heart failure: The Framingham study. *J Am Coll Cardiol* 1993;22:6A-13A.
2. Fletcher PJ, Pfeffer JM, Pfeffer MA, Braunwald E. Effects of hypertension on cardiac performance in rats with myocardial infarction. *Am J Cardiol* 1982;50:488-496
3. Nass O, Yang X-P, Liu Y-H, Carretero OA, Khaja F, Goldstein S, Sabbah HN. Effects of pre-existing left ventricular hypertrophy on ventricular dysfunction and remodeling following myocardial infarction in rats. *J Heart Lung Transplant* 2002;21:1113-1119.
4. Anversa P, Li P, ,Malhotra A, Zhang X, Herman MV, Capasso JM. Effects of hypertension and coronary constriction on cardiac function, morphology, and contractile proteins in rats. *Am J Physiol Heart Circ Physiol* 1993;265:H713-H724.
5. Jain M, Liao R, podesser BK, Ngoy S, Apstein CS, Eberli FR. Influence of gender on the response to hemodynamic overload after myocardial infarction. *Am J Physiol Heart Circ Physiol* 2002;283:H2544-H2550.

6. Atkinson J. Arterial calcification: mechanisms, consequences and animal models. *Path Biol* 1999;47:677-684.
7. Boutouyrie P, Tropeano AI, Asmar R, Gautier I, Benetos A, Lacolley P, Laurent S. Aortic stiffness is an independent predictor of primary coronary events in hypertensive patients. A longitudinal study. *Hypertension* 2002;39:10-15.
8. Safar ME, Levy BI, Struijker-Boudier H. Current perspectives on arterial stiffness and pulse pressure in hypertension and cardiovascular diseases. *Circulation* 2003;107:2864-2869.
9. Kass DA, Saeki A, Tunin RS, Recchia FA. Adverse influence of systemic vascular stiffening on cardiac dysfunction and adaptation to acute coronary occlusion. *Circulation* 1996;93:1533-1541.
10. Hass GM, Trueheart RE, Taylor CB, Stumpe M. An experimental histologic study of hypervitaminosis D. *Am J Pathol* 1958;34:395-431.
11. Niederhoffer N, Lartuad-Idjuadiene I, Giummelly P, Duvivier C, Peslin R, Atkinson J. Calcification of medial elastic fibres and aortic elasticity. *Hypertension* 1997;29:999-1006.
12. Lartaud-Idjouadiene I, Lompre A-M, Kieffer P, Colas T, Atkinson J. Cardiac consequences of prolonged exposure to an isolated increase in aortic stiffness. *Hypertension* 1999;34:63-69.
13. Lartaud-Idjouadiene I, Niederhoffer N, Debets JJM, Struijker-Boudier H, Atkinson J, Smits JFM. Cardiac function in a rat model of chronic aortic stiffness. *Am J Physiol Heart Circ Physiol* 1997;272:H2211-H2218.
14. Marque V, van Essen H, Struijker-Boudier H, Atkinson J, Lartaud-Idjouadiene I. Determination of aortic elastic modulus by pulse wave velocity and wall tracking in a rat model of aortic stiffness. *J Vasc Res* 2001;38:546-550.

15. Jegger D, da Silva R, Jeanrenaud X, Nasratullah M, Tevaearai HT, von Segesser LK, Segers P, Gaillard V, Atkinson J, Lartaud I, Stergiopulos N. Ventricular-arterial coupling analyzed by a conductance catheter in a rat model of reduced arterial compliance provoked by hypervitaminosis D and nicotine. *Am J Physiol Heart Circ Physiol* 2006 (In press)
16. Baan J, van der Velde ET, de Bruin HG, Smeenk GJ, Koops J, van Dijk AD et al. Continuous measurement of left ventricular volume in animals and humans by conductance catheter. *Circulation* 1984;70:812-823.
17. Henrion D, Chillon JM, Godeau G, Muller F, Capdeville-Atkinson C, Hoffman M, Atkinson J. The consequences of aortic calcium overload following vitamin D3 plus nicotine treatment in young rats. *J Hypertens* 1991;9:919-926.
18. Chien YW, Barbee RW, MacPhee AA, Frohlich ED, Trippodo NC. Increased ANF secretion after volume expansion is preserved in rats with heart failure. *Am J Physiol Heart Circ Physiol* 1988;254:R185-91.
19. Anthonio RL, van Veldhuisen DJ, Scholtens E, van Bekkum C, de Boer E, van Gilst WH. Myocardial infarction with aortic banding. A combined rat model of heart failure. *Jpn Heart J* 1997;38:697-708.
20. Zabalgoitia M, Berning J, Koren MJ, Stoylen A, Nieminen MS, Dahlof B, Devreux RB. Impact of coronary artery disease on left ventricular systolic function and geometry in hypertensive patients with left ventricular hypertrophy (the life study). Am J Cardiol 2001;88:646-650.
21. Yoshiyama M, Kamimori K, shimada Y, Omura T, Kino N, Iida H, Yoshikawa J. Left ventricular remodelling after myocardial infarction in antecedent hypertensive patients. *Hypertens Res* 2005;28:293-299.

22. Richards AM, Nicholls MG, Troughton RW, Lainchbury JG, Elliott J, Frampton C, Espiner EA, Crozier IG, Yandle TG, Turner J. Antecedent hypertension and heart afilre after myocardial infarction. *J Am Coll Cardiol* 2002;39:1182-8.
23. Atkinson J, Poitevin P, Chillon J-M, Lartaud I, Levy B. Vascular Ca overload produced by vitamin D_3 plus nicotine diminishes arterial distensibility in rats. *Am J Physiol Heart Circ Physiol* 1994;35:H540-H547.
24. Zdrojewski T, Gaudron P, Whittaker P, Poelzl S, Schiemann J, Hu K, Ertl G. Ventricular remodelling after myocardial infarction and effects of ACE inhibition on hemodynamics and scar formation in SHR. *Cardiovascular Pathology* 2002;11:88-93.
25. Omland T, Aakvaag A, Bonarjee VVS, Caidahl K, Lie RT, Nilsen DWT, Sundsfjord JA, Dickstein K. Plasma brain natriuretic peptide as an indicator of left ventricular systolic function and long-term survival after acute myocardial infarction. Comparison with plasma atrial natriuretic peptide and N-terminal proatrial natriuretic peptide. *Circulation* 1996;93:1963-1969.
26. Uusimaa P, tokola H, Ylitalo A, Vuolteenaho O, Ruskoaho H, Risteli J, linnaluoto M, Peuhkurinen K. Plasma B-type natriuretic peptide reflects left ventricular hypertrophy and diastolic function in hypertension. *Int J Cardiol* 2004;97:251-256.
27. Vanderheyden M, Goethals M, Verstreken S, De Bruyne B, Muller K, Van Scheurbeeck E, Bartunek J. Wall stress modulates brain natriuretic peptide production in pressure overload cardiomyopathy. *J Am Coll Cardiol* 2004;44:2349-54.
28. Falkensammer G, Lechleitner P, Hammerer-Lercher A, Theurl A, Puschendorf B, Mair J. B-type natriuretic peptide and N-terminal pro brain natriuretic peptide are

related to systolic and diastolic left ventricular function assessed by radionuclide ventriculography. *Int J Cardiol* 2005;105:340-341.

29. Weber T, Auer J, O'Rourke MF, Kvas E, Lassnig E, Berent R, Eber B. Arterial stiffness, wave reflections, and the risk of coronary artery disease. *Circulation* 2004;109:184-189.
30. Franklin SS, Khan SA, Wong ND, Larson MG, Levy D. Is pulse pressure useful in predicting risk of coronary heart disease? The Framington heart study. *Circulation* 1999;100:354-60.
31. Safar ME. Systolic blood pressure, pulse pressure and arterial stiffness as cardiovascular risk factors. *Curr Opin Nephrol Hypertens* 2001;10:257-261.
32. Bolli R, Kuo LC, Roberts R. Influence of acute arterial hypertension on myocardial infarct size in dogs without left ventricular hypertrophy. *JACC* 1984;4:522-8.

Conclusions and future perspectives

We have employed an established model of ISH to examine the combined effects of increased aortic stiffness (ISH) and MI on cardiac performance and ventricular-arterial coupling in rats. A complete set of noninvasive (TTE) and invasive techniques were employed and a comprehensive set of cardiac, arterial and coupling parameters were evaluated. The major findings are:

Paper 1: This paper addresses the issue of the universality of the normalized time-varying elastance curve. It is demonstrated that the waveform of the normalized time-varying elastance curve ($E_n(t_n)$) is qualitatively comparable between the control and MI hearts, however, when $E_n(t_n)$ is compared quantitatively between the two groups, statistical significance is found at the ejection phase and during diastole. These differences need to be taken into account when assessing cardiac contractility based on a generalized $E_n(t_n)$ in different animal models or in the human in different physiological or pathological states.

Paper 2: Using trans-thoracic echo (TTE), we were able to follow serial changes of cardiac function post MI using two novel parameters, the myocardioal performance index (MPI) and its ratio to left ventricular fractional shortenin (LVFS/MPI), both indices being monitor successfully and as efficiently as other classical TTE parameters. More so, LVFS/MPI visually expressed better the serial modifications in cardiac function. Both MPI and LVFS/MPI were correlated to the load-independent contractile parameter, PRSW, and to the preload parameter, LVEDP, being thus pertinent in following preload changes post MI. Finally, chamber remodeling post MI can successfully be followed due to the fact that ESV and EDV both correlate to MPI and LVFS/MPI.

Paper 3: We studied hemodynamics, arterial function, cardiac function and ventricular-arterial coupling in a rat model of reduced arterial compliance. The results show that arterial stiffening after VDN treatment provokes important changes in vascular impedance and wave

reflections, leading to isolated systolic hypertension and LV hypertrophy, Ventricular-arterial coupling was also altered. The effects are quantitatively similar to those of arterial stiffening with age.

Paper 4: We studied changes in cardiac geometry, structure and function in response to MI in control and VDN-treated (stiffened aorta) rats. The combined VDN/MI model showed the largest compromise in cardiac structure and function and exhibited the strongest biochemical signs of heart failure as compared to all other groups. The addition of MI on top of a raised afterload, seems to have accelerated the progression of heart failure. Vascular alterations also reflected well a model of ageing and calcification. This combined pathology model of failing hearts in presense of a stiff arterial tree might be fruitful in better understanding the evolution of disease and may help improving or developing novel treatment therapies.

Future perspectives:

1. The utilization of the combined model will be employed using non viral gene transfer in order to elucidate the effect of gene therapy on a heart suffering from HTN and MI.
2. Subsequently, when patients are in acute or chronic heart failure, they are placed on cardiac or ventricular assist devices, which offload the heart. During this period, the heart is capable of recovering its contractile function by a phenomenon called "Reverse Remodeling" (RR). Little is known about RR or understood at a molecular and cellular level. The intention is to perform myocardial infarctions and provoke arterial hypertension in rats or rabbits (even combine the two pathologies). Then, these damaged hearts are extracted and transplanted into the abdomen's of recipient rats (or necks re rabbits) over a certain defined time period. During this period, the RR occurs, or not and finally the hearts will be removed at sacrifice in order to perform genomic and proteomic assays in order to better understand the mechanisms involved in the RR

process.

3. Finally, drug discovery strategies could be defined and proposed later in collaboration with drug companies using MI, VDN and the combination of the two.

Curriculum vitae

1. General information:

Name and first name: JEGGER David
Citizenship: Swiss and South African
Origin: Cape Town – South Africa
Date of birth: June 16th, 1972
Personal address: Avenue de la dole 19
1005 Lausanne
Switzerland
41.21.3124947 (home), 41.79.6304845 (handy)

Professional address:
Department of Cardiovascular Surgery
CHUV (University Hospital of Lausanne)
Rue du Bugnon 46
1011 Lausanne
Switzerland
Tel: +41(0)21-3142153
Fax: +41(0)21-3142158
E-mail: David.Jegger@chuv.hospvd.ch

Laboratory of Haemodynamics and Cardiovascular Technology
Swiss Federal Institute of Technology
Batiment AI.1014, station 15
1015 Lausanne
Switzerland
Tel. +41.21.6938342
Fax. +41.21.6939635
e-mail : David.Jegger@epfl.ch

2. Education:

Primary School in Cape Town (South Africa) - 1978 to 1984
High School in Cape Town (South Africa) - 1985 to 1989
Military service (South Africa) -1990
Polytechnic College in Cape Town (South Africa) – 1991 to 1994
BSc (Hons), Open University, UK. -1997 to 2000
MEng, Open University, UK. -2001 to 2003
PhD, EPFL, Lausanne, Switzerland – 2003 to 2006

3. Diplomas

Matriculation Certificate of the Joint Matriculation Board with matric/bac/abitur university exemption (1989)
National Diploma in Clinical Technology (Perfusion) (1993)
Registration with the South African Medical and Dental Council (1994)
Certificate in French (1994)
Certificate in German (1994)
European Certificate in Cardiovascular Perfusion (1995)
Certificate in computer literacy, Office-1996
Certificate for Quality Control conference, Lausanne, Switzerland-1999
Certificate: workshop on temporary ventricular assistance, Zurich, Switzerland-1999
BSc (Hons) -Open University (2000)

Course as animal researcher Module 1 (2003)

MEng -Open University (2003) Thesis title: "Evaluation of a new venous cannula design for use in CPB operating procedures"
PhD (2006 at the Swiss Federal Institute of Technology) Title: "Effects of a stiffened arterial tree on ventricular-arterial coupling in healthy and diseased hearts"
Course as independent animal researcher Module 2 (2006)

4. Post-graduate education:

1991-1994:	Student Cardiovascular Perfusionist, Groote Schuur University Hospital, Cape Town, South Africa. (Prof. U.von Oppell)
1995 to date:	Certified Cardiovascular Perfusionist, University Hospital of Lausanne, Switzerland. (Prof.LK von Segesser)
2004:	Exchange program via FNS, 3 months visit to Prof Hunter, Auckland, New Zealand
2003-2006:	Biomedical researcher for PhD thesis at the Laboratory of Haemodynamics and Cardiovascular Technology, EPFL (Prof N Stergiopulos) and at the Department of cardiovascular surgery, CHUV, Lausanne (Prof LK von Segesser).

5. Prizes awarded:

- Foundation European Congress on Extra-Corporeal Circulation Technology (FECECT) : The best presentation regarding perfusion safety on Cardiopulmonary Bypass. [Czech Republic, 1997]
- Société suisse de Chirurgie Thoracique et Cardio-vasculaire (Swiss Society for Thoracic and Cardiovascular Surgery) : The best presentation in the perfusion session. [Lausanne, 1998]
- Société suisse de Chirurgie Thoracique et Cardio-vasculaire (Swiss Society for Thoracic and Cardiovascular Surgery) : The best presentation in the perfusion session. [Zurich, 2001]

6. Society memberships and reviewer status:

- Swiss Society of Thoracic and Cardiovascular Surgery
- Swiss Society of Perfusionists (SSdP)
- European Board of Cardiovascular perfusion (EBCP)
- Institute of Physics and Engineering in Medicine (IPEM-UK)
- Chief Editor of the "SwissPerfusion" Journal
- Swiss Society of Biomedical Engineering (SSBE)
- European Society of Artificial Organs (ESAO) pending
- American Society of Artificial Internal Organs (ASAIO) pending
- Quality Control Manager for CPB applications
- Reviewer for "European Journal of Cardio-thoracic Surgery"
- Reviewer for "Artificial Organs"
- Reviewer for "Investigative Radiology"
- Reviewer for "Circulation"
- Cardiovascular System Dynamics Society
- IEEE (applied)
- American Physiological Society
- Swiss cardiovascular research and training network (SCRTN)
- European society of biomechanics

7. Publications

58 papers published in scientific journals (33 now mentioned in medline under "Jegger D"), 14 papers in press or submitted for publication.

8. Published Abstracts

47 abstracts published in scientific journals

9. Collaborations

- Prof P Hunter, University of Auckland, New Zealand.
- Prof J Atkinson, University of Nancy, France, Dept of Pharmacology.
- Prof P Segers, University of Gent, Belgium, Dept of Biomechanics.
- Prof N Westerhof, Free University, Amsterdam, The Netherlands.
- Dr H Duplain: Internal Medicine, CHUV, Lausanne– TTE analysis of the effect of specific peptides on cardiac function post MI.
- Dr G Milano, CHUV, Lausanne: Effect of Viagra on myocardial preconditioning post MI.
- Dr Zaugg, USZ, Zurich: The effect of different anaesthetic agents on myocarfdial preconditioning post MI.

10. Funding

- Fondation Scientifique Cardiovasculaire (CHF 25 000, 2003)
- FNS exchange program bursary (PBOIA-102080) to undertake specialist training in New Zealand (CHF 13 000, 2003)
- Novartis Foundation (CHF 60 000, 2004)
- Swiss National Science Foundation, FNS (CHF 175 000, 2004-2007)
- Swisslife (CHF 20 000, 2004)
- Euroecho 8 travelling grant (Euro 500, 2004)

11. Congress participation and presentations:

- XIX South African Cardiac Society Congress, Cape Town-1994
- Société suisse de Chirurgie Thoracique et Cardio-vasculaire à Lugano-1995
- French Society of Perfusion, Paris,France-1995
- ECLS, Stockholm, Sweden-1996
- Société suisse de Chirurgie Thoracique et Cardio-vasculaire à Lausanne-1997
- Fédération de perfusion en Europe (FECECT) Tchécoslovaquie-1997
- Société suisse de Chirurgie Thoracique et Cardio-vasculaire, Lausanne- 1998
- SCANSECT , Helsinki -1998
- European association of cardiovascular surgery, Paris-1998
- Reunion annuelle commune Société Suisse de Chirurgie Thoracique et Cardio-vasculaire, Bale, -1999.
- Fédération de perfusion en Europe (FECECT) Greece- 1999
- XXVI Congress of European Society for Artificial Organs -Edinburgh-1999
- Annual meeting of the Swiss society of cardiovascular surgery, Lucern, Switzerland-2000
- American Society for Artificial Internal Organs (ASAIO), New York-2000
- World congress for Physics and Engineering in Medicine, Chicago-2000
- European Society for Artificial Organs (ESAO) Lausanne-2000
- Société suisse de Chirurgie Thoracique et Cardio-vasculaire, Zurich - 2001
- German perfusion society, Wurzburg, Germany-2001

- European Society for Artificial Organs (ESAO) Belguim-2001
- World society of cardiothoracic surgeons, Lucern,CH, 2002
- Union des societes chirurgicales suisses, Lausanne, 2002
- ESAO, Vienna, Austria 2002.
- SSCTCV, Lausanne, Switzerland 2003
- SSC, Interlaken, Switzerland 2003
- FECECT, Funchal, Madeira 2003
- ESC, echocardiography, Barcelona Spain 2003
- American Academy of Perfusion and STS, San Antonio, USA, 2004
- Cardiovascular System Dynamics Society, Banff, Canada 2004.
- SSBE meeting in Zurich, 2004
- ESAO, Warsaw, Poland, 2004
- Euroecho 8, Greece, 2004
- FECECT, Sardinia, 2005
- SSCTCV, Lausanne, 2005
- EACTS, Barcelona, 2005
- ESAO, Bologna, 2005
- International society of biomechanics, Munich, 2006

12. Invited talks organized and given, plenary lectures and seminars

- Invitation to the annual congress of the Dutch Perfusion society, Amsterdam-2000: "*Minimally invasive cardiac surgery*"
- Moderator for ESAO congress in poster session, Lausanne-2000
- Invitation to the SSdP in Basel 2003. The Smartcanula™: from idea to reality
- Invited review article for the peer reviewed journal "Artificial Organs" edited by Professor Pascal Verdonck: "*Vascular Access for Cardiopulmonary Bypass Procedures". 2004*
- Invited Prof P Hunter, New Zealand for talk on Cardiome project-2004
- Invited Prof J Atkinson for talk on vascular biology-2004
- Invited talk on rat echocardiography: Program of course on Rodent Phenotyping Course April 29-30, 2005
- Invited talk on rat myocardial infarction: Program of course on Rodent Phenotyping Course November 25-26, 2005

13. Referees

Prof. Nikos Stergiopulos
Laboratory of Hemodynamics and Cardiovascular Technology
Building AA.B.023.
PSE A - Ecublens
1015 Lausanne
Switzerland
nikolaos.stergiopulos@epfl.ch

Prof. LK.von Seggeser
Department of Cardiovascular Surgery
CHUV (University Hospital of Lausanne)
Rue du Bugnon 46
1011 Lausanne
Switzerland
Ludwig.Von-Segesser@chuv.hospvd.ch

Dr. Hendrik Tevaearai
Clinic for Cardiovascular Surgery
University Hospital - Inselspital
CH-3010 Bern
Tel: +41 31 632-2373
Fax: +41 31 632 9766
Email: hendrik.tevaearai@inselch
Hendrik.Tevaearai@insel.ch

Scientific publications:

2006

1. Jegger D, da Silva R, Lartaud I, Gaillard V, Tevaearai H, Jeanrenaud X, Nasratullah M, von Segesser LK, Atkinson J, Stergiopulos N. A novel cardiovascular research model: combined myocardial infarction and isolated systolic hypertension in rats. (submitted to Circulation)
2. Jegger D, Mallik AS, Nasratullah M, Jeanrenaud X, Tevaearai H, Westerhof N, von Segesser LK, Stergiopulos N. Evaluating the Effect of Heart Failure Post Myocardial Infarction on the Normalised Time-Varying Elastance Curve. (manuscript in preparation for J Biomech)
3. Jegger D, Di Gilio C, Lartaud I, Gaillard V, da Silva R, Tevaearai HT, von Segesser LK, Atkinson J, Stergiopulos N. Mechanical properties and structure of carotid arteries in hypervitaminosis D and nicotine treated rats. (manuscript in preparation for AJP or Cardiovasc Res)
4. Jegger D, da Silva R, Jeanrenaud X, Nasratullah M, Tevaearai HT, von Segesser LK, Segers P, Gaillard V, Atkinson J, Lartaud I, Stergiopulos N. Ventricular-arterial coupling analyzed by a conductance catheter in a rat model of reduced arterial compliance provoked by hypervitaminosis D and nicotine. (accepted AJP)
5. Jegger D, Jeanrenaud X, Nasratullah M, Chassot P-G, Tevaearai HT, von Segesser LK, Stergiopulos N. Serial TTE follow-up of cardiac structural and functional alterations in a model of isolated systolic hypertension. (manuscript in preparation for JASE)
6. da Silva R, Jegger D, Tevaearai HT, Koch W, Stergiopulos N. G-protein expression and alterations in a novel cardiovascular research model. (manuscript in preparation for Circulation)
7. da Silva R, Jegger D, Tevaearai HT, von Segesser LK, Stergiopulos N. Skeletal muscle alterations in a novel cardiovascular research model. (manuscript in preparation for AJP)

2005

8. Jegger D, Jeanrenaud X, Nasratullah M, Chassot P-G, Mallik A, Tevaearai HT, von Segesser LK, Segers P, Stergiopulos N. Noninvasive Doppler-derived myocardial performance index in rats with myocardial infarction: validation and correlation by conductance catheter. *Am J Physiol Heart Circ Physiol* 2005 (accepted)

Conferences attended:

1. Jegger D, Mallik AS, Nasratullah M, Jeanrenaud X, Tevaearai H, von Segesser LK, Stergiopulos N. Evaluating the Effect of Heart Failure Post Myocardial Infarction on the Time-Varying Elastance Curve. *CSDS meeting booklet* 2004: page 6. Cardiovascular System Dynamics Society, Banff, Canada 2004.
2. Jegger D., Nasratullah M., Jeanrenaud X., Chassot P-G., Mallik A., Tevaearai H., von Segesser LK., Stergiopulos N.. The evolution of global ventricular function using the myocardial performance index during heart failure induced by myocardial infarction in rodents. *Eur J Echocardiography* 2004;5 Suppl I,S82. Euroecho 8, Greece, 2004
3. Jegger D, Jeanrenaud X, Nasratullah M, Chassot P-G, Mallik A, Tevaearai HT, von Segesser LK, Segers P, Stergiopulos N. Noninvasive Doppler-derived myocardial performance index in rats with myocardial infarction: validation and correlation by conductance catheter. (Submitted to World congress of cardiology, Barcelona, 2006)
4. Jegger D, da Silva R, Jeanrenaud X, Nasratullah M, Tevaearai HT, von Segesser LK, Segers P, Gaillard V, Atkinson J, Lartaud I, Stergiopulos N. Ventricular-arterial coupling analyzed by a conductance catheter in a rat model of reduced arterial compliance provoked by hypervitaminosis D and nicotine.
5. Jegger D, Di Gilio C, Lartaud I, Gaillard V, da Silva R, Tevaearai HT, von Segesser LK, Atkinson J, Stergiopulos N. Mechanical properties and structure of carotid arteries in hypervitaminosis D and nicotine treated rats. (Both submitted to World congress of biomechanics, Munich, 2006; Summer Bioengineering Conference, Florida, 2006; 16th European meeting on Hypertension, Madrid, 2006)
6. Jegger D, Jeanrenaud X, Nasratullah M, Chassot P-G, Tevaearai HT, von Segesser LK, Stergiopulos N. Serial follow-up of cardiac structural and functional alterations in a model of isolated systolic hypertension. (submitted to Euroecho, Prague, 2006)
7. Jegger D, da Silva R, Lartaud I, Gaillard V, Tevaearai H, Jeanrenaud X, Nasratullah M, von Segesser LK, Atkinson J, Stergiopulos N. A novel cardiovascular research model: combined myocardial infarction and isolated systolic hypertension in rats. (submitted to AHA, Chicago, 2006 and CSDS, The Netherlands 2006)